D2.6 Petrophysics Report of all Regions

Release Status:

Authors: Marc Fleury, João Barradas, Paula Canteli, Julio Carneiro, António Correia, Elena Fernandez de Arévalo, Jesús García Crespo, David García F.-Valderrama, Nikolaos Koukouzas, Cristina Manrique, Javier Martinez, Jose Mediato, Patricia Moita, Francisco Pangaro Bedoya, Pavlos Tyrologou, Carlos Ribeiro, Nicolas Rousseau, Mark Wilkinson

PilotSTRATEGY (H2020- Topic LC-SC3-NZE-6-2020 - RIA)

1. Document History

1.1 Location

This document is stored in the following location:

Filename	D2.6_PilotSTRATEGY_Petrophysics
Location	https://pilotstrategy.eu/about-the-project/work-packages/geo-characterisation

1.2 Revision History

This document has been through the following revisions:

Version No.	Revision Date	Filename/Location stored:	Brief Summary of Changes
1.0	27 Feb 23		
1.1	07 March 2023		Request figure with lithological schematic section with samples and pictures placed in

1.3 Authorisation

This document requires the following approvals:

AUTHORISATION	Name	Signature	Date
WP Leader	M. Wilkinson,		04/04/2023
Project Coordinator	Fernanda de Mesquita Lobo Veloso		04/04/2023

1.4 Distribution

This document has been distributed to:

Name	Title	Version Issued	Date of Issue
		PUBLIC	00/00/0000

The PilotSTRATEGY project has received funding from the European Union's Horizon 2020 research and innovation programme under grant agreement No. 101022664

Disclaimer

The information and views set out in this report are those of the author(s) and do not necessarily reflect the official opinion of the European Union. Neither the European Union institutions and bodies nor any person acting on their behalf may be held responsible for the use which may be made of the information contained therein.

The PilotSTRATEGY project has received funding from the European Union’s Horizon 2020 research and innovation programme under grant agreement No. 101022664

2. Executive summary

This deliverable reports on the petrophysical data collected for all sites in France, Spain (off-shore and on-shore), Portugal and Greece. The source of information and sample gathering can be extremely variable: for France and Spain (on-shore), well samples were available from the oil exploration period and in the case of Spain onshore, outcrop samples were analysed as well; in Spain off-shore and Portugal, well log data were used essentially together with a few samples; in Greece, outcrop samples were used. For each region, a brief geological description is made to describe the formation target and the general context.

Petrophysical information such as porosity and permeability are obviously key information. However it is also important to gather information about the effective porosity, i.e. the fraction of the total porosity that can be in practice be used to store CO_2; indeed, the porosity can be large but if the pore size is too small (microporosity in carbonates, clays bound water in sandstones), the capillary pressure will be too large to allow CO_2 to penetrate into that porosity fraction.

For the Paris Basin area, core samples from 2 wells were analysed. Neither well is in the study area, but the reservoir and seal are laterally homogeneous, and the wells are close. For the target reservoir, the reservoir section is not uniform vertically in terms of petrophysical properties and contains several barriers of low porosity and permeability. Permeability is governed by the amount of macroporosity. For the Vulaines 1 well, some porosity and permeability data are available from a database courtesy of the Vermilion oil company; the measurements performed in this study are consistent with these data.

For the onshore Ebro Basin (Spain), petrophysical characterization was carried out by both laboratory and on-site tests. Samples were from the Peñas Royas Section, the Torre de las Arcas outcrop and the Chiprana well. All are outside of the target structure but are thought to be representative of the reservoir and seal lithologies.

For the offshore Ebro area, samples of reservoir and seal were mostly taken from the Amposta Marino C2 well core, plus cuttings were available. Petrophysical analysis was conducted using available well logs and the results obtained were calibrated with the measured data. Porosity curves calculated with the neutron-density and density methods are very similar and calibrate well with core data.

For the Lusitania Basin (Portugal), outcrop samples from both reservoir complexes were collected onshore due to a lack of core samples. 13 wells were analysed, 7 offshore and 5 onshore; these are old and there are uncertainties in the calculate data. Samples covered three reservoirs of interest: Silves Group, Alcobaça Formation, Torres Vedras Formation. The Late Triassic Silves Group, has very low N/G, and overall low porosity that does not exceed 10%. The early Cretaceous Torres Vedras Formation has better N/G results, although with a large variability. The Torres Vedras Formation presents very good porosities, with an average value of 20%, this is the best reservoir target.

For West Macedonia (Greece), samples were collected from surface exposures of the Tsotyli, Pentalofos and Eptachori formations. All permeabilities of potential reservoirs were too low to be measured (< 0.01 mD).

The PilotSTRATEGY project has received funding from the European Union's Horizon 2020 research and innovation programme under grant agreement No. 101022664

Table of Contents

The PilotSTRATEGY project has received funding from the European Union's Horizon 2020 research and innovation programme under grant agreement No. 101022664

The PilotSTRATEGY project has received funding from the European Union's Horizon 2020 research and innovation programme under grant agreement No. 101022664

The PilotSTRATEGY project has received funding from the European Union's Horizon 2020 research and innovation programme under grant agreement No. 101022664

3. Samples from France

3.1 Geological aspects

3.1.1 Geological settings of the area of interest

French study area is located in the Paris Basin, at 60 km Southwest to Paris (Figure 3.1a), next to the Nangis locality. This area has been a preferential target for oil exploration at the second half of the 20th century, as shown in Figure 3.1b with the numbers of wells used in our study. Nowadays a large volume of wells, well logs, and cores data are in the public domain and used in this study to understand the "Oolithe Blanche" Formation, the targeted reservoir in the French Area for PilotSTRATEGY Project (Figure 3.1c). Thanks to this important array of data, the French team were able to conduct the import works of thin section analyses, core description (477m) through 12 wells (Figure 3.1b) and well correlation in the area (51 wells correlated).

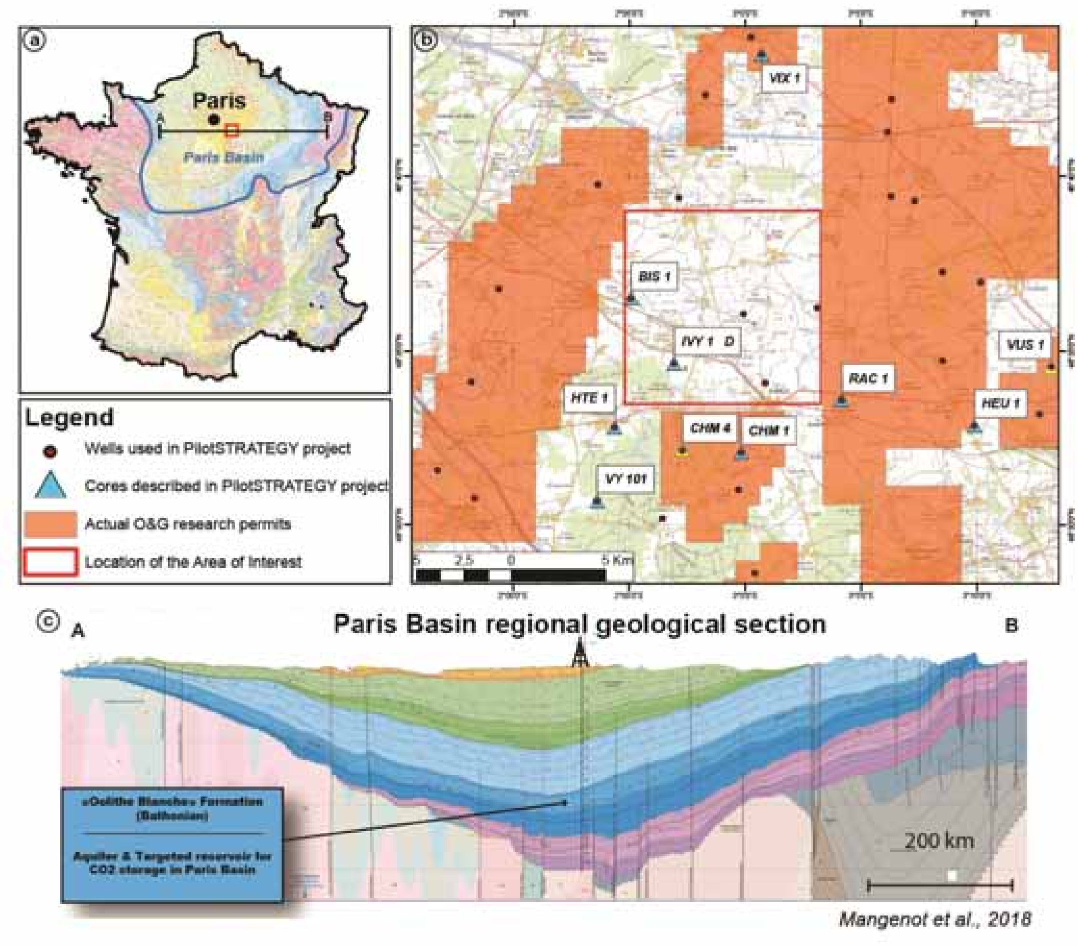

Figure 3.1: Location of the study area and data used in the French area for PilotSTRATEGY project. a) French geological map of France (1:1 000 000) showing location of the study area and the geological section presented in (c). b) Location map of the study area and data used in PilotSTRATEGY project. c) Geological section from Paris Basin, showing location of the targeted reservoir in PilotSTRATEGY project. Geological section from Mangenot et al., 2018.

One of the features of cores drilled in the area is the poor representation of the target reservoir. During oil exploration, coring was only conducted on the Callovian transgressive deposits. Consequently, only the topmost part of the targeted reservoir is cored and it is known from regional studies that this specific part of the reservoir has poor reservoir properties compared to rest of the formation.

Consequently, a sampling strategy has been conducted with the objective of having a better understanding of the reservoir property variations and how they depend to sedimentary facies; using well log data. This strategy is also adopted due to the small number of samples analysed for Petrophysical study. Sampling strategy is based on:

- Wells, which cores reach the deepest part of the Oolithe Blanche Formation
- Cores, which samples can be taken without damage to the core integrity. This is linked to previous systematic sampling conducted by Petroleum Company during exploration stage.
- Cores, which sampled an important sedimentary facies. This allowed us to understand which facies drive the good reservoir properties of the Oolithe Blanche Formation as well as which facies would have sealing properties.
- Well logs, which show important reservoir properties variations through the same sedimentary facies. This is dedicated to understand the role of diageneses in the Oolithe blanche.

After a screening of all cores described in the project, using the criteria of the sampling strategy, two wells have been selected for sampling: Charmottes 4 (CHM4) and Vulaines-1 (VUS1). Unfortunately, these cores are located slightly outside of the area of interest. However, because of the homogenous and low heterogeneity of sedimentary units at the local scale, and the absence of good representative cores in the AOI, CHM4 and VUS 1 cores are the best samples for our study.

3.1.2 Charmotte 4 cores and samples:

Charmottes-4 well is located at 2 Km south of the Area of Interest (Figure 3.1b). From depth -1790 to -1826m (TVD), 36 meters of the sedimentary pile have been cored with a 95% recovery. Stratigraphic interval correspond to:

- Dalle Nacrée Formation: Callovian transgressive system tract with development of isolated oolitic shoals. It corresponds to the oil reservoir targeted during exploration and poor hydrocarbon accumulations were found.
- Comblanchien Formation: latest Bathonian lagoonal facies, which correspond to the downward shift of the Oolitic ramp at the end of the Bathonian. In our study, this interval is interpreted as a relative low-permeable interval, despite very local and small scale permeable layers related to diagenesis and fracturing.
- Oolithe Blanche: Bathonian oolitic ramp that corresponds to the CCS reservoir target. Two main depositional environments are defined in the top reservoir interval with well-developed oolitic shoals and back-barrier facies (bioclastic packstone).

Six samples have been chosen from the Charmottes 4 cores. The Table below indicates for each samples:

- Samples location in the well (core number ; core section ; depth ; stratigraphic interval)
- Unique sample code number
- Type of analyses for sample

The PilotSTRATEGY project has received funding from the European Union's Horizon 2020 research and innovation programme under grant agreement No. 101022664

- Main lithology
- Purpose of the sampling

Results will be presented in sections 3.2 and 3.3

3.1.3 Vulaines-1 cores and samples:

Drilled in 1978, Vulaine-1 well is located at 11 Km east to the Area of Interest (Figure 3.1b). From depth -1819 to -1919m (TVD), 100 meters of the sedimentary pile have been cored. Compared to Charmottes-4 well, recovery is under 60% with only 57m thick preserved and described in our study. Stratigraphic interval identified in Vulaines-1 cores correspond to:

- "Marnes de Massengis" Formation: Callovian caprock. This formation corresponds to the proper seal of the reservoir system. It is indurated marls with calcareous nodules.
- Dalle Nacrée Formation: Callovian transgressive system tract with the development of isolated oolitic shoals. It is characterised by meter-thick coarsening upward sequence of oo-bioclastic Grainstone in Vulaines-1 well.
- Comblanchien Formation: represented in Vulaines-1 well by oncolitic and coral rich wackstones and packstones. This formation representa s shallow water environment recording an important regressive stage at the end of Bathonian.
- Oolithe Blanche: Bathonian oolitic ramp that correspond to the reservoir targeted. Due to relative low core penetration of the formation, only two main depositional environments are defined in the top reservoir interval with well-developed oolitic shoals and back-barrier facies (bioclastic packstone).

Six samples have been chosen in Vulaines-1 cores. Details of spreadsheets entries are explained in the section 3.1.2.

The PilotSTRATEGY project has received funding from the European Union's Horizon 2020 research and innovation programme under grant agreement No. 101022664

Table 3-1: List of samples taken and analysed in Charmottes-4 cores

Core	section	Depth	Lithology	Sample Name	Purpose	Interval
2	2/18	1809,5	Oobioclastic GST with cm-thick brachiopods and bivalves clast	CHM4_C2_1809,5	Reservoir properties of Oolithe Blanche : reservoir targeted (coarse-grained oo-bioclastic shoal)	DOGGER RESERVOIR
2	3/18	1811,7	Bioclastic PST/GST with gastropods, brachiopods, bivalves	CHM4_C2_1811,7	Reservoir properties of Oolithe Blanche : reservoir targeted (back-barrier facies with stylolites)	
2	5 / 18	1812,4	Oolitic Grainstone	CHM4_C2_1812,4	Reservoir properties of Oolithe Blanche : reservoir targeted (oolitic shoal)	
3	9 / 18	1815,9	PST/GST with pelloids, and brachiopods, bioclast and bivalve clasts	CHM4_C2_1815,9	Reservoir properties of Oolithe Blanche : reservoir targeted (back-barrier facies)	
2	15 / 18	1822,1	Oobioclastic GST with corals and bivalve clast. Dune stratifications	CHM4_C2_1822,1	Reservoir properties of Oolithe Blanche : reservoir targeted (oolitic shoal with specific well logs results)	
2	17 / 18	1824,8	Oolitic GST with cm-thick bioclastic layers and inclined stratifications	CHM4_C2_1824,8	Reservoir properties of Oolithe Blanche : reservoir targeted (oolitic shoal with specific well logs results)	

The PilotSTRATEGY project has received funding from the European Union's Horizon 2020 research and innovation programme under grant agreement No. 101022664

Table 3-2: List of samples taken and analysed in Vulaines-1 cores

Core	Section	Depth	Lithology	Sample Name	Purpose	Interval
6	4/11	1843,45	Argillaceous wackstone with large brachiopods, rare oolites. Extremely bioturbated.	VUS1_c6_1843,45	Reservoir properties at the Caprock / reservoir Transition: internal seal (lagoonal facies)	
6	5/11	1844,05	Argillaceous wackstone with large brachiopods, rare oolites. Extremely bioturbated.	VUS1_c6_1844,05	Reservoir properties at the Caprock / reservoir Transition: internal seal (lagoonal facies)	
10	1/8	1891,80	very well sorted oolitic Grainstone passing to oo-bioclastic megaripples	VUS1_c10_1891,8	Reservoir properties of Oolithe Blanche : reservoir targeted (specific sedimentary facies)	DOGGER RESERVOIR
10	6/8	1896,5	Megaripples with oo-bioclastic Grainstone : poorly rounded surficial oolites, echinoderms, “gravelles”, lamellibranches	VUS1_c10_1896,5	Reservoir properties of Oolithe Blanche : reservoir targeted (specific sedimentary facies – oolitic shoal)	
11	3/10	1911,2	Oobioclastic Grainstone passing to planar laminated Oolitic Grainstone	VUS1_c11_1911,2	Reservoir properties of Oolithe Blanche : reservoir targeted (specific sedimentary facies)	
11	9/10	1917	Oblique laminations in Oobioclastic facies	VUS1_c11_1917	Reservoir properties of Oolithe Blanche : reservoir targeted (specific sedimentary facies – oolitic shoal)	
11	10/10	1918	Very well sorted Oobioclastic Grainstone. Bioclasts are not dissolved and correspond to brachiopods & echinoderms fragments.	VUS1_c11_1918	Reservoir properties of Oolithe Blanche : reservoir targeted (specific sedimentary facies)	

The PilotSTRATEGY project has received funding from the European Union’s Horizon 2020 research and innovation programme under grant agreement No. 101022664

3.2 Petrophysical measurements: results

3.2.1 Reservoir section

Permeability, formation factor, irreducible water saturation and NMR T_2 distribution were measured on samples from the Charmottes 4 and Vulaines 1 wells (Table 3-3) following the various methodologies described in the Appendix (Section 7). The geological context of these samples is summarized in Table 3-1 and Table 3-2. When plotted as a function of depth, one can observe large variations of porosity (from 3 up to 18%) and permeability (0.1 up to 200 mD). The reservoir section is not uniform in terms of petrophysical properties (Figure 3.2, Figure 3.3) and contains several barriers of low porosity and permeability. As will be seen later in paragraph 3.2.2, permeability is governed by the amount of macroporosity. Macroporosity can be clearly distinguished in the T_2 distributions (proxies of pore size distributions) by considering components above about 150 ms (dashed line in Figure 3.2 and Figure 3.3). For the Vulaines 1 well, some porosity and permeability data are available from a database (courtesy of Vermilion oil company); the measurements performed in this study are consistent with these data and show in more detail the succession of low and high porosity-permeability layers a few meters thick.

The irreducible water saturation values both measured and deduced from the T_2 distributions are around 0.4, meaning that only about 60% at best of the total porosity can be occupied by CO_2; it corresponds to the maximum amount of macroporosity.

The pore entry size distributions measured by mercury injection (Figure 3.4 and Figure 3.5) are mostly bimodal or unimodal in the absence of macroporosity: pore entry size below about 2 µm corresponds to microporosity. They give a similar information as NMR T_2 distributions ((Vincent et al., 2011).

Concerning the cementation exponents calculated from the formation factor measurements (Table 3-3) $m = -\frac{\log(FF)}{\log(F)}$ where FF = the formation factor (the ratio of brine to sample conductivity measured at the same temperature), we can observe that m is systematically lower in the Vulaines well (1.71<m<1.76) compared to Charmottes (1.85<m<1.93).

The PilotSTRATEGY project has received funding from the European Union's Horizon 2020 research and innovation programme under grant agreement No. 101022664

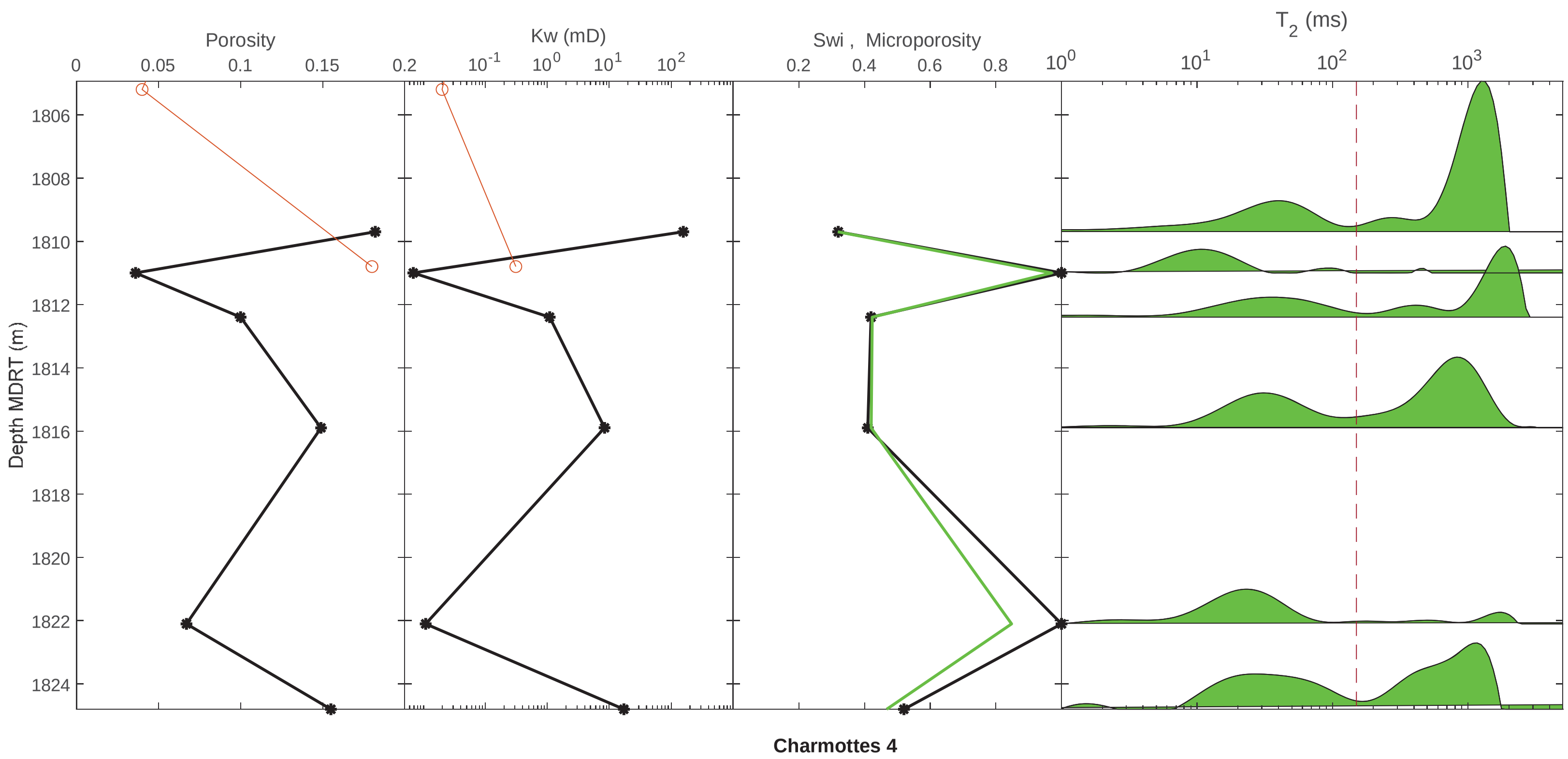

Figure 3.2: Overview of the results for well Charmottes 4. The red curve in the porosity-permeability panels represents data from Vermilion company. The dashed line in the NMR T_2 panel represents the separation between micro and macroporosity.

The PilotSTRATEGY project has received funding from the European Union's Horizon 2020 research and innovation programme under grant agreement No. 101022664

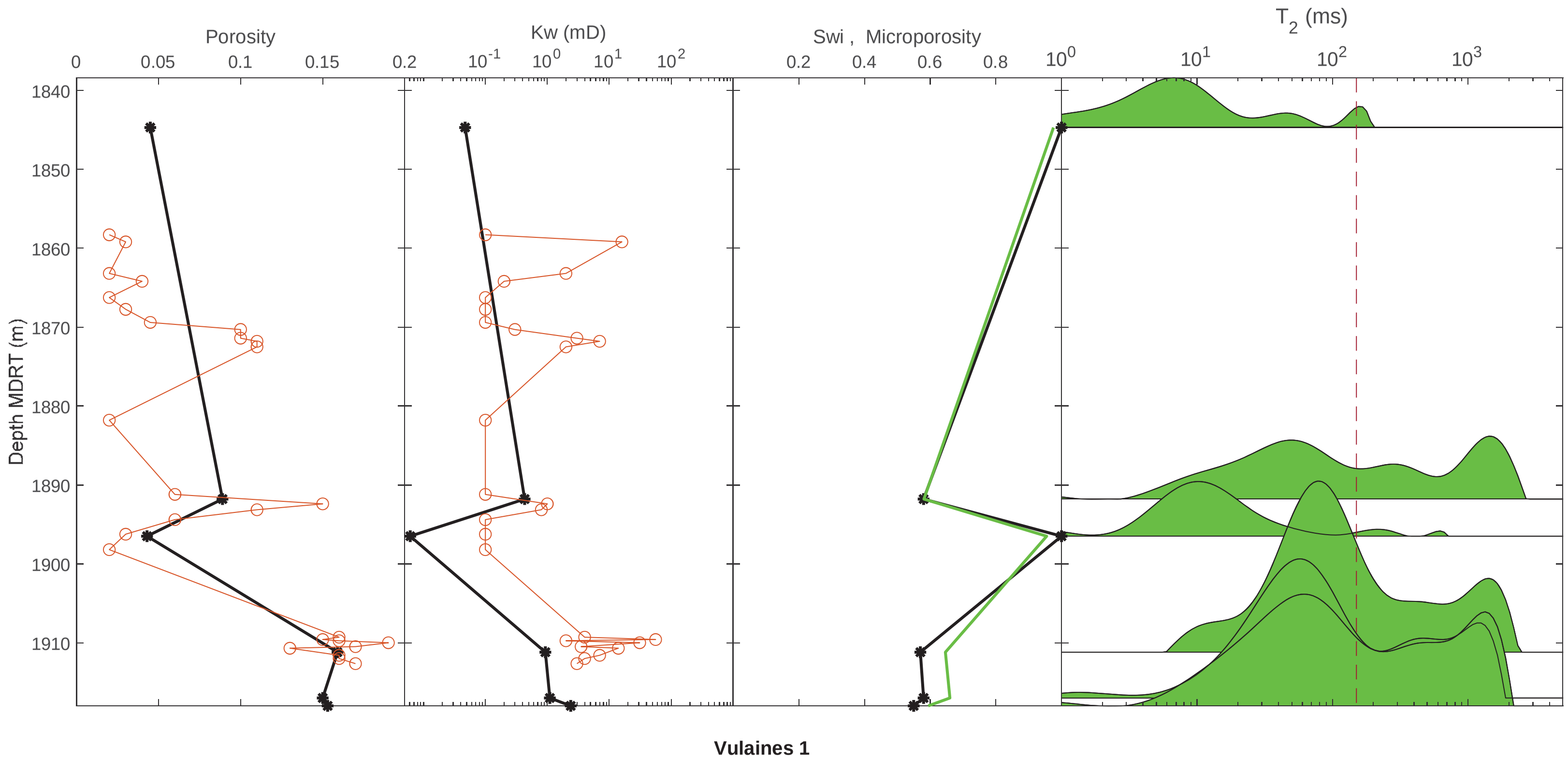

Figure 3.3: Overview of the results for well Vulaines 1. The red curve in the porosity-permeability panels represents data from Vermilion company. The dashed line in the NMR T_2 panel represents the separation between micro and macroporosity.

The PilotSTRATEGY project has received funding from the European Union's Horizon 2020 research and innovation programme under grant agreement No. 101022664

Table 3-3: Results of porosity, water permeability Kw, water saturation Sw after air-brine centrifuge at 7 bar, irreducible water saturation Sw deduced from NMR, PE: entry pressure, FF formation factor and m cementation exponent. .

PETRA ref	Name	Well	Depth (m)	Porosity (%)	Kw (mD)	PE (bar)	FF	m	Centrifuge Sw (%)	NMR Sw (%)
4859	CHM4_C2_1809,7	Charmottes 4	1809.7	18%	157	/	36	1.93	33	32
4860	CHM4_C2_1811	Charmottes 4	1811.0	4%	0.007	/	/	/	/	0
4861	CHM4_C2_1812,4	Charmottes 4	1812.4	10%	1.09	/	96	1.93	42	42
4862	CHM4_C2_1815,9	Charmottes 4	1815.9	15%	8.4	/	42	1.85	44	41
4863	CHM4_C2_1822,1	Charmottes 4	1822.1	7%	0.011	/	/	/	/	/
4864	CHM4_C2_1824,8	Charmottes 4	1824.8	16%	17.2	/	/	/	42	52
4868	VUS1_c6_1844,7	Vulaines 1	1844.7	5%	0.047	/	/	/	/	/
4870	VUS1_c10_1891,8	Vulaines 1	1891.8	9%	0.43	/	81	1.72	54	58
4871	VUS1_c10_1896,5	Vulaines 1	1896.5	4%	0.001	1,6 - 2,0	/	/	/	/
4873	VUS1_c11_1911,2	Vulaines 1	1911.2	16%	0.93	/	28	1.71	56	57
4874	VUS1_c11_1917	Vulaines 1	1917.0	15%	1.10	/	32	1.75	54	58
4875	VUS1_c11_1918	Vulaines 1	1918.0	15%	2.39	/	31	1.76	51	55

The PilotSTRATEGY project has received funding from the European Union's Horizon 2020 research and innovation programme under grant agreement No. 101022664

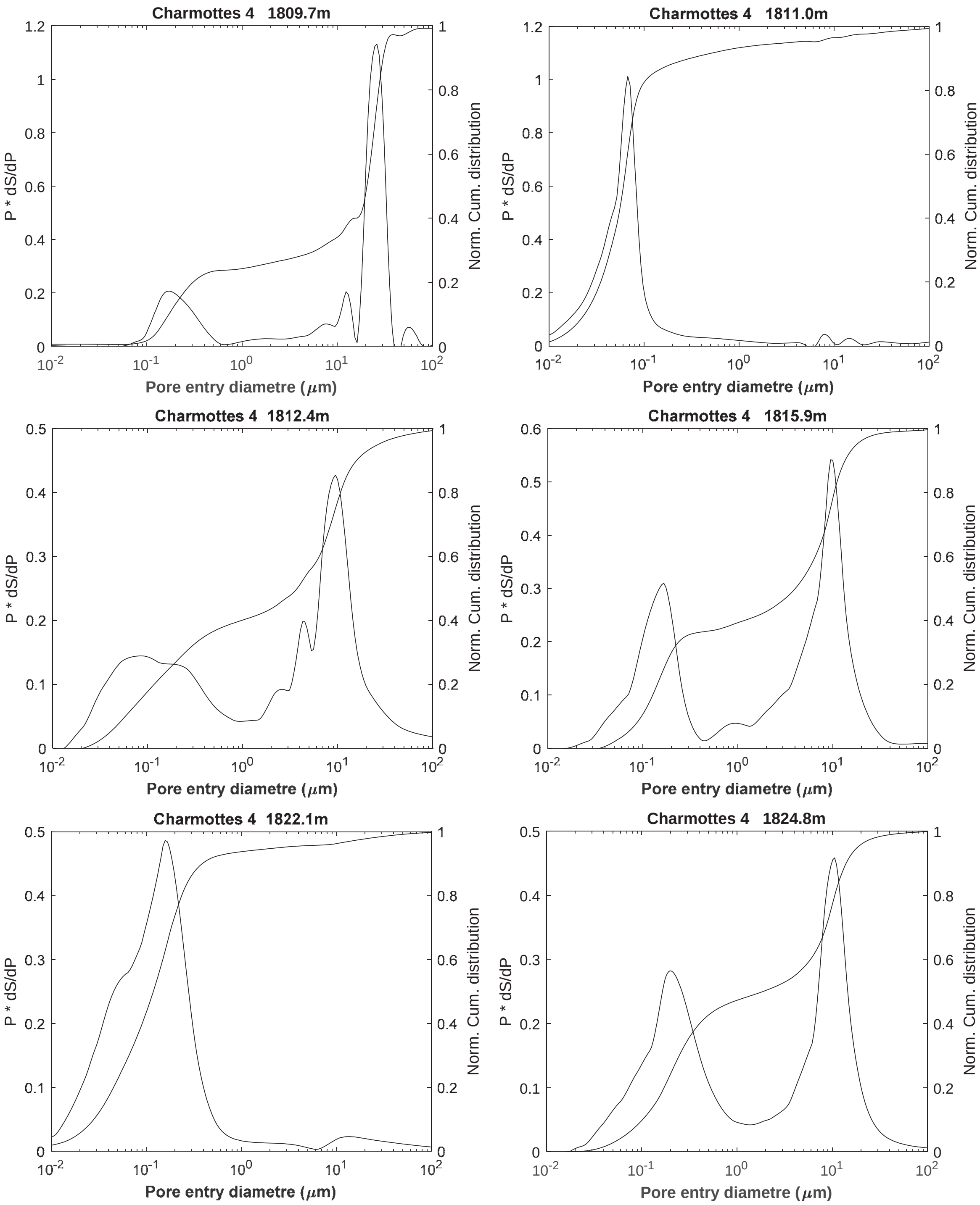

Figure 3.4: Pore size distribution from mercury injection experiments; Charmottes 4 well.

The PilotSTRATEGY project has received funding from the European Union’s Horizon 2020 research and innovation programme under grant agreement No. 101022664

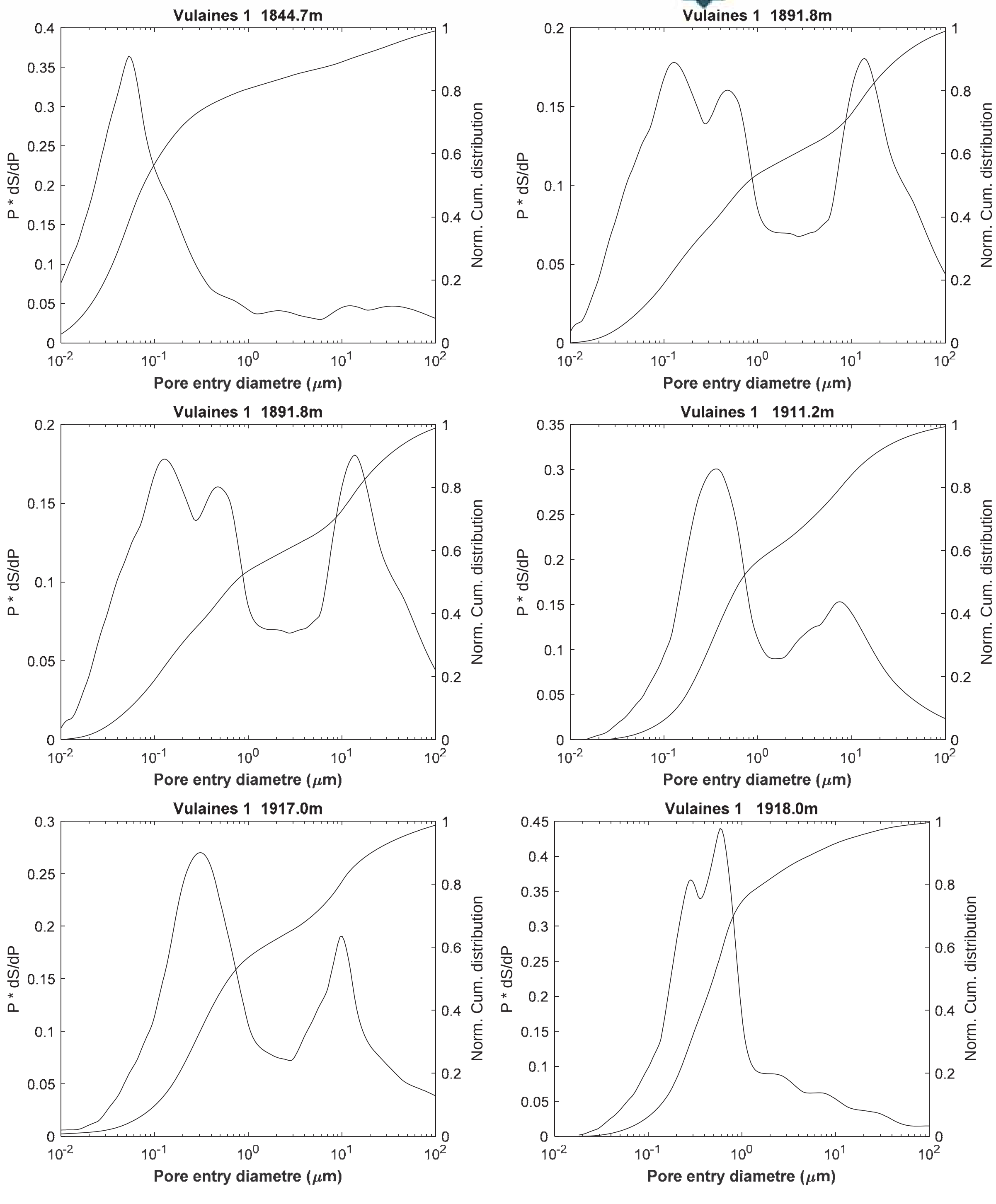

Figure 3.5: Pore size distribution from mercury injection experiments; Vulaines 1 well.

The PilotSTRATEGY project has received funding from the European Union's Horizon 2020 research and innovation programme under grant agreement No. 101022664

3.2.2 Permeability-porosity relationship

In a study of the Dogger formation in the context of geothermal exploitation in the centre of the Paris basin (city of Bobigny), Catinat and co-workers (Catinat et al., 2023) tested several permeability-porosity relationships on a set of about 70 samples comprising essentially 4 facies. The best one was obtained by taking the amount of macroporosity Φ_m instead of the total porosity Φ:

$$Kw = CF_m^n$$

where C=2.738x10^7 and n=5.18 (Kw in units of mD and porosity as a fraction). This relationship has an error factor of 2.6 (meaning that the predicted permeability can statistically be multiplied or divided by a factor of 2.6 with 90% confidence). When taking total porosity, the relationship was:

$$Kw = CF^n$$

where C=5.81x10^9 and n=4.49 with an error factor of 4.5. Performing the same analysis on the present dataset, it is clearly seen that the choice of macroporosity has the effect of aligning the data on a power law with little scatter (Figure 3.6) when considering macroporosity values above about 4%. At values below this, macroporosity may not percolate through the pore network. However the constant C in the above relationship needs to be adjusted to C=0.5x10^7 while keeping the same value of n (5.18). This is shown in Figure 3.6 (line "Adjusted Dogger corr."). Hence for the present and limited dataset, the suggested correlation is:

$$Kw = 0.5x10^7 F_m^{5.18}$$

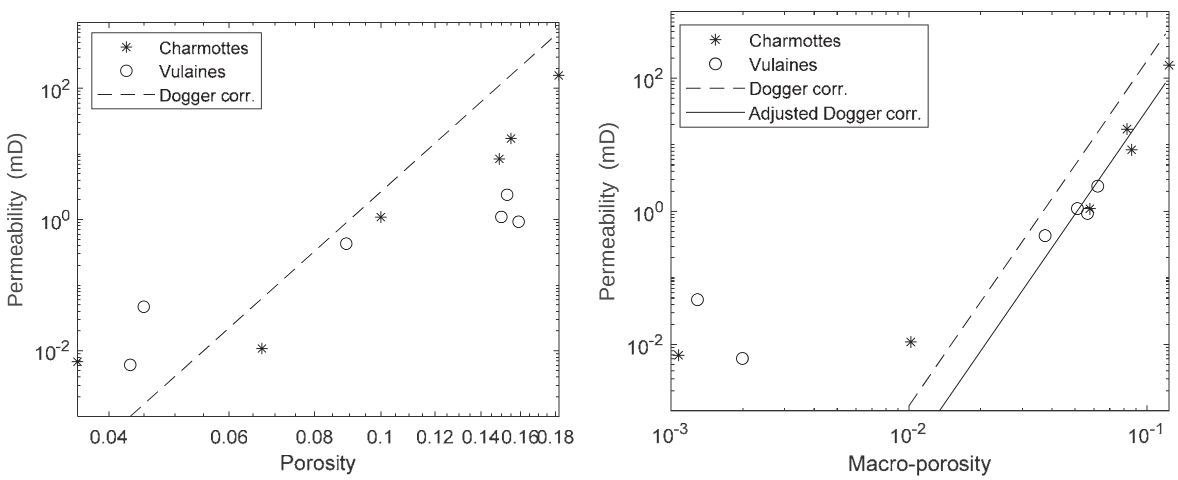

Figure 3.6: Permeability-porosity relationships using total porosity (left) and macroporosity (right). The dashed line indicates the correlations obtained in the study of Catinat et al. (2023)

Since microporosity cannot be quantified easily using log data in old wells from petroleum exploration, it would be useful to use a combination of porosity and formation factor (i.e. resistivity) to predict

The PilotSTRATEGY project has received funding from the European Union's Horizon 2020 research and innovation programme under grant agreement No. 101022664

permeability. This has been attempted in Figure 3.7 in which a relationship of the form $Kw=C\Phi^aFF^b$ gives a reasonable trend in the case of the data set of Bobigny, but not in the present study.

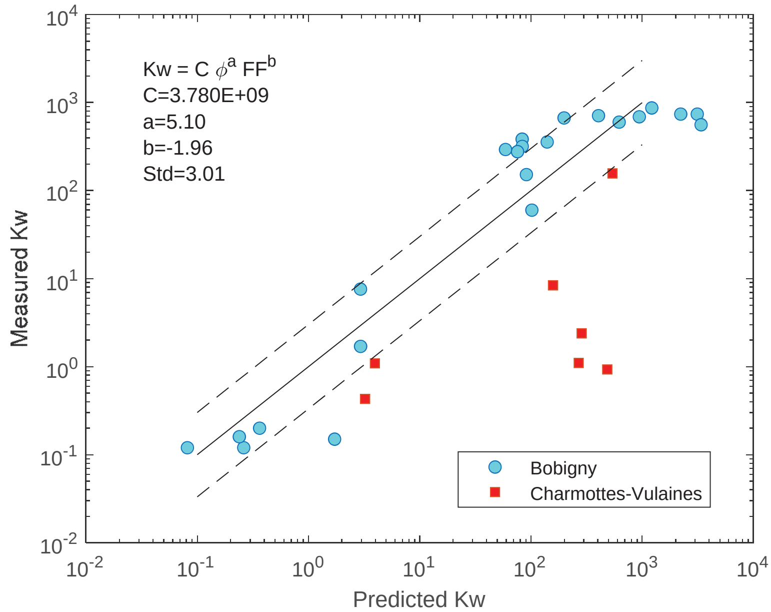

Figure 3.7: Attempt to relate permeability to a combination of porosity and formation factor ($Kw=C\Phi^aFF^b$). The dataset of Bobigny (unpublished, work of Catinat et al. 2023) indicates a clear trend whereas the data collected in this work is only partially consistent with the trend of Bobigny.

The PilotSTRATEGY project has received funding from the European Union's Horizon 2020 research and innovation programme under grant agreement No. 101022664

3.2.3 Caprock permeability and entry pressure measurements

Permeability and entry pressure measurements were performed on samples classified as caprocks (**Erreur ! Source du renvoi introuvable.**) using the methods described in the appendix (Section 7). Actually, they belong to a transition layer between the reservoir and the true caprock that has not been sampled by oil producing companies in the past, as is usually the case. The pore size distributions measured by mercury injection (Figure 3.8) indicate that the samples are essentially composed of microporosity (pore entry size < 2 µm); they have a low porosity and a low permeability (Table 3-4**Erreur ! Source du renvoi introuvable.**), and sometimes very low (7 nD). The measured entry pressure values are relatively small (~1 bar) when the permeability is of the order of 1 µD and much larger (44 bars) when the permeability is very small (~10 nD).

Table 3-4: Results of water permeability Kw and entry pressure PE measurements on caprock samples from Charmottes 4 and Vulaines 1 wells.

	Name	Well	Depth (m)	Porosity (%)	Kw (µD)	PE (bar)
4856	CHM4_C1_1800,5	Charmottes 4	1800.5	8%	0.4	~ 0,5
4857	CHM4_C1_1803,25	Charmottes 4	1803.25	4%	0.8	~ 1
4866	VUS1_c6_1843,45	Vulaines 1	1843.45	4%	0.007	42 - 46
4867	VUS1_c6_1844,05	Vulaines 1	1844.05	5%	5	1.0 – 1.5

The PilotSTRATEGY project has received funding from the European Union's Horizon 2020 research and innovation programme under grant agreement No. 101022664

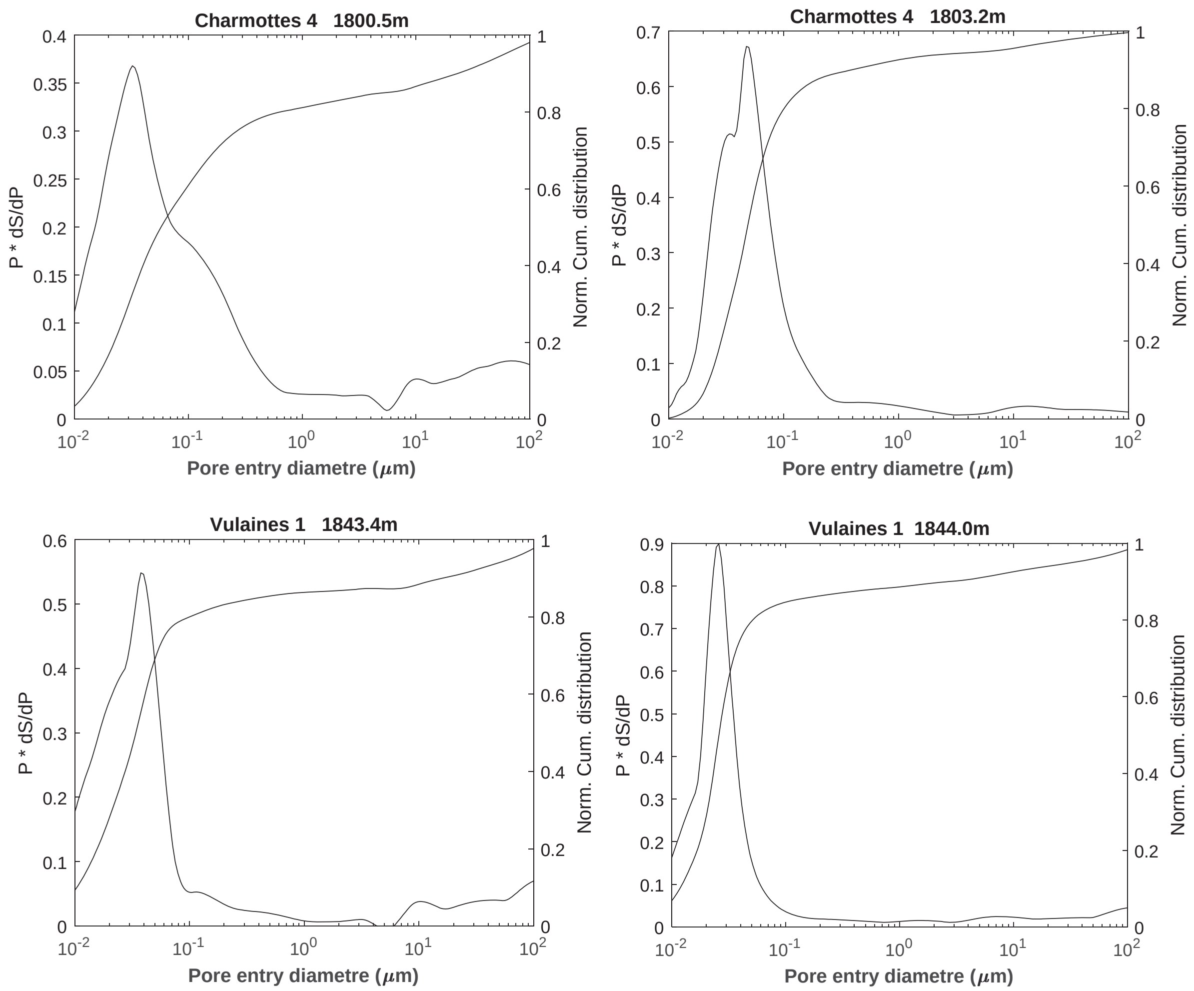

Figure 3.8: Pore size distribution from mercury injection experiments; Charmottes and Vulaines well, caprock section.

The PilotSTRATEGY project has received funding from the European Union's Horizon 2020 research and innovation programme under grant agreement No. 101022664

3.3 References

Bemer E. and J.M. Lombard J.M. (2010), From Injectivity to Integrity Studies of CO2 Geological Storage, OGST, Vol. 65.

Bemer E., et al (2004), Geomechanical Log Deduced from Porosity and Mineralogical Content, OGST, Vol. 59

Catinat M., Fleury M., Brigaud B., Antics M., Ungemach P. (2023), Estimating permeability in a limestone geothermal reservoir from NMR laboratory experiments, Geothermics, in revision.

Vincent, B., Fleury, M., Santerre, Y., & Brigaud, B. (2011). NMR relaxation of neritic carbonates: An integrated petrophysical and petrographical approach. Journal of Applied Geophysics, 74(1), 38–58.

The PilotSTRATEGY project has received funding from the European Union's Horizon 2020 research and innovation programme under grant agreement No. 101022664

4. Samples from Spain – On Shore

4.1 Geological aspects. Sampling.

The Spanish onshore study area is located in the Lopín Structure (Zaragoza, Ebro basin) (Figure 4.1). Rock samples for petrophysical (and geomechanical) characterization were obtained from two different sources: 1) samples from stratigraphic sequences studied in natural outcrops (Torre de las Arcas section and Peñas Royas section); and 2) samples from rock cores (Chiprana well) stored at the Rock Sample Storage Centre (IGME-CSIC).

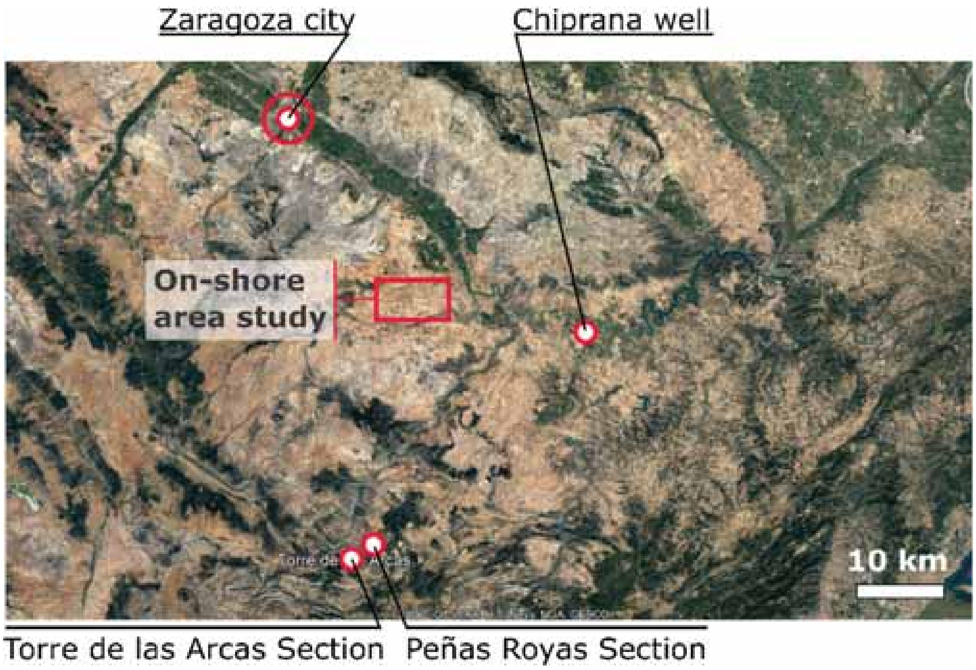

Figure 4.1. Location of the onshore area study and the Chiprana well as well as the outcrops where both the Torre de las Arcas and Peñas Royas sections are described.

Both natural outcrops (Torre de las Arcas and Peñas Royas) are located 55 km south of the study area (Lopín structure). They are extensive outcrops where a complete stratigraphic sequence of both the reservoir and the seal rock formation can be studied and sampled. Even though rocks exposed in natural outcrops are affected by subaerial weathering processes and, consequently, the petrographic characteristics of these exhumed rocks can be slightly different than the buried materials, these natural outcrops have been considered in this project because of two main reasons:

1) A unlimited number of samples can be taken

2) Large-scale stratigraphic structures can be observed that are not visible in borehole core

The Chiprana well is located 30 km east of the study area. 90 m of rock core of the reservoir formation is preserved at the Rock Sample Storage Centre (IGME-CSIC).

Stratigraphic Units.

Proposed reservoir and seal rocks are a sedimentary sequence formed by The Buntsandstein Facies. The Buntsandstein predominantly consists of red sandstone layers of the Lower Triassic series and is one of three characteristic Triassic units, together with the Muschelkalk and Keuper that form the Germanic Triassic Supergroup.

The reservoir is identified as the Tierga Fm, which is divided in the Aranda, Carcalejos and Rané members. They are composed mainly of sandstones with intercalations of shales of variable thickness, which tend to be thicker towards the top (Rané Mb). It also contains some levels of conglomerates, which usually appear between the base and middle areas of the unit. They have been interpreted as fluvial channels braided in intermediate zones of alluvial fans that pass vertically to distal deposits and finally a tidal deltaic system (Arribas, 1984). More recently there are parts that have been interpreted as erg deposits (Soria et al., 2009). The average thickness of the Tierga Fm in the area is around 120 m.

Seal rocks are formed by the Cálcena Fm, which is composed by red shales with some sandstone intercalations towards the base, green marls, gypsum/anhydrites, and dolomites. Towards the top, the carbonate and gypsum content increases. In the field, it shows pseudomorphs of evaporites and tepee structures. Its thickness varies from 10 to 70 m, and the contacts with both the lower and upper formations are gradual and concordant.

Samples

75 samples were taken in all (see table below). conventionally, samples from natural outcrops are irregular in shapeshape of decimeter scale. However, due to exceptional accessibility in the Torre de las Arcas outcrop, small regular cores were taken with a portable core drill. These cores are cylindrical samples with 5.5 cm in diameter and up to 10 cm in length. Only the strongest and most cohesive levels were sampled with the portable core drill.

In addition, 10 samples were taken from the Chiprana well. Due to the strict regulations of the Rock Sample Storage Centre (IGME-CSIC), only small samples of the most representative levels have been obtained.

The total number of stratigraphic levels sampled in each section and the total number of rock samples taken is indicated in Table 4-1.

Table 4-1. Stratigraphic levels sampled in each section

	Stratigraphic levels Sampled	Total Number of samples
Torre de las Arcas Section	12	44
Peñas Royas Section	11	21
Chipriana Section	10	10

4.1.1 Torre de las Arcas Section

Torre de las Arcas section is a stratigraphic sequence studied in a large outcrop located in the Gabardal Valley, close to the Torre de las Arcas town (Teruel, Spain) (Figure 4.1). 44 samples were taken from Torre de las Arcas Section, corresponding to 12 representative stratigraphic levels (Table 4-2). 10 samples of red quartzarenite with planar and trough cross-stratification or with lamination of ripples were analysed. The table below shows the complete list of samples. Three samples from the seal formation were composed of silts, clays, and marls and many pseudomorphs of gypsum were analysed. A Hyphen in Table 4-2 indicates flat and slab samples.

The PilotSTRATEGY project has received funding from the European Union's Horizon 2020 research and innovation programme under grant agreement No. 101022664

Table 4-2. Samples taken from Torre de las Arcas Section.

Reservoir/Seal	Sampled stratigraphic levels	Number of samples irregular	cores	Sample codes
Reservoir	PS.TA.01		6	01A; 01B; 01C; 01D; 01E; 01F
Reservoir	PS.TA.02		7	02A; 02B; 02C; 02D; 02E; 02F; 02G
Reservoir	PS.TA.03		4	03A; 03C; 03D; 03F
Reservoir	PS.TA.04		3	04A; 04B; 04C
Reservoir	PS.TA.05	2, -		
Reservoir	PS.TA.06	2, -		
Reservoir	PS.TA.07	-*		
Reservoir	PS.TA.08	1		
Reservoir	PS.TA.09	5		
Reservoir	PS.TA.10	11		
Seal	PS.TA.11	-*		
Seal	PS.TA.12	-*		
Seal	PS.TA.13	3		

* Non-cohesive and crumbly samples

4.1.2 Peñas Royas Section

The Peñas Royas section is a stratigraphic sequence studied in an extensive outcrop located in Martin River Cultural Park, near Peñas Royas village (Teruel, Spain) (Figure 4.1). 21 samples were taken from the Peñas Royas Section, corresponding to 11 representative stratigraphic levels (Table 4-3). The table below shows the complete list of samples. The samples of the reservoir formation (Tierga Fm) are composed of red quartzarenites with quartz and OFe-oxide cements, with cross-stratification or ripple laminations. Three samples from the seal formation composed of silts, clays and marls were analysed. Asterisk in Table 4-3 indicates non-cohesive and crumbly samples. Hyphen in Table 4-3 indicates flat and slabs samples.

Table 4-3. Samples taken from Peñas Royas section.

Reservoir/Seal	Sampled stratigraphic levels	Number of samples
Reservoir	PS.PR.01	9
Reservoir	PS.PR.02	1
Reservoir	PS.PR.03	1
Reservoir	PS.PR.04	-
Reservoir	PS.PR.05	2
Reservoir	PS.PR.06	-
Reservoir	PS.PR.07	- *
Reservoir	PS.PR.08	3
Seal	PS.PR.09	2
Seal	PS.PR.10	2
Seal	PS.PR.11	1

* Non-cohesive and crumbly samples

4.1.3 Chiprana Section

This stratigraphic section has been studied from well cores available at the Rock Core Storing Centre (IGME-CSIC). A complete 90 m of rock cores from the Chiprana well preserves the reservoir formations

The PilotSTRATEGY project has received funding from the European Union's Horizon 2020 research and innovation programme under grant agreement No. 101022664

studied in this project. 10 samples were taken Chiprana Section, corresponding to 10 representative stratigraphic levels (Table 4-4). The samples of the reservoir formation are composed of red quartzarenites with cross-stratification and red silts with fine ripple lamination. Table 4-4 shows the complete list of samples.

Table 4-4. Samples taken from Chiprana Section

Reservoir/Seal	Sampled stratigraphic levels	Number of samples
Reservoir	CH.1743	1
Reservoir	CH.1747	1
Reservoir	CH.1752	1
Reservoir	CH.1758	1
Reservoir	CH.1764	1
Reservoir	CH.1768	1
Reservoir	CH.1773	1
Reservoir	CH.1788	1
Reservoir	CH.1796	1
Reservoir	CH.1824	1

4.2 Petrophysical measurements: results

Petrophysical characterization was carried out by two procedures: 1) Laboratory tests (porous system characterization and standard hydraulic characterization); and 2) On-site tests (non-destructive and portable hydraulic tests).

4.2.1 Porous system characterization

The porous system characterization of studied rocks was carried out by IGME, using the following parameters and methods:

1. The connected porosity (ϕ_{Hg}), the mean pore size (r_M) and bulk density (ρ_{bulk}) were obtained by Autopore IV 9500 Micromeritics mercury porosimetry (MIP). The pore size interval ranges from 0.002 to 200 µm. The relative pore volume (%) was also obtained considering the sequent pore size classes: <0.01 µm (class 1); 0.01-0.1 µm (class 2); 0.1-1 µm (class 3); 1-10 µm (class 4); 10-100 µm (class 5); and >100 µm (class 6).
2. The nano-porosity (ϕ_{N2}) and the specific surface (S_{BET}) were determined using the conventional Brunauer, Emett and Teller (BET) procedure (Brunauer et al., 1938) using the N_2 adsorption isotherm at 77K obtained from a Micromeritics ASAP 2020 automatic analyzer (ASAP-N2).
3. Effective porosity (ϕ_{eff}) defined as the ratio of the volume of connected voids to total rock volume and expressed as a percentage, was determined using the vacuum water saturation test (UNE-EN 1936:2007).
4. Bulk density and apparent density were also determined by means of MIP and UNE-EN 1936:2007 procedure, respectively.

In addition, a series of tests were performed by IFPEN (see methodologies in the Appendix):

5. Permeability measured with brine (NaCl 20g/l).
6. Formation factor, measured only on 40 mm samples.
7. Desaturation. Samples centrifuged under air.
8. NMR measurements.

The PilotSTRATEGY project has received funding from the European Union's Horizon 2020 research and innovation programme under grant agreement No. 101022664

One sample of each sampled stratigraphic level of the three studied stratigraphic sections were tested under MIP and ASAP (43 samples). The vacuum water saturation test was exclusively carried out on all the cylindrical samples obtained from the Torre de las Arcas Section (13 samples).

In general terms, the sandstone reservoir has an average connected porosity (MIP determination) of 10.25%, with an average Mean Pore Radius of 6.36 µm (tables below). Table 4-5 and Table 4-6 show the pore size distribution. The sandstone reservoir presents a porous system with pores centered on the range of 1-10 µm (32.57 % of the pores in this size range) with another important population of pores (26.56 % of the total porosity) with radius in the range 0.1-10 µm.

Table 4-5. Mean values and Standard Deviation (SD) of the density and porosity measured in the sandstones considered as reservoir, including all samples of the three studied sections.

	ϕ_{eff} [%]		ϕ_{Hg} [%]		r_M [µm]		ρ_{ap} [g/cc]		ρ_{bulk} [g/cc]	
	mean	SD	mean	SD	mean	SD	mean	SD	mean	SD
Reservoir	12.57	1.61	10.25	4.17	6.36	9.74	2.33	0.05	2.31	0.14

Table 4-6. Mean values and Standard Deviation (SD) of the pore size distribution of the sandstones considered as reservoir, including all samples of the three studied sections.

	Pore class [µm]											
	<0.01		0.01-0.1		0.1-1		1-10		10-100		>100	
	mean	SD	mean	SD	mean	SD	mean	SD	mean	SD	mean	SD
Reservoir	7.30	13.42	14.66	9.97	26.56	15.23	32.57	20.08	15.84	13.00	3.01	1.31

Table 4-7 shows the porosity value (connected porosity, %) and bulk density (g/cc) obtained in each stratigraphic level of each studied sedimentary columns.

Table 4-7. Bulk density (ρ_{bulk}) and porosity (MIP, ϕ_{Hg}) measured in the sandstones of Torre de las Arcas section, Peñas Royas section and Chiprana section.

Torre de las Arcas			Peñas Royas			Chiprana		
Level	ϕ_{Hg} [%]	ρ_{bulk} [g/cc]	Level	ϕ_{Hg} [%]	ρ_{bulk} [g/cc]	Level	ϕ_{Hg} [%]	ρ_{bulk} [g/cc]
1	13.48	2.19	1	8.99	2.33	1	8.92	2.28
2	10.80	2.32	2	9.65	2.32	2	11.15	2.36
3	10.84	2.28	3	9.65	2.31	3	9.11	2.43
4	6.85	2.42	4	12.46	2.20	4	14.18	2.18
5	9.82	2.26	5	11.16	2.16	5	3.26	2.63
6	7.87	2.39	6	7.69	2.45	6	5.49	2.48
7	15.26	2.16	7	12.76	2.24	7	3.51	2.56
8	12.40	2.28	8	11.28	2.30	8	2.58	2.22
9	13.39	2.20				9	7.29	2.41
10	17.81	2.05				10	17.72	2.14
11	19.39	2.05						
12	7.90	2.44						
13	5.21	2.56						

The PilotSTRATEGY project has received funding from the European Union's Horizon 2020 research and innovation programme under grant agreement No. 101022664

Table 4-8 shows the pore size distribution obtained in each stratigraphic level of Torre de las Arcas Section. The most frequent pore family are highlighted in bold.

Table 4-8. Mean radius (r_M) and pore size distribution of the sandstones of Torre de las Arcas section.

Torre de las Arcas							
Level	r_M	Pore radius ranges [µm]					
	[µm]	<0.01	0.01-0.1	0.1-1	1 a 10	10 - 100	>100
1	2.41	1.75	9.13	36.33	**39.43**	9.46	3.98
2	0.45	1.81	20.82	**46.37**	17.83	11.42	1.70
3	6.83	3.27	15.28	22.57	**38.36**	17.71	2.74
4	0.32	8.89	33.11	**45.31**	0.95	8.47	3.24
5	1.37	4.85	16.18	**37.77**	32.93	6.56	1.66
6	0.57	1.74	14.50	**48.09**	22.09	9.99	3.61
7	11.20	0.81	9.21	15.12	**58.54**	12.47	3.85
8	2.86	1.38	16.38	30.78	**37.69**	11.83	1.93
9	3.99	0.00	3.14	30.59	**56.00**	7.62	2.62
10	40.29	0.11	4.35	7.34	25.72	**60.26**	2.18
11	31.88	2.11	7.08	7.07	30.14	**50.82**	2.12
12	0.29	12.79	30.44	**33.25**	8.54	13.79	1.14
13	0.94	2.57	26.02	**37.25**	19.67	10.03	4.36

Table 4-9 shows the pore size distribution obtained in each stratigraphic level of Peñas Royas Section. The most frequent pore family is highlighted in bold.

Table 4-9. Mean radius (rM) and pore size distribution of the sandstones of Peñas Royas section.

Peñas Royas							
Level	r_M	Pore radius ranges [µm]					
	[µm]	<0.01	0.01-0.1	0.1-1	1 a 10	10 - 100	>100
1	1.82	0.88	11.47	**44.22**	31.45	8.38	3.55
2	1.54	0.97	14.24	**46.14**	31.00	5.46	2.08
3	2.32	1.22	11.42	34.83	**36.15**	12.11	4.16
4	12.71	0.00	3.51	13.50	**61.04**	17.93	4.09
5	6.22	0.00	0.30	18.97	**61.21**	12.95	6.48
6	0.41	7.78	31.17	**46.12**	6.23	7.17	1.62
7	4.60	0.60	9.58	28.83	**41.45**	17.41	2.10
8	1.85	0.63	15.25	**37.09**	36.90	6.21	4.01

Table 4-10 shows the pore size distribution obtained in each stratigraphic level of Chiprana Section. The most frequent pore family is highlighted in bold.

The PilotSTRATEGY project has received funding from the European Union's Horizon 2020 research and innovation programme under grant agreement No. 101022664

Table 4-10. Mean radius (rM) and pore size distribution of the sandstones of Chiprana section.

Chiprana							
Level	r_M	Pore radius ranges [µm]					
	[µm]	<0.01	0.01-0.1	0.1-1	1 a 10	10 - 100	>100
1	10.46	0.00	0.30	9.68	**77.31**	10.87	1.83
2	8.75	3.34	11.26	18.01	**53.78**	11.46	2.23
3	0.76	8.68	24.36	**41.88**	14.34	7.27	3.34
4	20.62	0.00	0.25	1.56	**53.69**	42.70	1.76
5	0.03	**44.10**	25.68	7.35	6.04	13.48	3.25
6	0.01	**55.18**	6.73	3.06	10.19	20.67	4.01
7	0.06	**36.82**	21.10	5.91	7.98	22.27	6.02
8	1.16	8.32	23.39	27.33	**32.49**	6.84	1.62
9	0.29	13.62	**32.56**	**32.95**	6.26	10.59	4.01
10	20.15	2.16	6.36	8.05	**54.32**	26.90	1.92

Finally, Table 4-11 and Table 4-12 show the porosity (ϕ_{N2}) and the specific surface (S_{BET}) measured by ASAP-N2 in the sandstone reservoir. Table 4-11 includes mean values (global values considering all the stratigraphic levels of all the three studied stratigraphic sections). Table 4-12 specifies the punctual values obtained in each one of the stratigraphic levels of each stratigraphic sections.

Table 4-11. Mean values and Standard Deviation (SD) of the porosity (ϕ_{N2}) and specific surface (SBET) of the sandstones considered as reservoir, including all samples of the three studied sections. Data obtained from ASAP-N2.

	Porosity (ϕ_{N2}) cm^3/g		Porosity (ϕ_{N2}) %		Maximum measured pore size	Specific surface (S_{BET}) m^2/g	
	mean	SD	mean	SD	nm	mean	SD
Reservoir	0.01067	0.00902	2.04	1.29	467	5.9579	8.0621

Table 4-12. Porosity (ϕ_{N2}) and specific surface (SBET) measured in the stratigraphic levels of Torre de las Arcas section, Peñas Royas section and Chiprana section. Data obtained from ASAP-N2.

Torre de las Arcas			Peñas Royas			Chiprana		
Level	ϕ_{N2} [cm^3/g]	S_{BET} [m^2/g]	Level	ϕ_{N2} [cm^3/g]	S_{BET} [m^2/g]	Level	ϕ_{N2} [cm^3/g]	S_{BET} [m^2/g]
1	0.00584	1.97	1	0.00386	0.93	1	0.00725	2.16
2	0.00488	1.37	2	0.00657	2.16	2	0.00681	2.34
3	0.00859	3.89	3	0.00529	1.47	3	0.0122	5.02
4	0.01128	5.75	4	0.00352	0.96	4	0.00415	1.1
5	0.00768	5.11	5	0.00747	2.38	5	0.0178	12.41
6	0.00372	0.94	6	0.01127	4.63	6	0.02374	14.35
7	0.00421	1.13	7	0.00439	1.45	7	0.014	9.64
8	0.00463	1.34	8	0.0054	2.35	8	0.0163	3.68
9	0.00585	1.84	9	0.01286	9.71	9	0.01203	3.78

The PilotSTRATEGY project has received funding from the European Union's Horizon 2020 research and innovation programme under grant agreement No. 101022664

10	0.00703	3
11	0.01891	15.12
12	0.04011	32.79
13	0.00944	6.24

10	0.04106	35.03

10	0.00522	1.1

4.2.2 Threshold pressures (Entry, displacement and capillary pressure)

In order to offer an assessed value of the threshold pressures related to this rock reservoir, an approximation has been carried out from obtained MIP data. These pressures are obtained following several empirical and theoretical equations and they do not represent the real or directly measured Injection Pressures. However, they can be used as indicative values.

The calculated threshold pressures are:

- Entry pressure (Pe, bar), according to Robinson (1966).
- Displacement pressure (Pd, bar), according to Schowalter (1979)
- Capillary pressure (apex method) (Pc-apex, bar), according to Swanson (1981)
- Capillary pressure (tangent method) (Pc-tg, bar), according to Cranganu and Soleymani (2015)

In general terms, the sandstone reservoir has a mean Entry pressure of 170 bar, with maximum and minimum values of 2067.97 bar and 0.41 bar, respectively. The Displacement Pressure vary between 0.07 bar and 2.59 bar, with average value of 0.45 bar. Finally, the average Capillary Pressure ranges between 6.7 and 14.62 bar, depending on the calculation method followed. All these data are showed in Table 4-13.

Table 4-13. Mean, maximum and minimum values obtained for the Entry Pressure (Pe), Displacement Pressure (Pd), Capillary Pressure (apex method) (Pc-apex) and Capillary Pressure (tangent method) (Pc-tg). All samples of the three studied sections are considered.

	Threshold pressures (bar)											
	Pe			Pd			Pc-apex			Pc-tg		
	mean	max	min	mean	max	min	mean	max	min	mean	max	min
Reservoir	169.99	2067.97	0.41	0.45	2.59	0.07	6.85	130.77	0.32	15.07	400.10	0.15

Table 4-14 shows the threshold pressures (Entry pressure, Pe; Displacement pressure, Pd; Capillary pressure obtained by the apex-method, Pc-apex; Capillary pressure obtained by the tangent method, Pc-tg) obtained in each stratigraphic level of Torre de las Arcas Section.

The PilotSTRATEGY project has received funding from the European Union's Horizon 2020 research and innovation programme under grant agreement No. 101022664

Table 4-14. Threshold pressures obtained in Torre de las Arcas Section.

Torre de las Arcas				
Level	Pe [bar]	Pd [bar]	Pc-apx [bar]	Pc-tg [bar]
1	22.54	0.21	1.38	1.90
2	82.42	0.52	0.52	6.50
3	52.91	0.21	0.72	0.31
4	82.51	0.21	35.72	19.00
5	82.46	1.38	2.07	1.80
6	82.49	0.14	0.89	0.42
7	2.45	0.27	1.10	4.70
8	130.67	0.41	1.10	1.5
9	82.71	0.58	2.07	0.8
10	1.10	0.14	0.32	0.18
11	1.10	0.21	0.41	0.17
13	1019.13	0.38	0.41	0.2

Table 4-15 shows the threshold pressures (Entry Pressure, Pe; Displacement Pressure, Pd; Capillary Pressure obtained by the apex-method, Pc-apex; Capillary pressure obtained by the tangent method, Pc-tg) obtained in each stratigraphic level of Peñas Royas Section.

Table 4-15. Threshold pressures obtained in Peñas Royas Section.

Peñas Royas				
Level	Pe [bar]	Pd [bar]	Pc-apx [bar]	Pc-tg [bar]
1	22.55	0.38	0.89	0.32
2	82.39	2.59	5.91	2.9
3	54.99	0.14	0.72	0.70
4	2.48	0.27	1.10	0.49
5	22.67	0.10	0.89	0.3
6	43.88	0.89	0.41	0.67
7	2.48	0.27	0.89	0.38
8	35.65	0.58	1.72	0.59

Table 4-16 shows the threshold pressures (Entry pressure, Pe; Displacement pressure, Pd; Capillary pressure obtained by the apex-method, Pc-apex; Capillary pressure obtained by the tangent method, Pc-tg) obtained in each stratigraphic level of Chiprana Section.

The PilotSTRATEGY project has received funding from the European Union's Horizon 2020 research and innovation programme under grant agreement No. 101022664

Table 4-16. Threshold pressures obtained in Chiprana Section.

	Chiprana			
Level	Pe [bar]	Pd [bar]	Pc-apx [bar]	Pc-tg [bar]
1	15.01	0.41	1.38	0.58
2	2.60	0.41	1.10	0.5
3	44.19	0.38	6.07	2.6
4	2.52	0.41	0.72	0.49
5	0.41	0.27	2.07	0.15
6	2067.97	0.14	130.77	400.1
7	0.41	0.07	0.38	2.6
8	43.99	1.10	1.72	0.602
9	1019.24	0.10	1.38	0.26
10	2.07	0.38	0.70	0.33

4.2.3 Hydraulic properties

Water-permeability, air-permeability, capillary coefficient, and water-absorption coefficient were calculated for the studied reservoir rock. The capillary behaviour of rocks was determined following the capillary imbibition test. Water-permeability and air-permeability were assessed from empirical equations using the MIP data (Pittman, 1992 and Bear, 1988). The water absorption coefficient was obtained by carrying out on-site tests (Karsten pipe) at the Torre de las Arcas outcrop (Hendrickx, 2013).

Global results for the studied reservoir rock are showed in Table 4-17.

Table 4-17. Mean, maximum and minimum values obtained for calculated hydric properties. All samples of the three studied sections are considered.

	Hydraulic properties											
	Capillary coefficient [$g \cdot m^{-2} \cdot s^{-0.5}$]			On-site Absorption Coefficient [$kg \cdot m^{-2} \cdot min^{-0.5}$]			Air-permeability [mD]			Water-permebility [mD]		
	mean	max	min	mean	max	min	mean	max	min	mean	max	min
Reservoir	17.4	27.2	8.8	7.96	16.19	0.77	488.02	3191.9	0.01	69.94	903.40	0.00

According to these results, the proposed reservoir rock is classified as a "*very good permeability*" rock using the measured value of air-permeability and the classification proposed by Schön (2015). However, it is important to consider that this air-permeability value has been obtained from empirical equations using the MIP data inputs. Moreover, it is important to highlight that this value is an average

The PilotSTRATEGY project has received funding from the European Union's Horizon 2020 research and innovation programme under grant agreement No. 101022664

obtained from different strata and different sections. A detailed analysis of these data is provided below.

Table 4-18 and Table 4-19 show the detailed hydric properties measured in the stratigraphic levels of the Torres de las Arcas Section (Table 4-18) and both the Peñas Royas and Chiprana sections (Table 4-19). The most permeable stratigraphic levels are shown in bold.

According to all these results, the proposed reservoir rocks can be considered to be a multilayer system with different porosity and hydraulic properties. Some of these strata act as impermeable (seal or baffle) layers, whilst most of them act as permeable and porous volume.

Table 4-18. Hydraulic properties measured in the Torre de las Arcas Section

Level	Hydraulic properties – Torre de las Arcas Section			
	Capillary coefficient [$g \cdot m^{-2} \cdot s^{-0.5}$]	On-site Absorption Coefficient [$kg \cdot m^{-2} \cdot min^{-0.5}$]	Air-permeability [mD]	Water-permebility [mD]
1	18.3	1.54	600.98	2.44
2	18.9	16.19	1066.05	0.07
3	15.0	0.77	518.16	**15.80**
4		0.92	0.10	0.02
5		7.05	53.16	0.58
6		6.94	306.28	0.08
7		4.62	224.65	**59.84**
8		7.94	215.94	3.17
9		14.08	56.78	6.67
10		11.31	3191.91	**903.40**
11		10.78	1612.35	**615.78**
12		6.41		
13		2.70	46.46	0.02

Table 4-19. Hydraulic properties (air-permeability and water-permeability) measured in both Peñas Royas and Chiprana Sections

Level	Hydraulic properties – Peñas Royas Section		Hydraulic properties – Chiprana well	
	Air-permeability [mD]	Water-permebility [mD]	Air-permeability [mD]	Water-permebility [mD]
1	314.78	0.93	124.50	**30.50**
2	5.53	0.72	210.37	**26.70**
3	505.83	1.62	5.17	0.16
4	215.30	**62.95**	548.17	**188.31**
5	329.69	**13.47**	42.06	0.00
6	1602.44	0.04	0.01	0.00
7	339.13	8.45	1637.27	0.00
8	81.00	1.21	59.21	0.11
9			119.28	0.02
10			608.15	**224.88**

The PilotSTRATEGY project has received funding from the European Union's Horizon 2020 research and innovation programme under grant agreement No. 101022664

The PilotSTRATEGY project has received funding from the European Union's Horizon 2020 research and innovation programme under grant agreement No. 101022664

4.2.4 Petrophysical results from IFPEN

4.2.4.1 *Torre de las Arcas*

Three samples from outcrops have been analysed. The results are shown in Erreur ! Source du renvoi introuvable.Table 4-20. In Figure 4.2 the graphics of the NMR test along with the image of the corresponding sample can be found.

Table 4-20. Samples taken from Torre de las Arcas Section

Sample	PS-TA-01-C	PS-TA-02-E	PS-TA-03-F1
Porosity (%)	12.0	12.4	12.9
Water Permeability (mD)	0.16	<0.01	0.44
Formation Factor/m	35.3 (1.44)	-	33 (1.53)
Swi @ 7 bar (fraction)	0.26	-	0.33
Clay bound water (fraction)	0.45	0.59	0.42

The PilotSTRATEGY project has received funding from the European Union's Horizon 2020 research and innovation programme under grant agreement No. 101022664

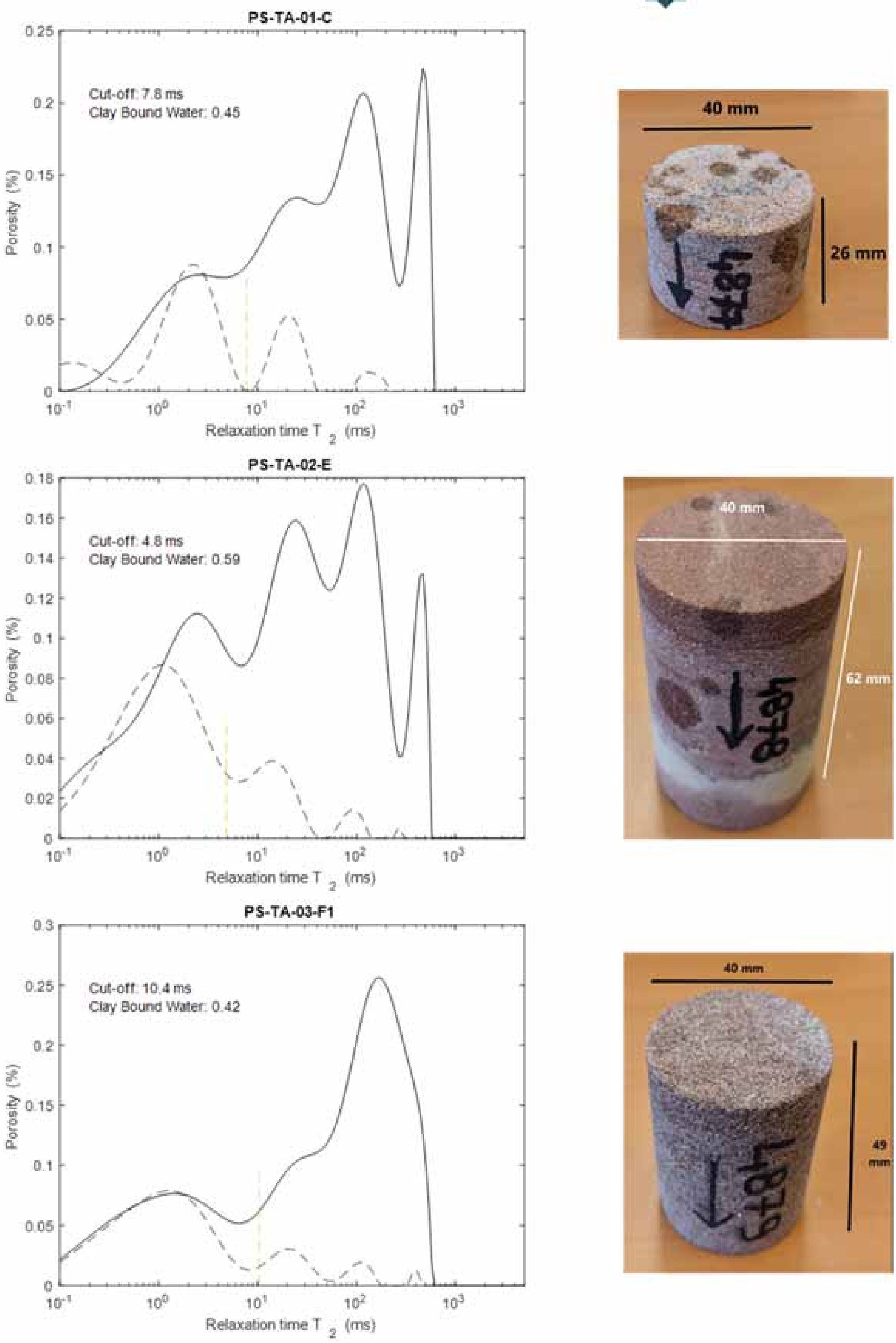

Figure 4.2. Measured NMR distributions (at Sw=100% and Swirr) for Torre de las Arcas samples.

The PilotSTRATEGY project has received funding from the European Union's Horizon 2020 research and innovation programme under grant agreement No. 101022664

4.2.4.2 Chiprana

From the Chiprana core, 5 samples were taken at different depth of the Buntsandstein facies. In this case, given the small size of the plugs, the Formation Factor could not be estimated. The results are shown in **Erreur ! Source du renvoi introuvable.** and in Figure 4.3, Figure 4.4, and Figure 4.5.

Table 4-21. Samples taken from Chiprana Section

Sample	1-Chiprana 1743	2-Chiprana 1747	4-Chiprana 1788	5-Chiprana 1796	6-Chiprana 1824
Porosity (%)	16.5	13.0	18.7	16.7	20.9
Water Permeability (mD)	13	13	16	28	14
Formation Factor/m	-	-	-	-	-
Swi @ 7 bar (fraction)	*	0.30	0.41	0.34	0.34
Clay bound water (fraction)	0.39	0.40	0.72	0.43	0.28

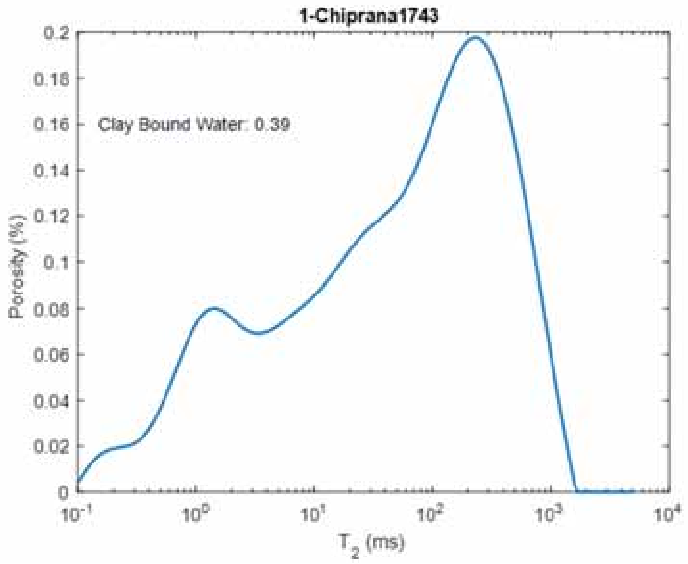

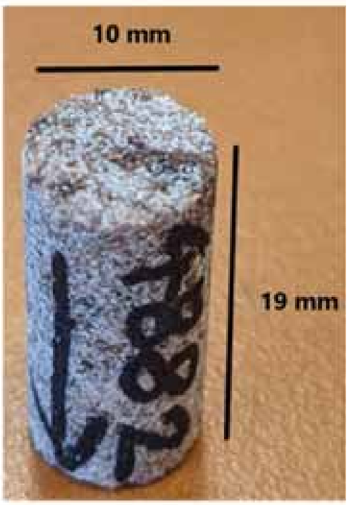

Figure 4.3. Measured NMR distributions (at Sw=100%) for Chiprana samples.

The PilotSTRATEGY project has received funding from the European Union's Horizon 2020 research and innovation programme under grant agreement No. 101022664

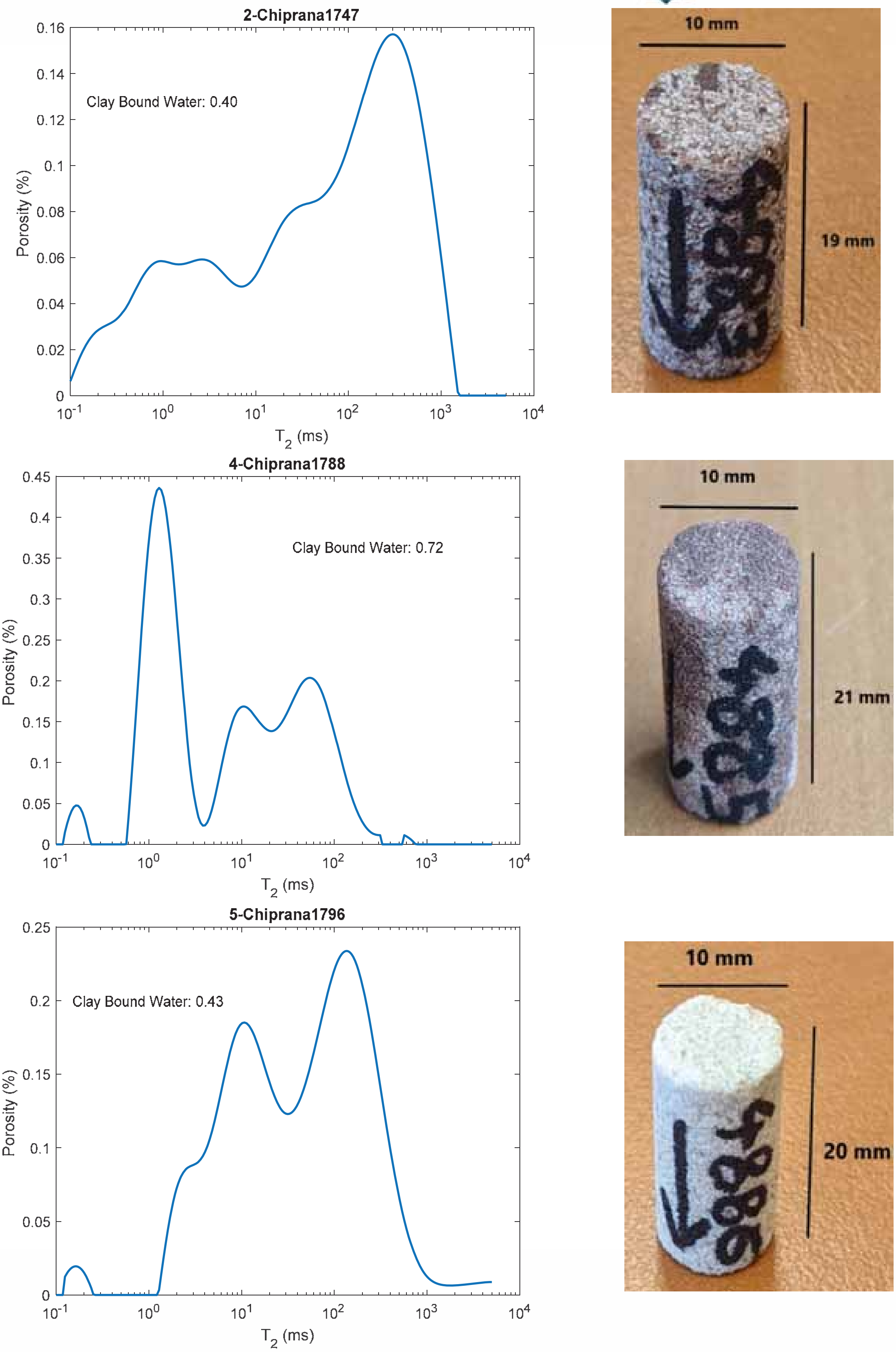

Figure 4.4. Measured NMR distributions (at Sw=100%) for Chiprana samples.

The PilotSTRATEGY project has received funding from the European Union's Horizon 2020 research and innovation programme under grant agreement No. 101022664

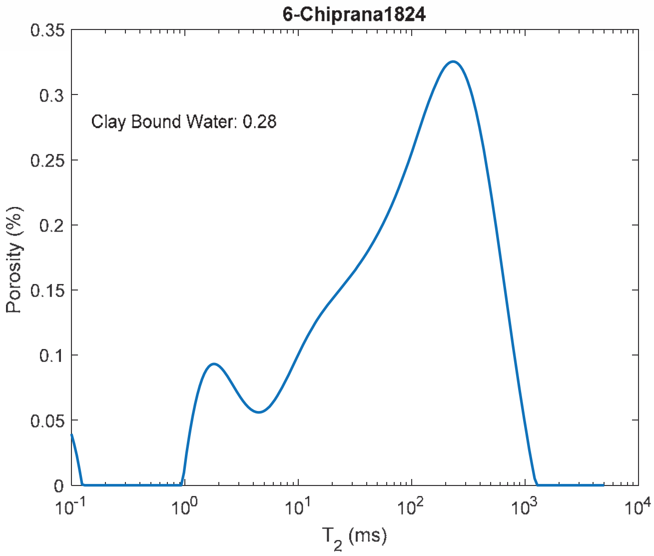

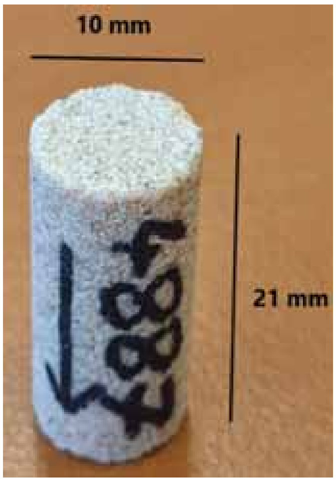

Figure 4.5. Measured NMR distributions (at Sw=100%) for Chiprana samples.

The PilotSTRATEGY project has received funding from the European Union's Horizon 2020 research and innovation programme under grant agreement No. 101022664

4.3 References

Arribas, J. (1984). *Estudio petrológico del Pérmico y Triásico de Malanquilla (Rama Aragonesa de la Cordillera Ibérica).* Tesis de Licenciatura, Universidad Complutense de Madrid.

Bear, J.: *Dynamics of fluids in porous media*. Dover publications, New York (1988)

Brunauer, S., Emmett P. H., and Edward Teller (1938). *Adsorption of Gases in Multimolecular Layers*. Am. Chem. Soc., 60, 2, 309–319

Clauser, C. (1992). *Permeability of crystalline rocks*. Eos, Transactions American Geophysical Union, 73(21), 233-238.

Cranganu, C., & Soleymani, H. (2015). *Carbon dioxide sealing capacity: Textural or compositional controls? A case study from the Oklahoma Panhandle*. AAPG/DEG Environmental Geosciences, 22(2), 57-74.

EN-1936:2007, Natural Stone Test Methods, 2007. *Determination of real density and apparent density, and of total and open porosity*. AENOR eCEN, 14 pp.

Hendrickx, R. (2013). *Using the Karsten tube to estimate water transport parameters of porous building materials*. Materials and structures, 46(8), 1309-1320.

Pittman, E. D. (1992). *Relationship of porosity and permeability to various parameters derived from mercury injection-capillary pressure curves for sandstone*. AAPG bulletin, 76(2), 191-198.

Robinson, R. B. (1966). *Classification of reservoir rocks by surface texture*. AAPG Bulletin, 50(3), 547-559.

Schön, J. H. (2015). *Physical properties of rocks: Fundamentals and principles of petrophysics*. Elsevier.

Schowalter, T. T. (1979). *Mechanics of secondary hydrocarbon migration and entrapment*. AAPG bulletin, 63(5), 723-760.

Soria, A., Liesa, C., Rodríguez-López, J., Meléndez, N., de Boer, P., & Meléndez, A. (2011). *An Early Triassic evolving erg system (Iberian Chain, NE Spain):* palaeoclimate implications. *Terra Nova*.

Swanson, B. F. (1981). *A simple correlation between permeabilities and mercury capillary pressures*. Journal of Petroleum Technology, 2498–2504.ASTM D5731 – 95: Standard Test Method for Determination of the Point Load Strength Index of Rock. ASTM International, West Conshohocken, PA.

The PilotSTRATEGY project has received funding from the European Union's Horizon 2020 research and innovation programme under grant agreement No. 101022664

5. Samples from Spain – Off shore

5.1 Geological context

The study area of the Spanish Offshore region for the Pilot Strategy Project (See Figure 5.1), has been traditionally explored for hydrocarbons aiming at early Tertiary and Mesozoic carbonates. These units are stratigraphically deeper than the clastic upper Miocene reservoir under evaluation in this project. For that reason, most of the available hard data corresponds to the deeper formations, mostly limestones and marls. The only clastic saline aquifer of interest for carbon storage within the AOI are the upper Miocene Castellón Sandstones and the Middle Miocene Salou sandstone.

Figure 5.1 Location Map and Area of Interest (yellow box)

In the Figure 5.2 the Rodaballo-1 well displays the Gamma Ray (GR) log showing the irregular signature in the Castellon Sandstones and the higher GR response, with a more constant character, depicting the sealing facies of the Ebro clays. Secondary clastic plays for carbon storage such as the Salou sandstones are out of the scope of this petrophysical analysis. The lower Miocene and Oligocene section correspond to the formations developed in the past three decades by the oil and gas industry.

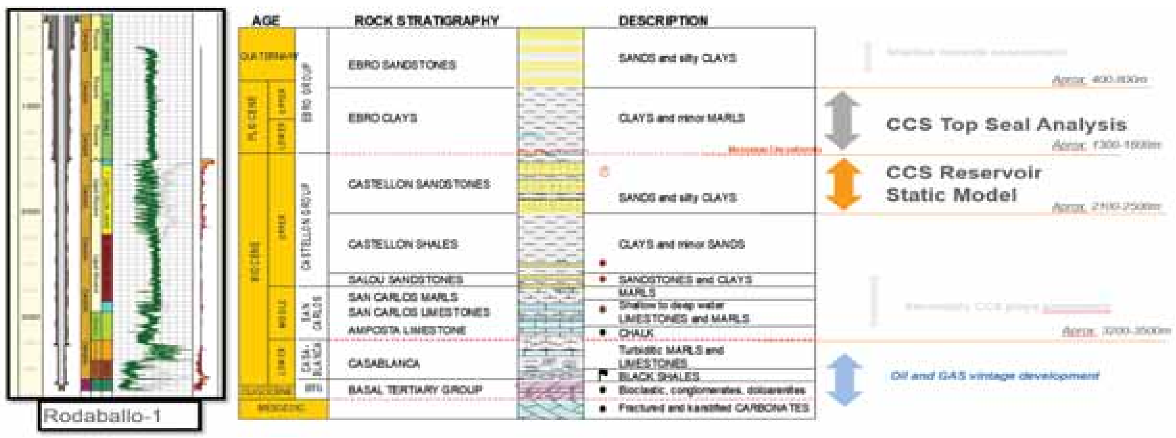

Figure 5.2 Stratigraphic Column and zones of interest Ebro Offshore

The PilotSTRATEGY project has received funding from the European Union's Horizon 2020 research and innovation programme under grant agreement No. 101022664

A 29m reservoir-seal core sample is available from the Amposta Marino C2 well in the AOI, plus 3 core pieces in the Amposta Marino B2 (AB2) and CastellónE-2 (CE2). Several vertical and horizontal plugs have been extracted from the Amposta Marino-C2 core to perform routine core analyses (RCAL). These core samples were sent to the IFPEN and IGME lab facilities. The AB2 and CE2 core pieces are not in an adequate condition to perform the IFPEN analyses (very fragile and or broken) so IGME has made use of them to perform mercury porosimetry analyses.

Figure 5.3 Reservoir Core plugs from wells (left to right) Amposta Marino C-2, Amposta Marino-B2 and Castellón-C1.

Additionally, cuttings set from the well Sardina-1 composed of 12 samples covering reservoir and seal sections has been selected for analysis and has been sent to IGME facilities to perform mercury porosimetry, XRD (X-ray diffraction) analysis and to IFPEN facilities to perform permeability and formation factor, porosity + clay bound water, irreducible water saturation and entry pressure analysis.

Figure 5.4 Cuttings Samples from Sardina-1 well covering seal (Ebro SH) and Reservoir (Castellón SST)

5.2 Petrophysical measurements and log analysis

Prior the lab results, a petrophysical analysis based on the available well logs from the Ebro Offshore region has been performed in the Area Of Interest (AOI); the results obtained are then calibrated with the results from IGME and IFPEN analyses when available and enough quality of the results is confirmed.

The PilotSTRATEGY project has received funding from the European Union's Horizon 2020 research and innovation programme under grant agreement No. 101022664

Using a complete suite of logs, Vsh (shale volume %), porosity and net to gross estimations were performed using GR method for Vsh, and a comparison between Density, Neutron Density and Sonic methods for Porosity determination. A cut-off of 8% porosity and 50% Vsh for net to gross flow reservoir determination has been used based on legacy core data available.

Near the structure under evaluation in the Ebro offshore region, the Rodaballo-1 and Sardina-1 wells were chosen for analysis, while further away the analysis of Amposta Marino B2, Amposta Marino C2 and Castellón E-1 was carried out to make use of hard data available for such wells (e.g. cores, core fragments and well-test results).

Figure 5.5 displays the IGME lab analysis results of Hg porosimetry. The results of porosity can be correlated with the total porosity curves calculated in the three wells, the matrix density has been used to calculate PHIE (effective porosity) vs PHIT (total porosity) relationships, and the threshold pressure to be used in the future calibrations of seal analyses and injectivity tests in seal and reservoir (not an objective of this study).

Samples	Depth	Porosity	Low P apparent density	matrix density at 207MPa	threshold pressure (Mpa)
Cuttings samples					
sample 11 (Seal)	1560-1581 m	25.67	1.9772	2.6598	0.0405
sample 12 (Seal)	1659-1674 m	21.2	2.0993	2.6639	0.0338
sample 5	1824-1845 m	23.26	2.038	2.6552	0.0354
sample 6	1863-1887 m	29.72	1.8459	2.6264	2.1231
sample 1	1956-1968 m	20.77	2.1214	2.6774	0.0574
sample 8	1992-2016 m	11.75	2.3691	2.6846	0.1364
sample 2	2061-2082 m	20.79	2.1098	2.6637	0.0354
sample 3	2121-2145 m	19.93	2.1954	2.7417	0.035
sample 10	2151-2178 m	18.9	2.1773	2.6846	0.0345
sample 4	2232-2247 m	17.35	2.2054	2.6684	0.11
sample 7	2307-2331 m	20.17	2.1184	2.6536	0.3875
sample 9	2451-2475 m	14.97	2.2655	2.6644	0.3116
Core plugs samples					
sample 13 (CE2 plug)	1658m	9	2.4277	2.6678	6.2552
sample 14 (AB2)	1517m	18.58	2.084	2.5596	0.0682
sample 15 (AB2)	1621m	6.85	2.4015	2.578	0.041

Figure 5.5 Summary of IGME Rock Lab Analysis - Hg Porosimetry.

5.2.1 Amposta Marino C-2

The Amposta Marino C-2 has available a complete set of logs plus core data for calibration (See Figure 5.6). We obtained the Vsh (Volume of Shales) from the GR reading picking the clean GR and the Shale line GR calibrated with the core data. We have found clean sands in the Castellón sandstones with GR readings in the order of 25-30ºAPI and clean shales in the range of 100-120ºAPI. To evaluate the porosity, we performed three different methods to check which one calibrates best with the core data.

The PilotSTRATEGY project has received funding from the European Union's Horizon 2020 research and innovation programme under grant agreement No. 101022664

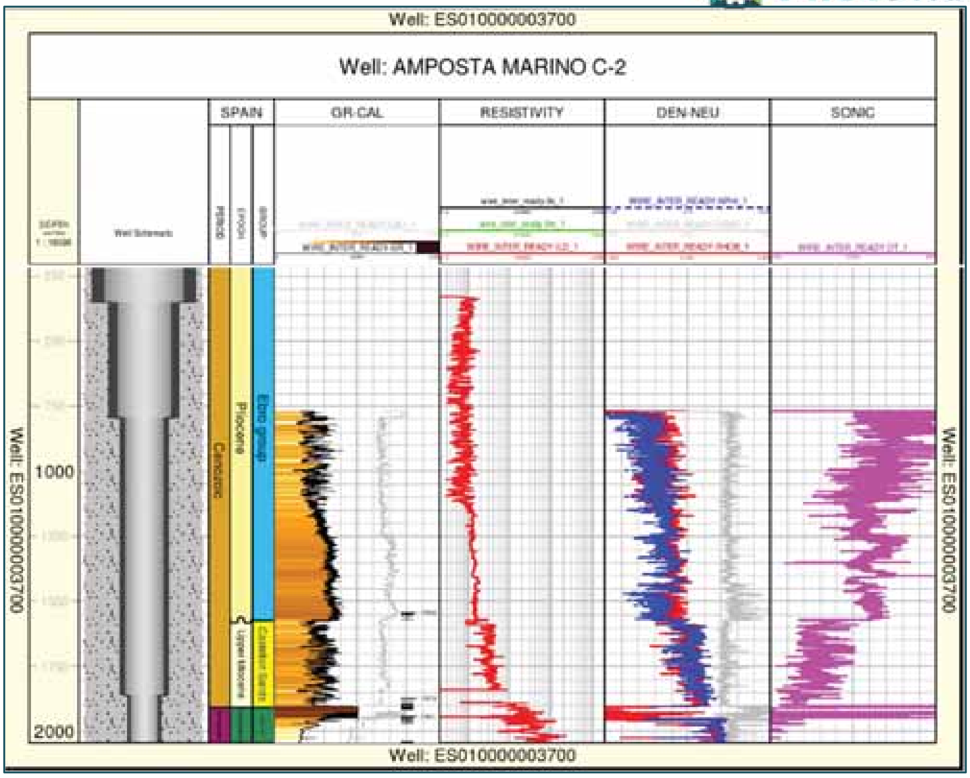

Figure 5.6 Input Data Amposta Marino C-2 – notice core depth at 1542mTVDSS in the reservoir of interest (Castellón Sands)

These methods are based on the density log, the neutron-density and the sonic log. The average effective porosities calculated range from 11% to 16% in this well depending on the method used but we have spot samples with a maximum porosity at around 25% proven by core analysis. The core grain density indicates a high calcareous content in agreement with core descriptions and there is a high variation on porosity and permeability along sands.

WELL	INTERVAL	TOP	BASE	GROSS	NET	N/G	PHIE_DEN	PHIE_DN	PHIE_SON
AMPOSTA MARINO C2	7_CASTELLON_SAND	1526.8	1872.3	345.5	39.319	0.11	0.15	0.157	0.11

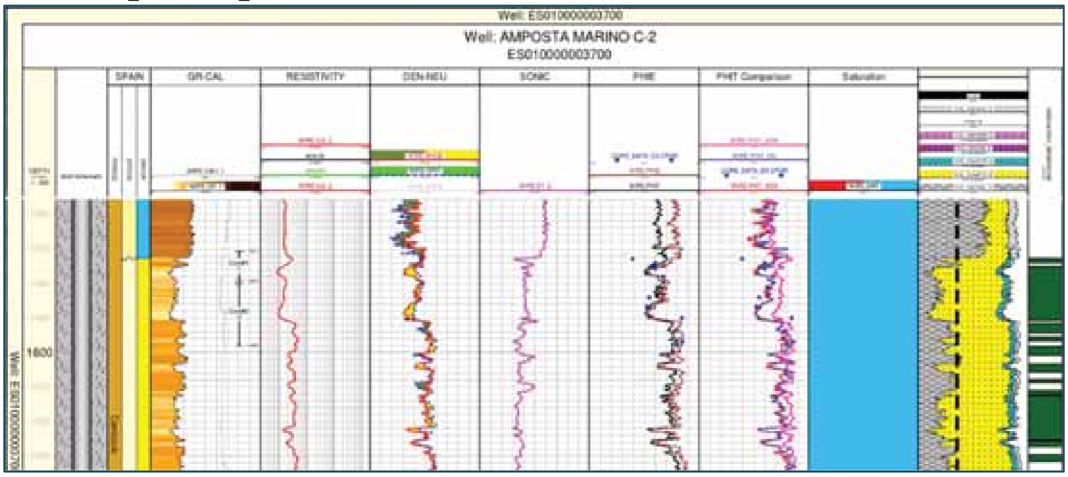

Figure 5.7 Reservoir Petrophysical Assessment for Castellón Sands, considering cutoffs of Vsh < 35% and PHIT > 10% for reservoir pay.

The PilotSTRATEGY project has received funding from the European Union's Horizon 2020 research and innovation programme under grant agreement No. 101022664

Clearly, the porosity curves calculated with the neutron-density and density methods are very similar to each other and calibrate well with core data, whereas the porosity calculated with the sonic method underestimates the porosity by more than 5% in the clean sandstones. Notice the Routine Core Analysis Porosity measurements in blue points attached to PHI logs showing the diminishing of porosity in the intraformational seals.

Below are the data produced by IFPEN from the analysis of plugs sent to their premises for lab analysis.

The sample of the Amposta C2 well at 1543 mTVDSS belongs to the upper part of the Castellon Reservoir and presents good porosity measurements of 21.6% and 90mD of permeability, predicting very good reservoir properties. They belong to facies of coastal Plain deltaic sandstones according to the sedimentological model.

Sample	P1 Amposta C2-1543mTVDSS
Porosity (%)	21.6
Water Permeability (mD)	90
Formation Factor/m	-
Swi @ 7 bar (%)	17
Clay bound water (%)	21

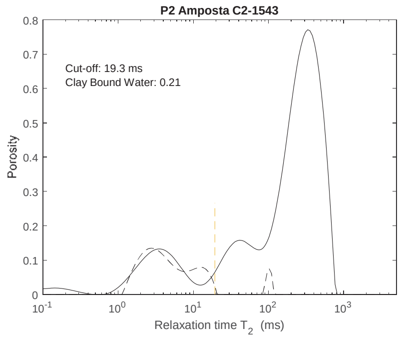

The sample at 1554mTVDSS belongs to the middle part of the Castellon core (upper part of the formation) and presents excellent measurements of porosity and permeability (22% and 550mD) that may correspond to the Shoreface Sand Bar facies.

Sample	P1 Amposta C2-1554mTVDSS
Porosity (%)	22.0
Water Permeability (mD)	550
Formation Factor/m	-
Swi @ 7 bar (fraction)	15
Clay bound water (fraction)	17

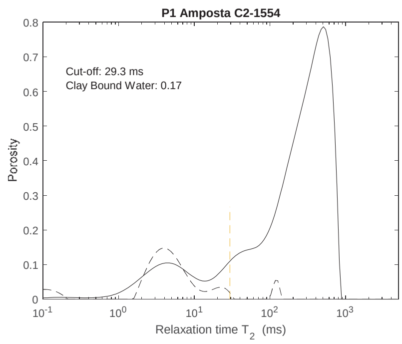

The Irreducible water saturation in both samples range between 15% and 17% providing excellent efficiency perspective for the saturation of the CO_2 in the trap that could go up to 85% if the sweep efficiency is high enough.

The PilotSTRATEGY project has received funding from the European Union's Horizon 2020 research and innovation programme under grant agreement No. 101022664

5.2.2 Amposta Marino B-2

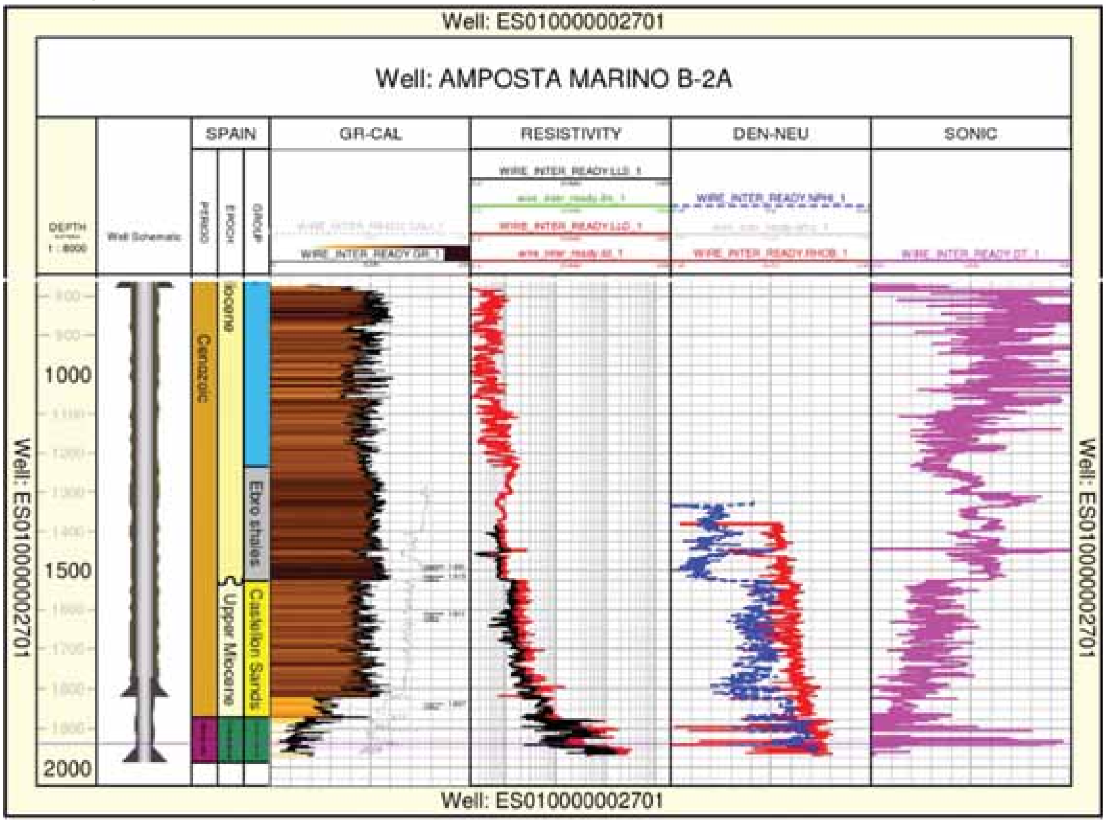

Figure 5.8 Input log data for Amposta Marino-B2 Well

The Amposta Marino B2 has a complete set of well logs, GR, Caliper, Resisitivity, Neutron-Denisty and Sonic. The final well report stated that SNP (sidewall neutron log) tool failure at 1533m, however there was second run performed to 1788mMD. There is no density correction (DRHO) log available so the measurement has less confidence.

Two sets of porosity measurements from Routine Core Analysis are available. Blue points correspond to legacy lab data performed during well operations. Meanwhile, red points are the measurement done by IGME Lab under the PilotSTRATEGY Program of two plugs analyzed by mercury porosimetry at 1517mMD of 21% and an intraformational seal at 1621 of 6%. Both sets of data correlates well with the computed porosity from logs.

The IFPEN analysis on this data delivered a result of 12% at 1621mMD (duplicate of IGME analysis using a similar sample, from the same depth) (see orange dot in the next plot)

The PilotSTRATEGY project has received funding from the European Union's Horizon 2020 research and innovation programme under grant agreement No. 101022664

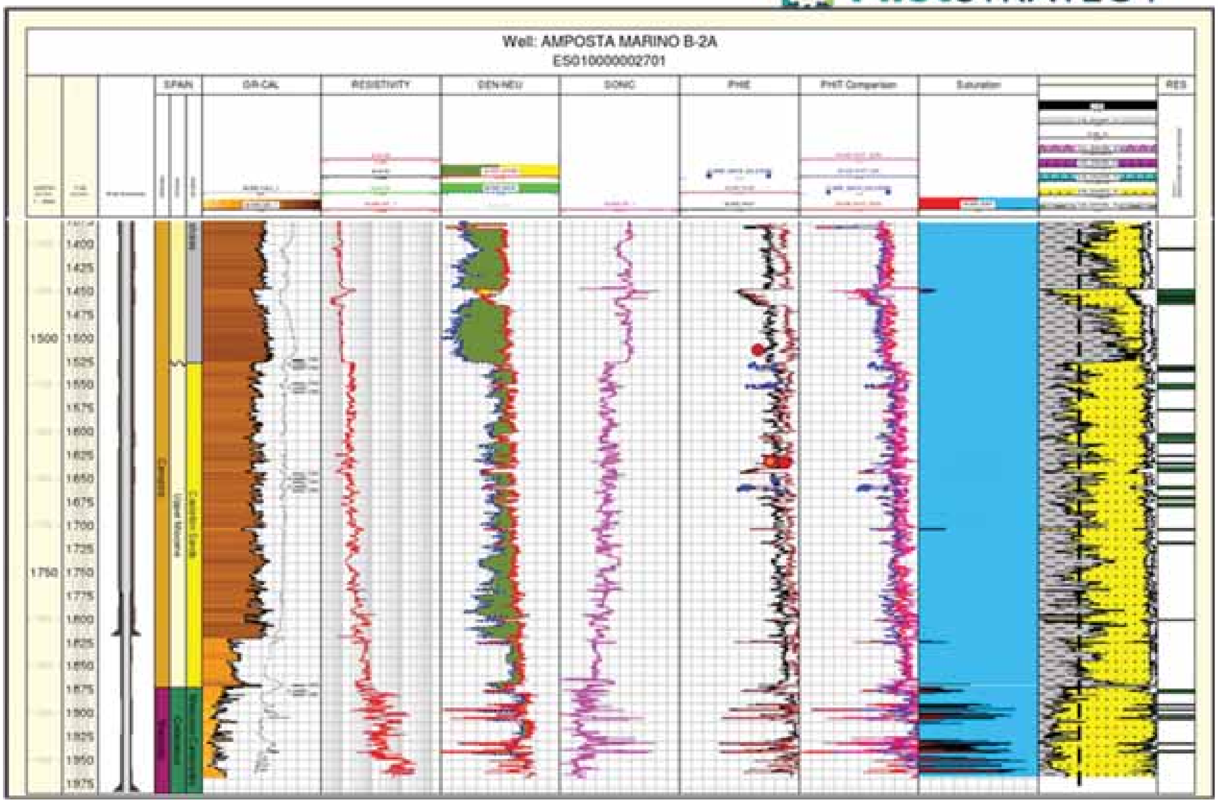

Figure 5.9 Reservoir Petrophysical Assessment in Amposta Marino B2A well for Castellón Sands, considering cutoffs of Vsh < 35% and PHIT > 10% for reservoir pay with calibrated samples from legacy data, and IGME and IFEPN Lab data.

WELL	INTERVAL	TOP	BASE	GROSS	NET	N/G	PHIE_DEN	PHIE_DN	PHIE_SON
AMPOSTA MARINO B2A	7_CASTELLON_SAND	1572.7	1907.7	335	100.736	0.30	0.16	0.144	0.093

Sample	P3 Amposta B2A-1621
Porosity (%)	12.7
Water Permeability (mD)	<0.04
Formation Factor/m	-
Swi @ 7 bar (fraction)	-
Clay bound water (fraction)	0.98

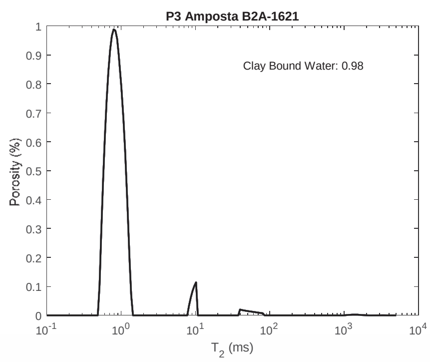

The PilotSTRATEGY project has received funding from the European Union's Horizon 2020 research and innovation programme under grant agreement No. 101022664

5.2.4 Castellón E-1

Castellon E-1 well presented some inconsistencies in the depths of tops provided for the sands reported as Salou sands. These are most likely the Castellón Sandstone (this is not an uncommon problem when working with old well logs). A log for corrected density is not available.

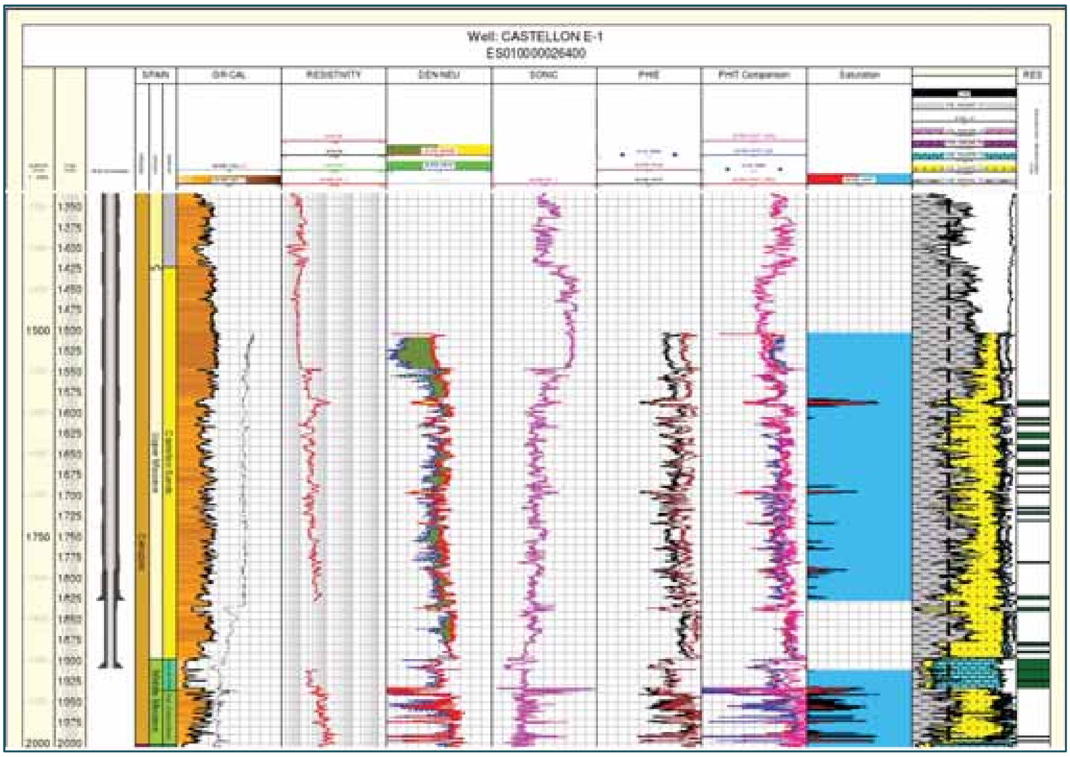

Figure 5.10 Reservoir Petrophysical Assessment in Castellón E-1 well for Castellón Sands, considering cutoffs of Vsh < 35% and PHIT > 10% for reservoir pay.

WELL	INTERVAL	TOP	BASE	GROSS	NET	N/G	PHIT_DEN	PHIT_DN	PHIT_SON
CASTELLON E-1	7_CASTELLON_SAND	1423.5	1897.5	474	59.893	0.13	0.16	0.165	0.127

Sample	P5 Castellon
Porosity (%)	15.4
Water Permeability (mD)	<0.04
Formation Factor/m	-
Swi @ 7 bar (fraction)	-
Clay bound water (fraction)	0.96

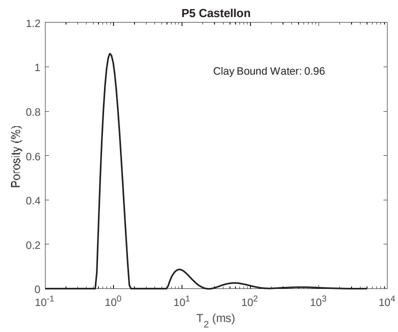

The PilotSTRATEGY project has received funding from the European Union's Horizon 2020 research and innovation programme under grant agreement No. 101022664

5.2.5 Rodaballo-1 Well

The Rodaballo well logs analysis showed an Interval highly affected by washout. There were no DRHO (density correction log) or PEF (Photoelectric Factor) logs available. There is no calibration point with hard data in this well.

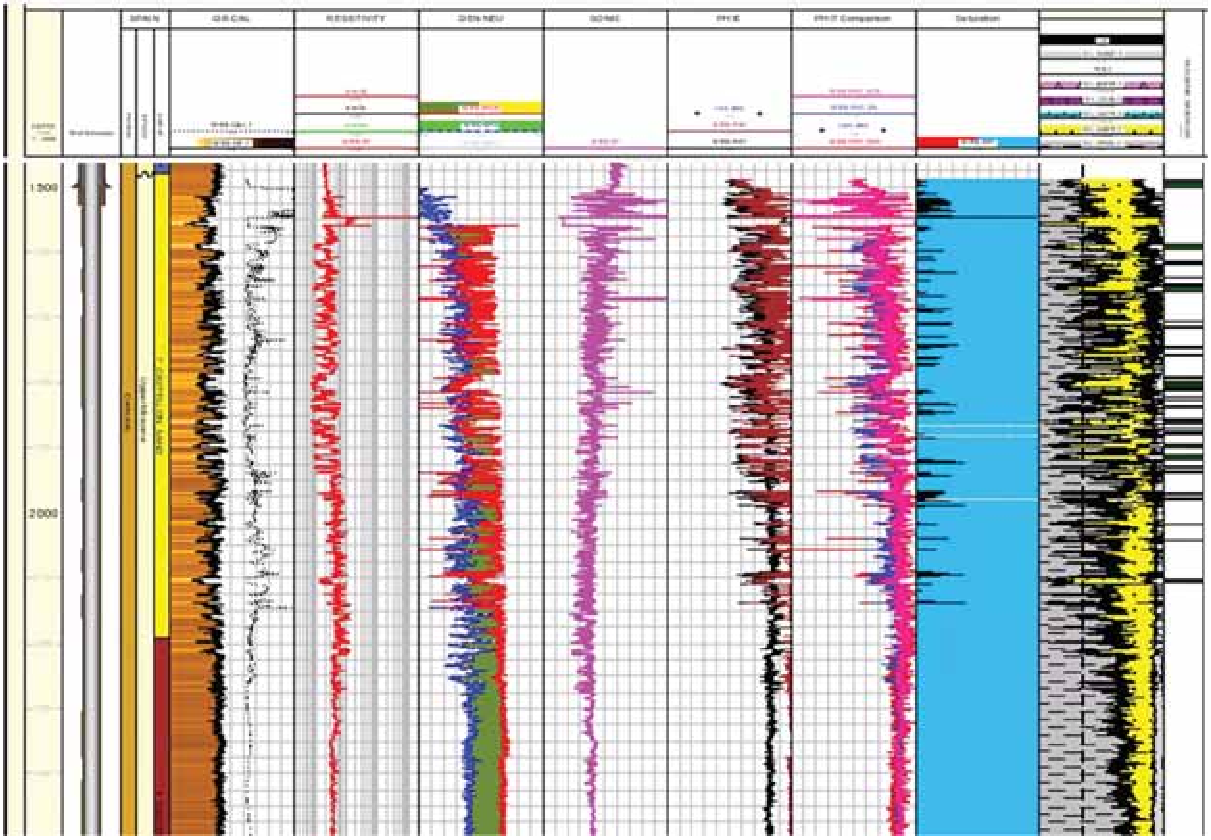

Figure 5.11 Reservoir Petrophysical Assessment in Rodaballo-1 well for Castellón Sands, considering cutoffs of Vsh < 35% and PHIT > 10% for reservoir pay

WELL	TOP	BASE	GROSS	NET	N/G	PHIT_DEN	PHIT_DN	PHIT_SON
RODABALLO-1	1488.034	2191.64	703.606	93.269	0.13	0.17	0.179	0.145

5.2.6 Sardina-1

The Sardina-1 well has the density log affected by borehole rugosity (irregularity) and no DRHO curve. It has the analysis performed by IGME of mercury porosimetry of cuttings samples of reservoir and seal facies.

The PilotSTRATEGY project has received funding from the European Union's Horizon 2020 research and innovation programme under grant agreement No. 101022664

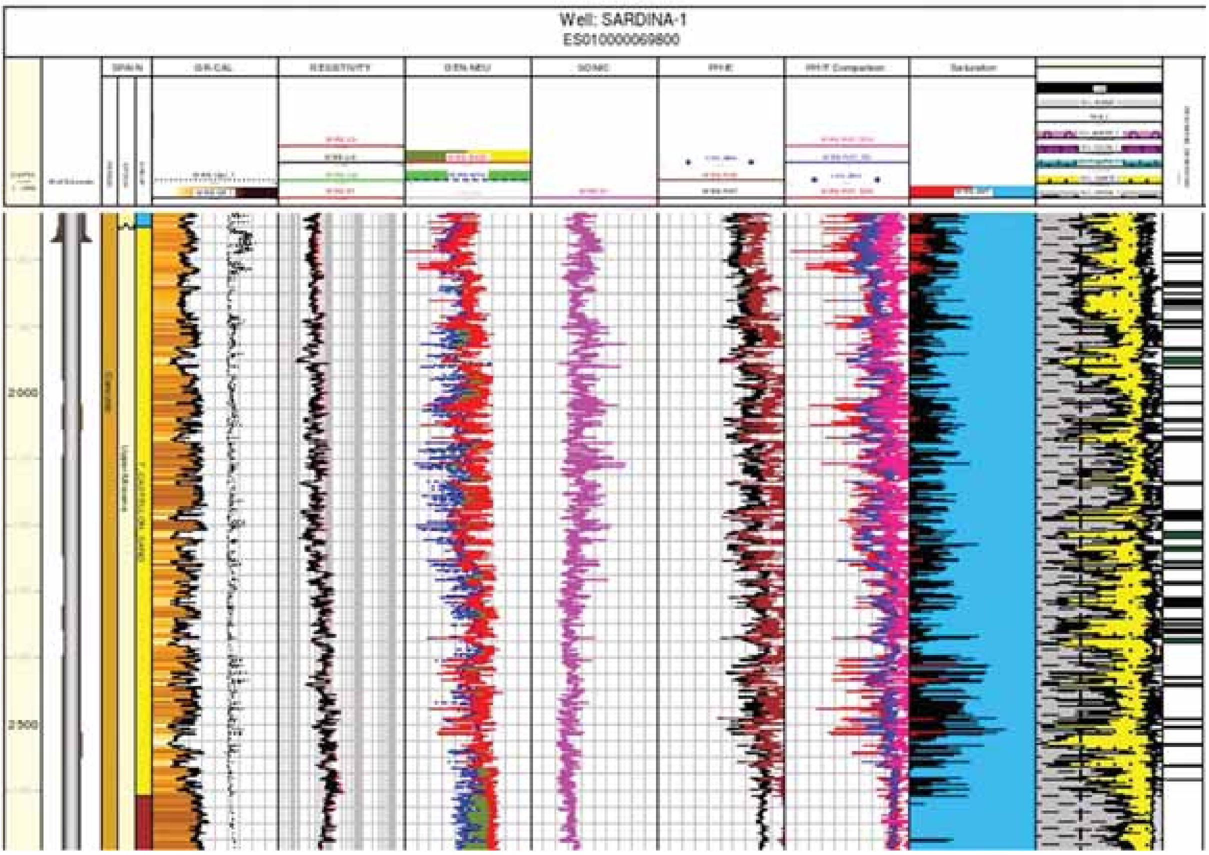

Figure 5.12 Reservoir Petrophysical Assessment in Sardina-1 well for Castellón Sands, considering cutoffs of Vsh < 35% and PHIT > 10% for reservoir pay

The PilotSTRATEGY project has received funding from the European Union’s Horizon 2020 research and innovation programme under grant agreement No. 101022664

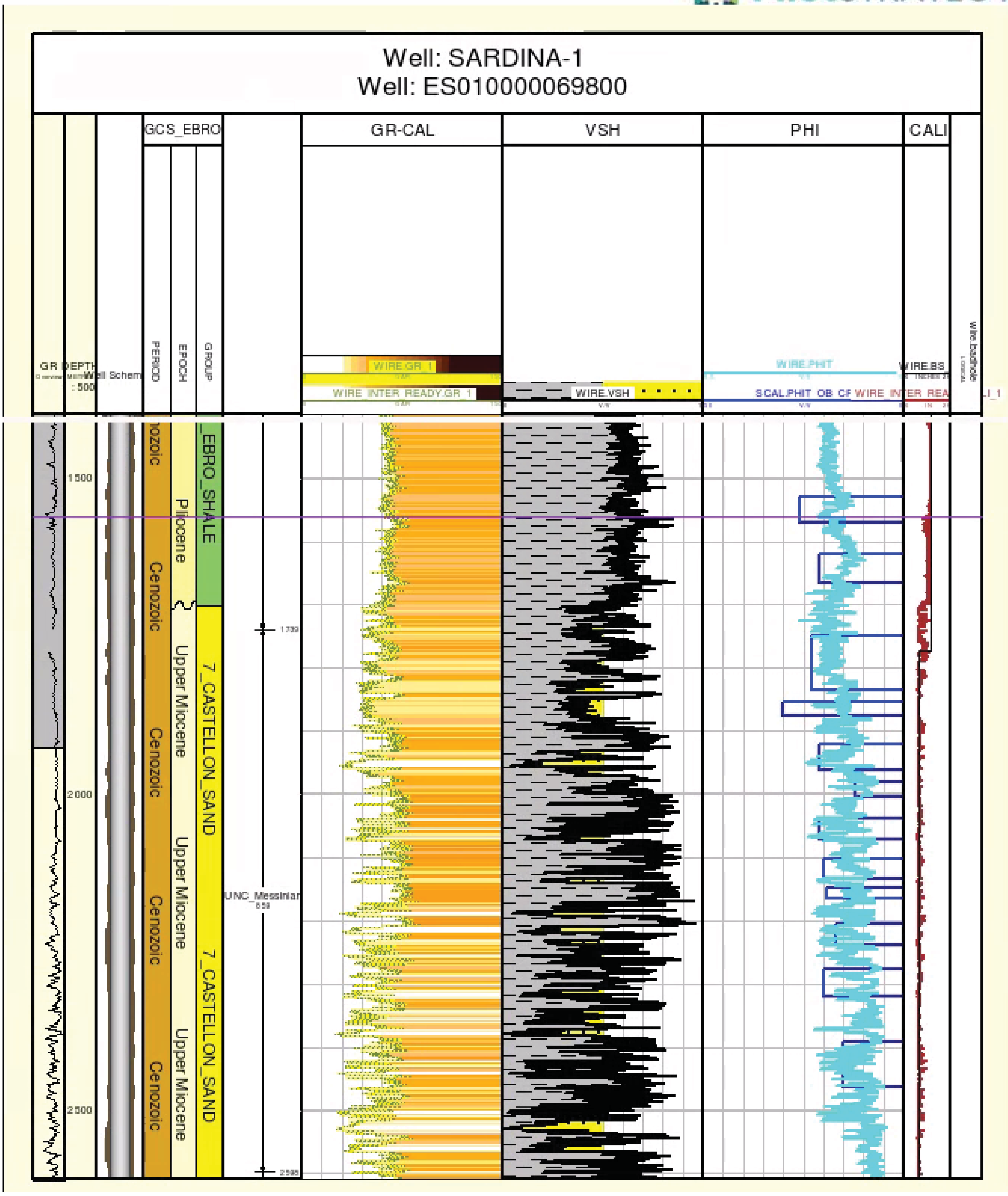

figure 5.13 Sardina-1 well Total Porosity Calculation and HG Porosimetry IGME lab analysis in cuttings sets (blue squares over porosity curve)

WELL	TOP	BASE	GROSS	NET	N/G	PHIT_DEN	PHIT_DN	PHIT_SON
SARDINA-1	1749.9	2608.92	859.02	133.198	0.16	0.17	0.156	0.1

The PilotSTRATEGY project has received funding from the European Union's Horizon 2020 research and innovation programme under grant agreement No. 101022664

5.2.7 Petrophysical Results Comparison

Reservoir summaries have been computed applying cutoffs of Vshales >0.35 and PHIT>10%. With a minimum thickness of 1m. Each column corresponds to log used for porosity calculation, porosity computed with density is in red, in green computed with neutron density and magenta with sonic. It can be observed that sonic log provides the lowest porosity calculation.

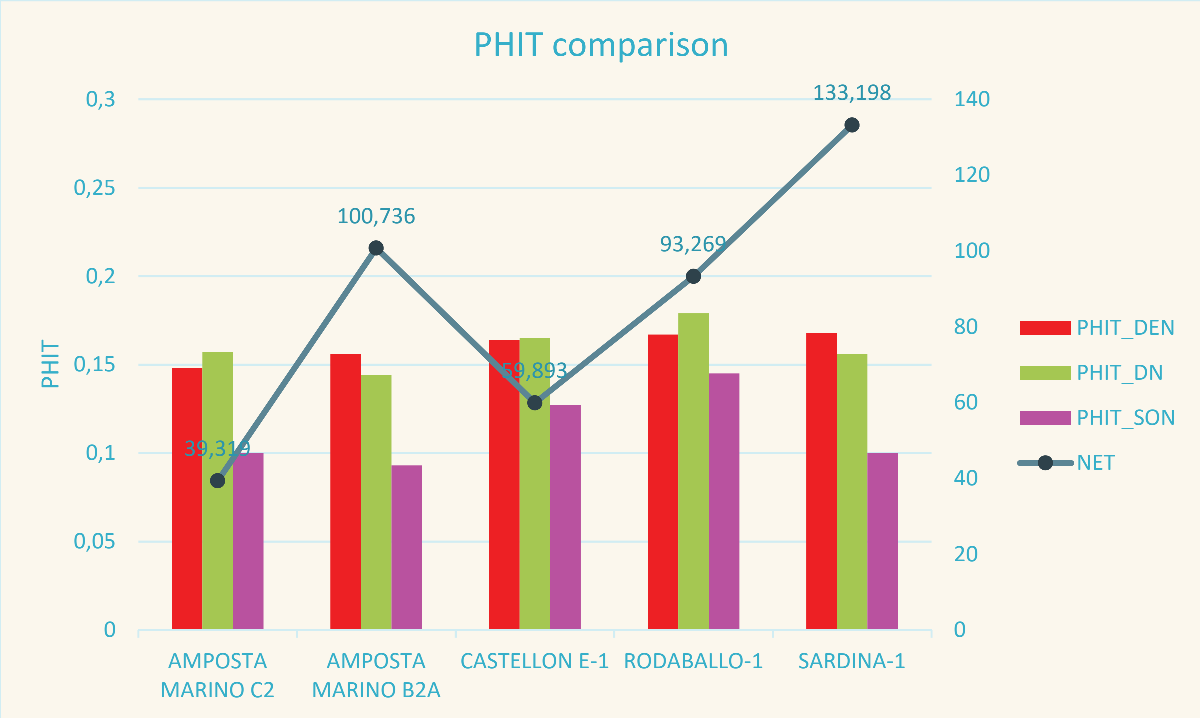

WELL	TOP	BASE	GROSS	NET	N/G	PHIT_DEN	PHIT_DN	PHIT_SON
AMPOSTA MARINO C2	1526.8	1872.3	345.5	39.319	0.11	0.148	0.157	0.1
AMPOSTA MARINO B2A	1572.7	1907.7	335	100.736	0.30	0.156	0.144	0.093
CASTELLON E-1	1423.5	1897.5	474	59.893	0.13	0.164	0.165	0.127
RODABALLO-1	1488.034	2191.64	703.606	93.269	0.13	0.167	0.179	0.145
SARDINA-1	1749.9	2608.92	859.02	133.198	0.16	0.168	0.156	0.1

The PilotSTRATEGY project has received funding from the European Union's Horizon 2020 research and innovation programme under grant agreement No. 101022664

5.3 References

Bowers, G.L., 1995. Pore pressure estimation from velocity data: accounting for overpressure mechanisms besides undercompaction. SPE Drill. Complet. 89 (95).

Castagna et al., 1985. Relationships between compressional-wave and shear- wave velocities in elastic silicate rocks. Geophysics, 50 (4). P.11

Eaton, B.A., 1975. The Equation for Geopressure Prediction from Well Logs. SPE5544-MS.

Gardner, G.H.F., Gardner, L.W., Gregory, A.R., 1974. Formation velocity and density: the diagnostic basics for stratigraphic traps. Geophysics 39, 770 (780).

Golubev, A.A., Robinovich, G.Y., 1976. Resultaty primeneia appartury akusticeskogo karotasa dlja predeleina proconstych svoistv gormych porod na mestorosdeniaach tverdych isjopaemych. Prikl Geofiz Moskova 73, 109–116.

Lal, M. Shale stability: drilling fluid interaction and shale strength. paper SPE 54356, 1999.

Matthews WR, Kelly J. How to predict formation pressure and fracture gradient. Oil Gas J. 1967;65(8):92–106.

McNally, G. H. N. 1987. “Estimation of coal measures rock strength using sonic and neutron logs,” Geoexploration Vol. 24, pp 381–395.

Militzer, H., Stoll, R., 1973. Einige Beiträige der Geophysik zur primädatenerfassung im Bergbau: Neue Bergbautechnik. Leipzig 3, 21–25.

Miller, J. B. (1967). A formula for average foliage density. Aust. J. Bot. 15, 141-4.

Terzaghi, K., 1943. Theoretical Soil Mechanics. Wiley, New York.

Zoback, M. 2007. “Reservoir Geomechanics” New York: Cambridge University Press.

The PilotSTRATEGY project has received funding from the European Union’s Horizon 2020 research and innovation programme under grant agreement No. 101022664

6. Samples from Portugal

6.1 Geological aspects: overview

In the Lusitanian Basin two complexes with storage potential were previously identified: (i) Triassic-L Jurassic complex and (ii) Lower Cretaceous-Upper Cretaceous complex.

Triassic-Early Jurassic complex includes a caprock of Hettangian sediments (evaporites – halite and gypsum mainly – marls, dolomites, dolomitic limestones and claystone), overlying the Triassic siliciclastic reservoir.

The Cretaceous complex includes an Upper Cretaceous carbonate seal overlying a Lower Cretaceous siliciclastic formation. Most of the seal lithologies are compact limestones, with some sporadic interlayered marls and clays. The Lower Cretaceous reservoir consists of sandstones of variable grain sizes with some silt/clay layers interlayered. In some sectors of the Lusitanian Basin, the Upper Jurassic is also siliciclastic, and ca be included in the reservoir complex.

During the field work campaigns, all the lithologies of both storage complexes were sampled.

6.2 Samples from the onshore

To overcome the lack of core samples to be studied outcrop samples from both reservoir complexes were collected onshore. The sampling strategy was to obtain a set of samples representative of the lithological variability of the reservoirs and the seals. Not all the samples were suited to the petrophysical and geomechanical analyses and a synthetic description of their mineralogical and textural characteristics are presented below in Table 6.1:

Table 6-1 - Studied Outcrop Samples

Sample	Age	Type	Observations
ARS-19	Triassic	Reserv.	Sandstone: mainly quartz grains; poorly calibrated; clast supported; abundant iron oxides/hydroxides. *XRD*: Quartz + K-feldspar ± Hematite
ARS-20	Triassic	Reserv.	Sandstone; quartz grains and lithoclasts; poorly calibrated; clast-supported; siliceous cement; iron oxides/hydroxides disseminated. *XRD*: Quartz + Orthoclase
ARS-22	Triassic	Reserv.	Sandstone; argillaceous cement. *XRD*: Quartz + K-feldspar + kaolinite
CC-CV-4	Triassic	Reserv.	Sandstone; sub-angular to subrounded grains; poorly calibrated; argillaceous cement. *XRD*: Quartz + K-feldspar + Kaolinite
PRVT-23	Triassic	Seal	Siltstone/claystone; abundant gypsum. *XRD*: Gypsum + K-felspar + Kaolinite + Dolomite ± Quartz ± Hematite
PPV-HT-28	Triassic	Seal	Fine grained sandstone; carbonate cement. *XRD*: Quartz + Calcite + Kaolinite ± Micas ± Microcline

The PilotSTRATEGY project has received funding from the European Union's Horizon 2020 research and innovation programme under grant agreement No. 101022664

RNA-16	Cretaceous	Seal	Wackstone; abundant bioclasts (gastropod and lamellibranchs); profusion of stylolites; *XRD*: Calcite
FR-SIB-26	Cretaceous	Seal	Dolomite, with some quartz and K-feldspar detrital grains and secondary calcite. *XRD*: Dolomite ± Calcite ± Quartz ± K-feldspar
CD-DARN-14	Cretaceous	Reserv.	Sandstone; fine grained; carbonate cement; quartz grains; poorly calibrated. *XRD*: Quartz + K-feldspar + Calcite
PAJ-29	Upper Jurassic	Reserv.	Sandstone; angular grains; carbonate cement; matrix-supported. *XRD*: Quartz + Orthoclase + Mg Calcite + Kaolinite

6.3 Petrophysical Results (conducted by IFPEN)

Results of mercury injection and helium porosity and MR are presented in Tables 6.2 and 6.3 and in Figures 6.1 to 6.3. See the appendix for methods.

The PilotSTRATEGY project has received funding from the European Union's Horizon 2020 research and innovation programme under grant agreement No. 101022664

Table 6-2 - Mercury injection and Helium porosity

Sample	Age	Type	Replica	Porosity (%)	Distribution mode (mícron)	Solid density (from He exp.)
ARS-20	Triassic	Reservoir	6	24.0	61.000	2.65
			7	23.1	32.200	2.65
PAJ-29	Upper Jurassic	Reservoir	6	10.0	2.600	2.67
			7	10.5	2.800	2.67
RNA-16	Upper Cretaceous	Seal	4	2.3	0.043	2.70
			5	2.0	0.035	2.71
PPV-HT-28	Triassic	Reservoir	4	21.9	0.700	2.70
			5	23.0	0.540	2.71
PRVT-23	Triassic	Seal	4	6.0	0.368	3 - 4
			6	5.6	0.022	2.36
			7	7.4	0.022	2.37

Table 6-3- Porosity, permeability Kw, water saturation Sw after air-brine centrifuge at 7 bar, and water saturation Sw deduced from NMR

Sample	Age	Type	Replica	Porosity (%)	Water Permeability (mD)	Formation Factor/m	Swi @ 7 bar (fraction)	Clay bound water (fraction)
ARS-20	Triassic	Reservoir	1	23.4	252.00	-	0.23	0.36
			2	19.9	375.00	16.7/1.73	0.23	0.34
			3	23.8	850.00	12.5/1.73	0.21	0.35
			4	22.9	368.00	-	0.27	0.39
			5	19.6	263.00	20.6/1.86	0.23	0.34
PAJ-29	Upper Jurassic	Reservoir	1	12.0	0.11	75.5/1.97	0.52	0.53
			2	11.6	0.10	96.3/2.05	0.53	0.54
			3	11.6	0.10	92.4/2.02	0.53	0.54
			4	11.3	0.10	96.5/2.02	0.54	0.55
			5	11.4	0.10	82.0/1.97	0.52	0.55

The PilotSTRATEGY project has received funding from the European Union's Horizon 2020 research and innovation programme under grant agreement No. 101022664

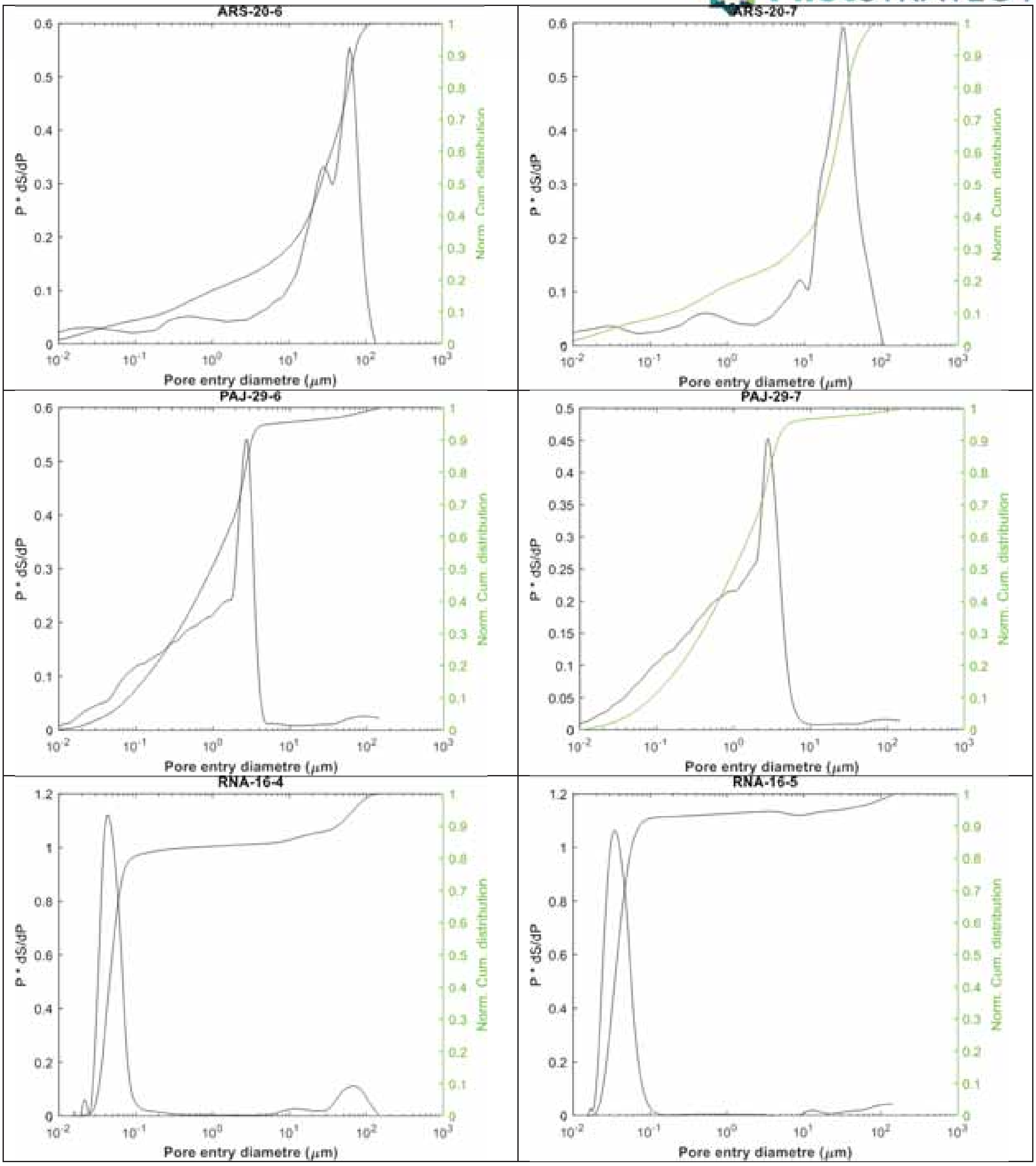

Figure 6.1 Mercury injection and Helium porosity results

The PilotSTRATEGY project has received funding from the European Union's Horizon 2020 research and innovation programme under grant agreement No. 101022664

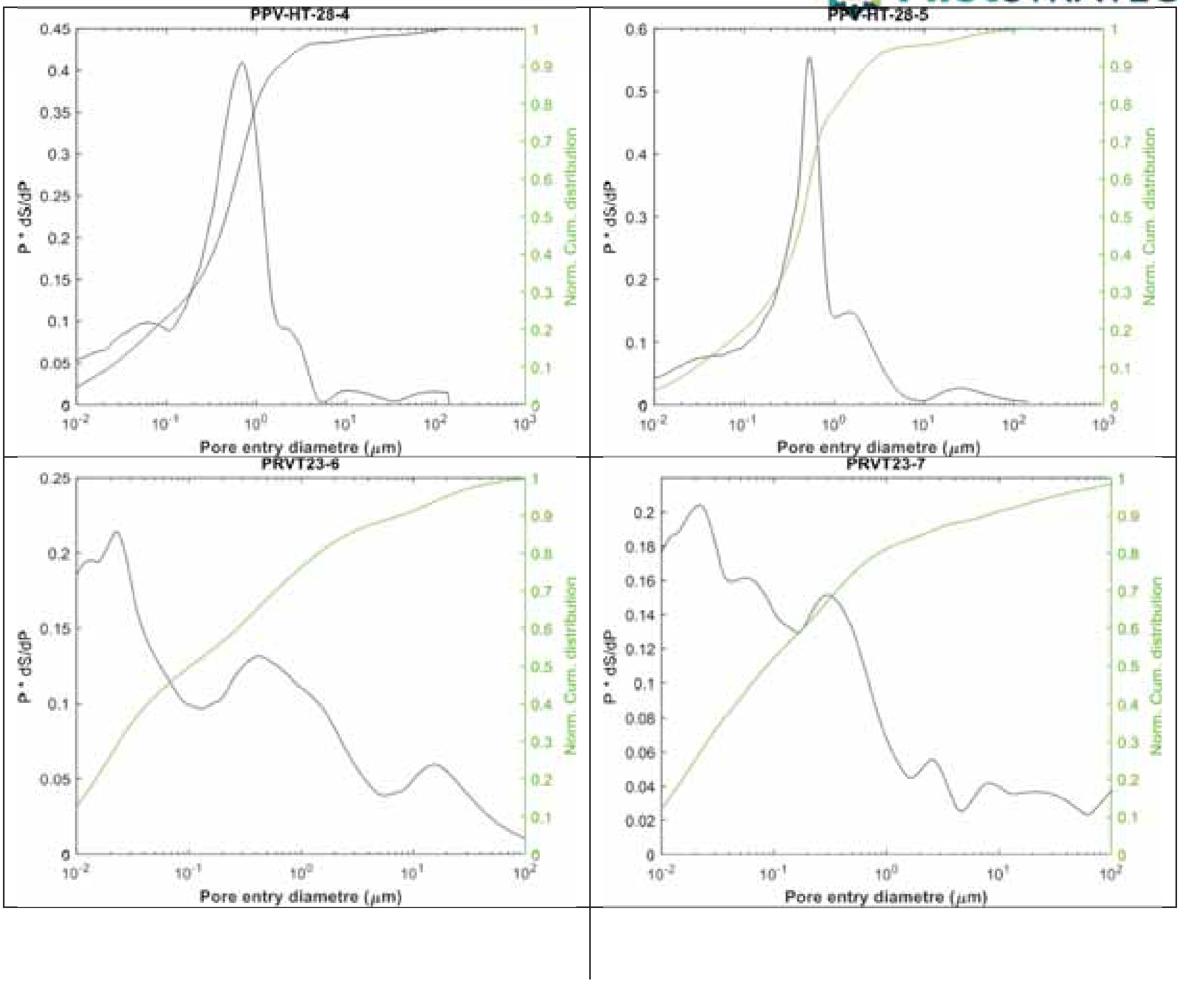

Figure 6.2 - Mercury injection and Helium porosity results (cont.)

The PilotSTRATEGY project has received funding from the European Union's Horizon 2020 research and innovation programme under grant agreement No. 101022664

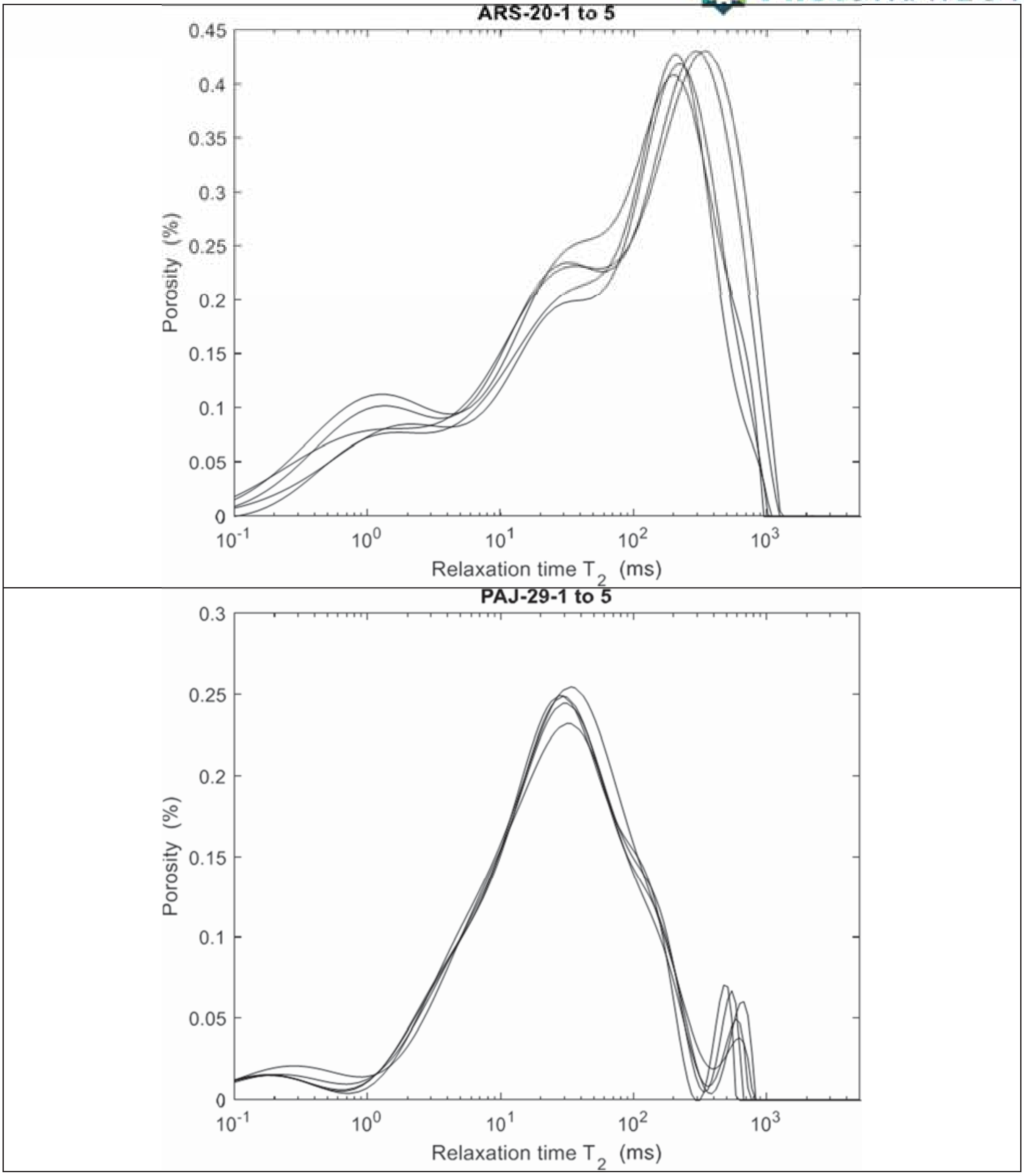

Figure 6.3- Porosity, permeability Kw, water saturation Sw after air-brine centrifuge at 7 bar, and water saturation Sw deduced from NMR

6.4 Conductivity and Thermal Capacity

Heat transfer properties of some selected samples were determined using an ISOMET 2104,

The PilotSTRATEGY project has received funding from the European Union's Horizon 2020 research and innovation programme under grant agreement No. 101022664

a portable measuring instrument for direct measurement of thermal conductivity, thermal diffusivity and volume heat capacity of rocks and other materials. It is equipped with two types of probes: needle probes (for porous, fibrous, or soft materials / rocks) and surface probes (for hard materials or rocks).

The principle of operation and measurement is based on the analysis of the temperature response of the rock samples to be analysed to heat flow impulses which are generated by electrical heating of a resistor; the resistor (heater) is inserted into the probe which is in direct thermal contact with the samples to be tested.

Evaluation of thermal conductivity and volume heat capacity is based on periodically sampled temperature records as a function of time; thermal diffusivity is internally evaluated dividing the thermal conductivity by the volume heat capacity of the sample. Samples should have a polished flat surface of at least 60 mm diameter and a minimal thickness ranging from 10 to 15 mm.

For the rock samples of the project only surface probes were used.

The obtained results are presented in Table 6.4.

The PilotSTRATEGY project has received funding from the European Union's Horizon 2020 research and innovation programme under grant agreement No. 101022664

Table 6-4 Conductivity and Thermal Capacity

Sample	Age	Type	Replica	Thermal Conductivity (W/mk)	Volumetric Thermal Capacity (J/m³.K) x10⁶	Thermal Diffusion (m²/s) x10⁻⁶	Observations
ARS-19	Triassic	Reserv	1	2.66	1.48	1.79	Medium-grained sandstone; sprayed liberally before each reading; specimens (5x5x5cm cubes); Probe Range (2.00…6.00 W/m.K).
			2	2.66	1.53	1.74	
			3	2.61	1.45	1.80	
			4	2.12	1.40	1.52	
			5	2.79	1.53	1.53	
			6	2.38	1.50	1.58	
			7	2.05	1.63	1.25	
			8	2.77	1.57	1.76	
			9	2.54	2.03	1.25	
ARS-22	Triassic	Reserv .	1	2.34	1.47	1.59	Consolidated fine sandstone; Samples (5x5x5cm cubes); sprinkled abundantly with water. Probe Range (2.00…6.00 W/m.K)
			2	3.03	2.15	1.40	
			3	2.75	1.92	1.43	
			4	2.56	1.42	1.80	
			5	3.15	2.03	1.56	
			6	2.49	1.41	1.76	
			7	3.08	2.13	1.44	
			8	2.44	1.44	1.69	
			9	2.21	1.38	1.60	
RNA-16	Cretaceous	Seal	1	2.81	2.11	1.33	Fractured limestone with clay filling in the fractures; submerged in water for 6 hours; specimens (5x5x5cm cubes); imperfect surface with cut saw marks; Probe Range (2.00…6.00 W/m.K).
			2	2.85	2.47	1.16	
			3	3.03	2.45	1.24	
			4	2.87	2.14	1.34	
			5	3.09	2.67	1.16	
			6	2.72	1.98	1.38	

			7	2.90	2.36	1.23	
			8	2.75	1.78	1.55	
			9	3.59	2.45	1.04	
FR-SIB-26	Cretaceous	Seal	1	1.83	1.93	0.950	Marly limestone; specimens (5x5x5cm cubes); submerged in water for 4 hours; imperfect surface with cut saw marks; Probe Range (2.00…6.00 W/m.K)
			2	1.89	2.00	0.947	
			3	2.00	1.74	1.150	
			4	1.68	2.00	0.840	
			5	1.97	1.94	1.010	
			6	1.82	1.74	1.050	
			7	1.69	1.96	0.863	
			8	1.82	2.19	0.830	
			9	1.78	1.93	0.923	
PAJ-29	Upper Jurassic	Reserv.	1	2.93	1.56	1.87	Very porous coarse sandstone; sprayed liberally before each reading; specimens (5x5x5cm cubes); Probe Range (2.00…6.00 W/m.K).
			2	2.60	1.84	1.41	
			3	2.07	1.39	1.48	
			4	2.08	1.57	1.33	
			5	2.71	1.38	1.97	
			6	2.51	1.75	1.44	
			7	2.84	1.70	1.67	
			8	2.42	2.30	1.05	
			9	3.14	2.05	1.53	

The PilotSTRATEGY project has received funding from the European Union's Horizon 2020 research and innovation programme under grant agreement No. 101022664

6.5 Well Data Availability

13 vertical wells were analysed in this study, 7 offshore and 5 onshore. The wells are mostly from the 70s (and some, the Monte-Real wells, from the 50s) with limited data acquisition and generally poor hole quality, which is illustrated through several wash-outs recorded in some of the most interesting formation targets. Figure 1 summarizes the available logs used in the interpretation.

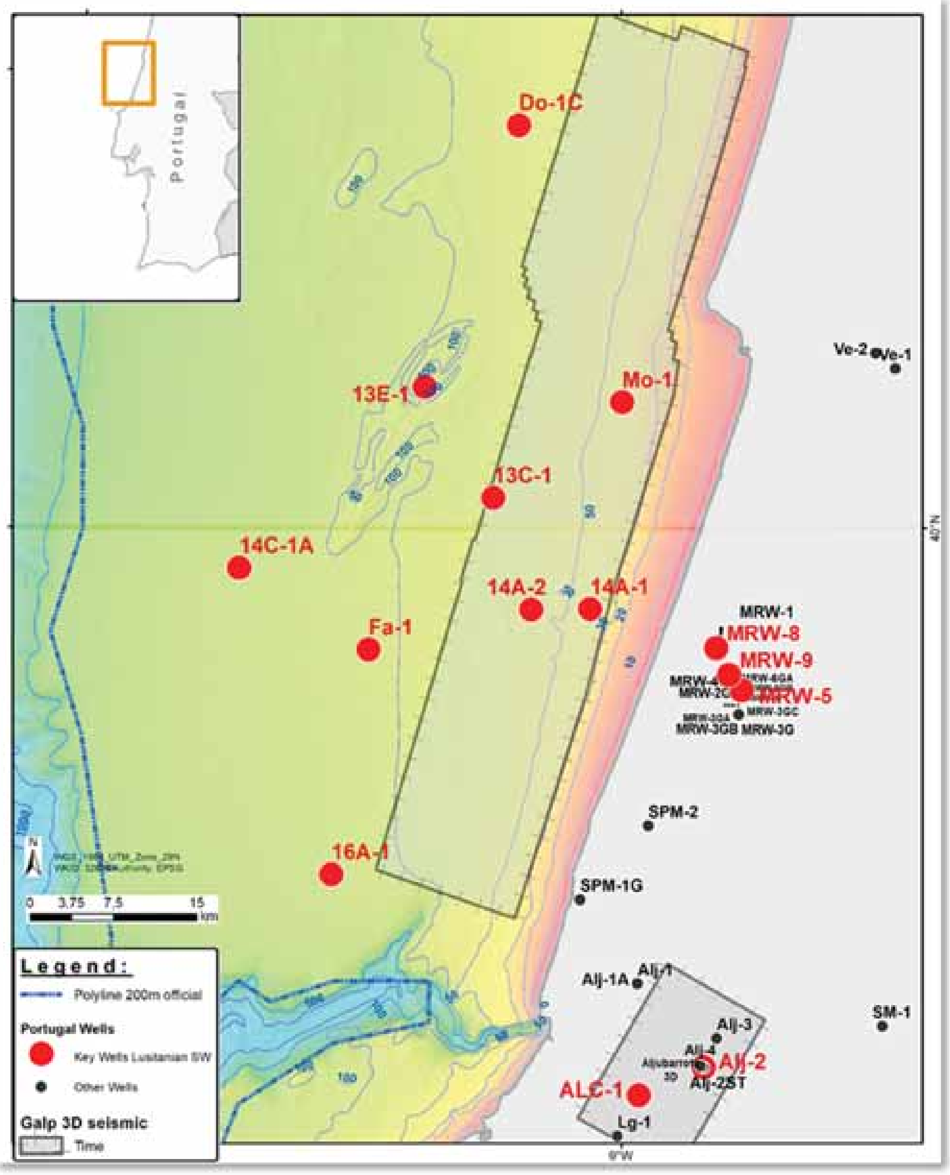

Figure 6.4 – Location map with the indication in red of the wells that were analyzed in this petrophysical study

The PilotSTRATEGY project has received funding from the European Union's Horizon 2020 research and innovation programme under grant agreement No. 101022664

Several washouts were identified based on Caliper, which influences the log readings and increases the uncertainty in the petrophysical assessment.

Due to the vintage character of some of the wells drilled in different exploration campaigns, and without routine core analysis and dynamic tests, it was impossible to calibrate the calculated porosities with 100% certainty.

Table 6-5: WELL LOG DATA AVAILABILITY

	Well	Formation		Available Logs							
		Silves	Torres Vedras	Cal	GR	Spec GR	Den	Neu	Pef	Res	Dt
Offshore	Do-1C	x	x	x	x	-	x	x	-	x	x
Offshore	Mo-1	-	x	x	x	-	x	x	-	x	x
Offshore	13E-1	-	x	x	x	-	x	x	-	x	x
Offshore	13C-1	x	x	x	x	-	x	x	-	x	x
Offshore	14C-1A	-	x	x	x	-	x	x	-	x	x
Offshore	Fa-1	x	x	x	x	-	x	x	-	x	x
Offshore	16A-1	-	x	x	x	-	x	x	-	x	x
Onshore	Alc-1	x	-	x	x	x	x	x	x	x	x
Onshore	Alj-2	x	-	x	x	x	x	x	x	x	x
Onshore	MRW-5	-	-	-	x	-	-	x	-	x	-
Onshore	MRW-8	-	-	-	x	-	-	x	-	x	-
Onshore	MRW-9	-	-	-	x	-	-	-	-	x	-

6.6 Well Log Analysis – Methodology

6.6.1 Shale Model

Galp's pore volume definition is presented in Figure 6.5. Shale volume (VSH) is dry clay volume (VCL) plus volume of clay bound water (VCBW).

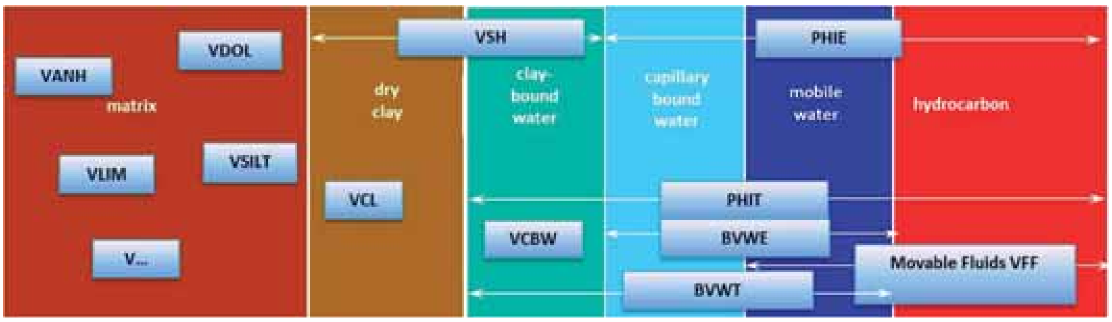

Figure 6.5: GALP'S PORE VOLUME DEFINITION

The PilotSTRATEGY project has received funding from the European Union's Horizon 2020 research and innovation programme under grant agreement No. 101022664

Equation 1 – Formulas used to determine Vshale

VSH (GR):

$$Linear_{method} = \frac{GR - GRclean}{GRshale - GRclean}$$

VSH (D-N):

$$Neutron - Density_{method} = \frac{(DEN_{ma2} - DEN_{ma1}) \times (NEU - NEU_{ma1}) - (DEN - DEN_{ma1}) \times (NEU_{ma2} - NEU_{ma1})}{(DEN_{ma2} - DEN_{ma1}) \times (NEU_{sh} - NEU_{ma1}) - (DEN_{sh} - DEN_{ma1}) \times (NEU_{ma2} - NEU_{ma1})}$$

Ma: Matrix

Sh: Shale

Ma1: Matrix low porosity

Ma2: Matrix high porosity

Shale volume is calculated by a dual shale indicator process. The chosen methods are gamma ray and density-neutron. The density-neutron method requires two clean points at low and high porosity to define a clean mineral line and a shale point. The volume estimation is based on the distance between input data and the clean mineral line and the shale point. Final shale volume is computed as a minimum of the GR and N-D method.

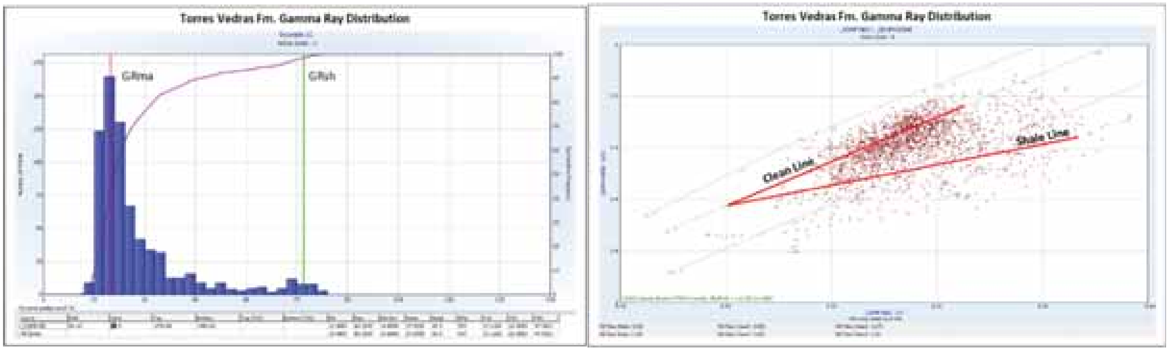

Figure 6.6: EXAMPLE OF GAMMA RAY HISTOGRAM AND NEUTRON-DENSITY CROSS-PLOT FOR THE DOURADA-1C WELL

The neutron-density cross plot is used to define the matrix line and shale points to apply in the previous neutron-density and shale volume equation. The clean line is adjusted by zone and fluid content. The shale point is shown as constant values by zone.

6.6.2 Porosity Model

Effective porosity is computed from density and neutron curves using a hydrocarbon corrected density porosity model or a hydrocarbon corrected neutron-density porosity model.

The PilotSTRATEGY project has received funding from the European Union's Horizon 2020 research and innovation programme under grant agreement No. 101022664

Equation 2 – Formulas used in the determination of effective porosity

$$\varnothing_{eff\_N-D} = \frac{(\rho_{ma} - \rho_b - V_{sh} \times (\rho_{ma} - \rho_{sh}))}{(\rho_{ma} - \rho_{fl} \times S_{xo} - \rho_{HyApp} \times (1 - S_{xo}))}$$

Where

ρ_{ma} – Matrix Density

ρ_b – Input Bulk Density

ρ_{sh} – Shale Density

ρ_{fl} – Filtrate Density

ρ_{HyApp} – Apparent Hydrocarbon Density

V_{sh} – Shale Volume

S_{xo} – Flushed Zone Water Saturation

$$\varnothing_{eff\_D} = \frac{(\rho_{ma} - \rho_b - V_{sh} \times (\rho_{ma} - \rho_{sh}))}{(\rho_{ma} - \rho_{fl} \times S_{xo} - \rho_{HyAp} \times (1 - S_{xo}))}$$

Where

ρ_{ma} – Matrix density

ρ_b – Input bulk density log

ρ_{sh} – Wet clay density

ρ_{fl} – Filtrate density

ρ_{HyAp} – Apparent hydrocarbon density

V_{sh} – Wet clay volume

S_{xo} – Flushed zone water saturation

Along washout zones, sonic porosity is calculated instead of previous mentioned porosity models:

Equation 3 – Raymer equation used to calculate sonic porosity

Raymer equation:

$$\phi_{clay} = \frac{(2 \times Vma - Vf) - \sqrt{(2 \times Vma - Vf)^2 - 4 \times Vma \times (Vma - Vclay)}}{2 \times Vma}$$

$$Vfc = \frac{1}{Dtfl \times Sxo + Dthy \times (1 - Sxo)}$$

$$\phi_{son} = \frac{(2 \times Vma - Vfc) - \sqrt{(2 \times Vma - Vfc)^2 - 4 \times Vma \times (Vma - V\log)}}{2 \times Vma}$$

$$\phi = \phi_{son} - \phi_{clay} \times Vcl$$

Where

Vma = 1/Dtma

Vf = 1/Dtfl

Vclay = 1/Dtclay

Vlog = 1/Dt

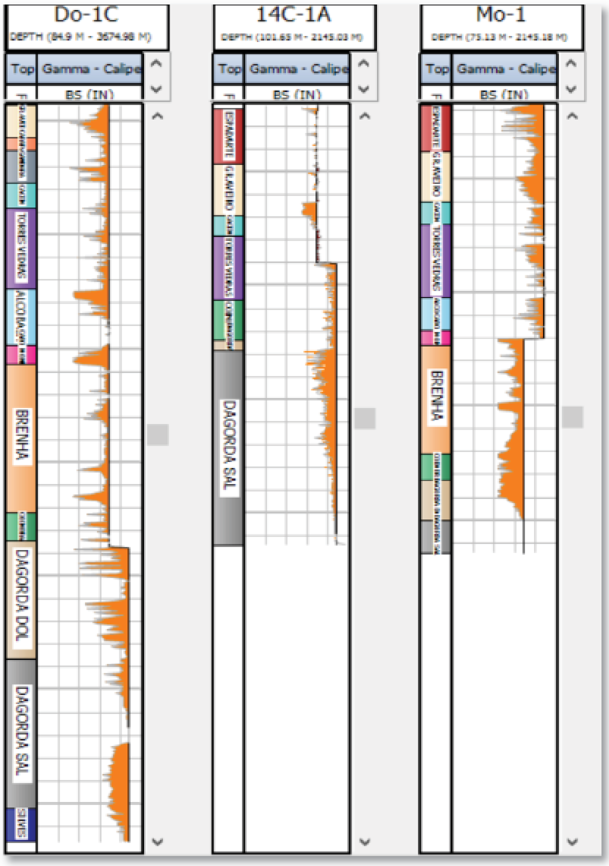

Figure 6.7: EXAMPLE OF WELL WASHOUT (GAMMA-CALIPER ORANGE PEAKS)

6.6.3 Water Saturation Model

Water saturation is calculated from the Archie equation (see equation 4), using the deep resistivity curve as true formation resistivity (R_t), together with effective porosity (ϕ_e) and water resistivity (R_w).

Equation 4 – Archie equation

$$S_{we} = \sqrt[n]{\frac{a \times R_w}{\emptyset_e^m \times R_t}}$$

The formation factor (a), cementation exponent (m) and saturation exponent (n) parameters are listed in the Table 6-6:

Table 6-6: *PARAMETERS USED IN THE WATER SATURATION MODEL*

	a	m	n
Lusitanian Basin	1	2	2

The PilotSTRATEGY project has received funding from the European Union's Horizon 2020 research and innovation programme under grant agreement No. 101022664

6.6.4 Formation Water Resistivity (Rw)

Based on the available information in well reports, two Rw values were used in the petrophysical interpretation. An average value of 30,000 ppm NaCl was used in onshore wells, and a higher value of 70,000 ppm NaCl was used for offshore wells.

6.6.5 Reservoir Summation and Cut-offs

As a standard practice in the oil & gas industry, pre-defined cut-offs were used for net-to-gross and net reservoir determination. Porosity cut-offs are illustrated in the Table 6-7:

Table 6-7: DOURADA-1C CPI DETERMINATION

Cut-offs	Curve	Value
Effective Porosity (Reservoir)	PHIE	> 8%
Effective Porosity (Seal)	PHIE	< 2%

The PilotSTRATEGY project has received funding from the European Union's Horizon 2020 research and innovation programme under grant agreement No. 101022664

6.7 Final Petrophysical Results

The final results are based on available data and on existing literature, as described in the Table 6-8.

Table 6-8: FINAL PETROPHYSICAL RESULTS IN THE MAIN FORMATIONS OF INTEREST (SILVES GROUP, ALCOBAÇA FORMATION, TORRES VEDRAS FORMATION)

	Well Name	WD (m)	Top (MD m)	Bottom (MD m)	Gross (m)	Net (m)	N/G (%)	Av Phi (%)
TORRES VEDRAS FM.	Do-1C	84	880	1238	358	289	81	19
	Mo-1	45	703	1024	321	262	82	23
	13C-1	83	412	761	349	37	11	19
	13E-1	129	356	748	392	114	29	22
	14C-1A	133	802	1062	280	70	27	22
	Fa-1	112	860	1300	440	109	25	17
	16A-1	125	974	1472	498	320	64	17
SILVES Grp.	Do-1C	84	3525	3668	141	0.5	0.3	10
	13C-1	83	2459	2737	278	0.3	0.1	12
	Fa-1	112	2065	2597	532	1.4	0.3	9
	Alc-1	-	2653	3240	587	10.4	1.8	10
	Alj-2	-	3027	3616	589	-	-	-
Alcobaça	MRW-5	-	778	1084	306	305	99*	18*

** non-reliable result – based on Neutron log*

According to our petrophysical analysis, some concluding remarks can be made. Starting with the Late Triassic Silves Group, our analysis from the available wells suggests there is no minimum requirements to be considered as a potential reservoir, mainly due to very low N/G properties, combined with overall low porosity that does not exceed 10%.

On other hand, the Early Cretaceous Torres Vedras Formation presents better N/G results, although with a large variability in the observed wells. This impose an additional challenge for proper well correlation of sand packages within this unit, which is displayed in the correlation panel in Figure 6.8. The Torres Vedras Formation presents very good porosities, with an average value of 20%. These combined properties and overall extension make this unit the best reservoir target to be pursued.

Regarding the Late Jurassic Alcobaça Formation, petrophysical analysis was limited to the log suite available for the MRW-5 well, which didn't allow full understanding of the reservoir characteristics. We, thus, recommend to discard this unit as a target due to the lack of good reservoir indicators.

The PilotSTRATEGY project has received funding from the European Union's Horizon 2020 research and innovation programme under grant agreement No. 101022664

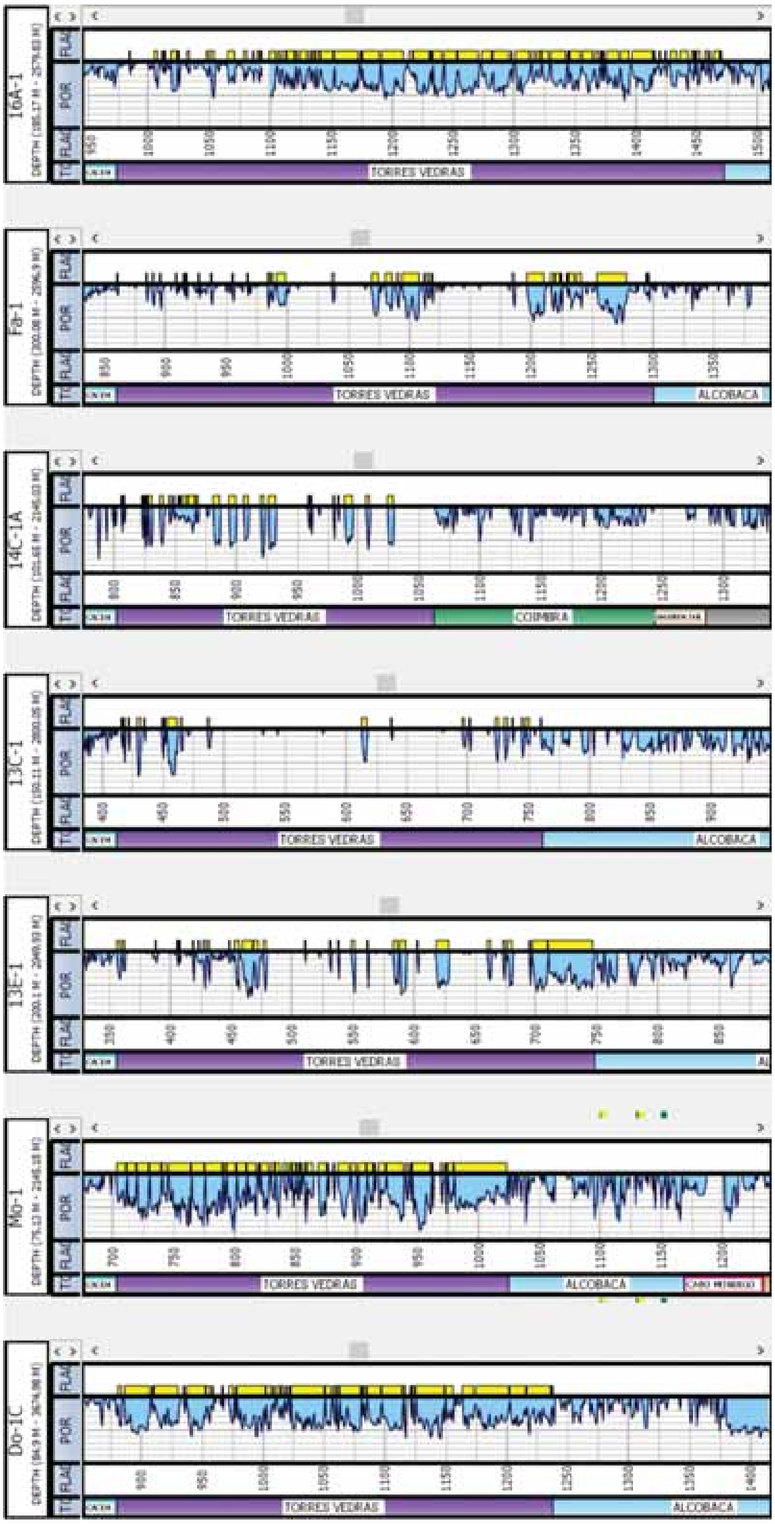

Figure 6.8 Well correlation panel focused on the most important reservoir target interval, the Torres Vedras Formation, in the offshore wells

The PilotSTRATEGY project has received funding from the European Union's Horizon 2020 research and innovation programme under grant agreement No. 101022664

6.8 References

[1] Alshkane, Y. M., & Hama Saeed, S. B. (2018). Effect of freezing and thawing on physical and mechanical properties of sedimentary rock. Journal of Garmian University, 5(2), 126-140.

[2] ASTM D 5731 – 95 - Standard Test Method for Determination of the Point Load Strength Index of Rock

[3] BS 1881 Part 203: Recommendations for measurement of velocity of ultrasonic pulses in concrete.1986

[4] Daoud, H. S. D., Rashed, K. A. R., & Alshkane, Y. M. A. (2017). Correlations of uniaxial compressive strength and modulus of elasticity with point load strength index, pulse velocity and dry density of limestone and sandstone rocks in Sulaimani Governorate, Kurdistan Region, Iraq. Journal of Zankoy Sulaimani, 19, 57-72.

[5] Deere, D. U., & Miller, R. P. (1966). Engineering classification and index properties for intact rock. Illinois Univ At Urbana Dept Of Civil Engineering.

[6] González de Vallejo, L. I., Ferrer, M., Ortuño, L., & Oteo, C. (2002). Ingeniería geológica. Pearson Educación.

[7] Katz, O., Reches, Z., & Roegiers, J. C. (2000). Evaluation of mechanical rock properties using a Schmidt Hammer. International Journal of rock mechanics and mining sciences, 37(4), 723-728.

[8] O'Rourke, J. E. (1989). Rock index properties for geoengineering in underground development. Min. Eng. (Littleton, Colo.);(United States), 41(2).

[9] Saleh Daoud, H., M Alshkane, Y., & Ahmad Rashed, K. (2018). Prediction of Uniaxial Compressive Strength and Modulus of Elasticity for Some Sedimentary Rocks in Kurdistan Region-Iraq using Schmidt Hammer. Kirkuk University Journal-Scientific Studies, 13(1), 52-67.

[10] Saptono, S., Kramadibrata, S., & Sulistianto, B. (2013). Using the Schmidt hammer on rock mass characteristic in sedimentary rock at Tutupan coal mine. Procedia Earth and Planetary Science, 6, 390-395.

[11] Singh, R., Hassani, F. P., & Elkington, P. A. S. (1983, June). The application of strength and deformation index testing to the stability assessment of coal measures excavations. In The 24th US Symposium on Rock Mechanics (USRMS). OnePetro.

[12] Yagiz, S. (2013). Comment on “Point Load Test on Meta-Sedimentary Rocks and Correlation to UCS and BTS” by Diyuan Li and Lous Ngai Yuen Wong, Rock Mechanics and Rock Engineering. Rock mechanics and rock engineering, 46(4), 909-912. Samples from Greece

7. West Macedonaia (Greece): Geological aspects

The Mesohellenic basin has a 150 km length and 30 km width. It is partly located in Northern Greece and partly in Albania and was developed from Middle Eocene to Upper Miocene. The Grevena sub-basin area has shown preliminary potential for CO_2 storage [Koukouzas et al, 2021].

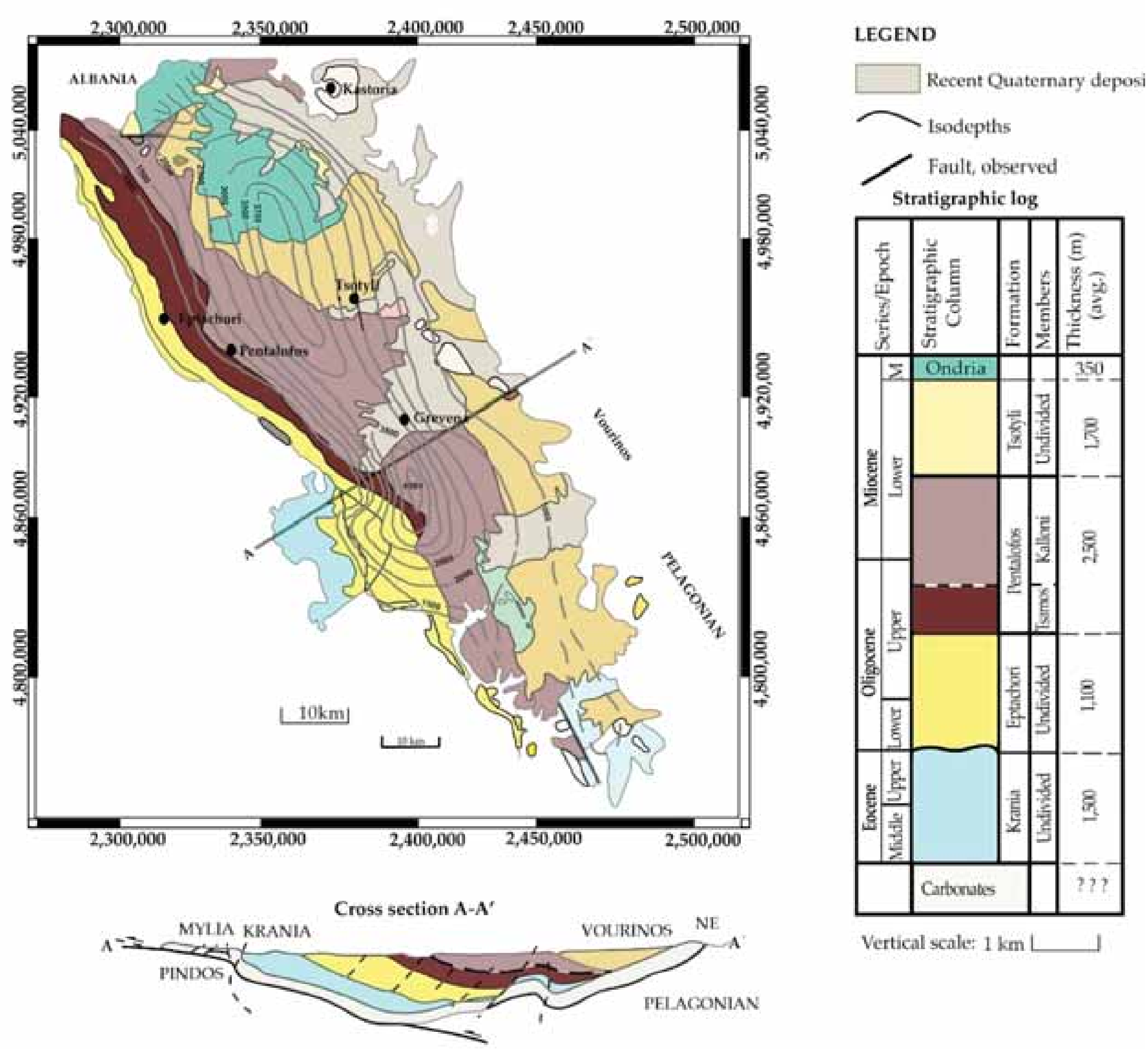

Figure 7.1.: Geological Map and stratigraphic column adapted from Ferriere et al., 2004, of the proposed CO2 Storage basins in Grevena area depicting Pentalofos and Eptachori formations, scale 1:1,000,000. Cross-sections of the Mesohellenic Trough. Lithological formations: Krania Turbidites, Eptachori, Taliaros, Pentalofos, Tsotyli. M stands for Middle Miocene, scale 1:500,000

During previous research three formations have identified with interest for further potential research related to CO2 storage. From top downwards, these are:

Tsotyli Formation. Alternation between units of varying grain size and strength:

1. 0.5 - 1.5 m-thick beds of medium weak to very strong, partially weathered, grey conglomerate. Clasts are poorly sorted (0.5 - 10+ mm with occasional larger clasts), sub-angular to sub-rounded,

The PilotSTRATEGY project has received funding from the European Union's Horizon 2020 research and innovation programme under grant agreement No. 101022664

predominantly limestone with igneous/metamorphic clasts and fossil corals, grain-supported with clastic matrix. No interior bedding or structures.

2. 10 cm – 1 m-thick beds of medium weak to very strong, partially weathered, grey greywacke. Grains are fine, angular, limestone-quartz-micas-various mafics.

Pentalofos Formation. Slightly weak to medium strong beds of partially weathered, grey sandstone. Grains are fine, crystalline, most are indistinguishable from matrix. Many mica and mafic grains. Sample effervesces in acid—either a calcareous matrix, or grains of limestone (could not be determined macroscopically). Some weak interior bedding. Occasional trace fossils (burrow casts). Iron oxide staining.

Eptachori Formation. Very strong, thickly bedded (20-30cm), partially weathered, medium grey-tan, fine greywacke. Joint fractures spaced 40-80cm apart, perpendicular to bedding. Trace fossils (invertebrate burrows) on bedding surfaces. Partially carbonized wood and leaf fragments. Water discoloration (Liesegang) penetrates 8-10cm into bedding.

From December 2021 to May 2023 several walk-over surveys were conducted to gather an initial set of data. During these surveys several field samples were collected from the Tsotyli, Pentalofos and Eptechori formation were collected and subsequently were sent to various laboratories for petrophysical (and geomechanical) investigation (Figure 7.**2**).

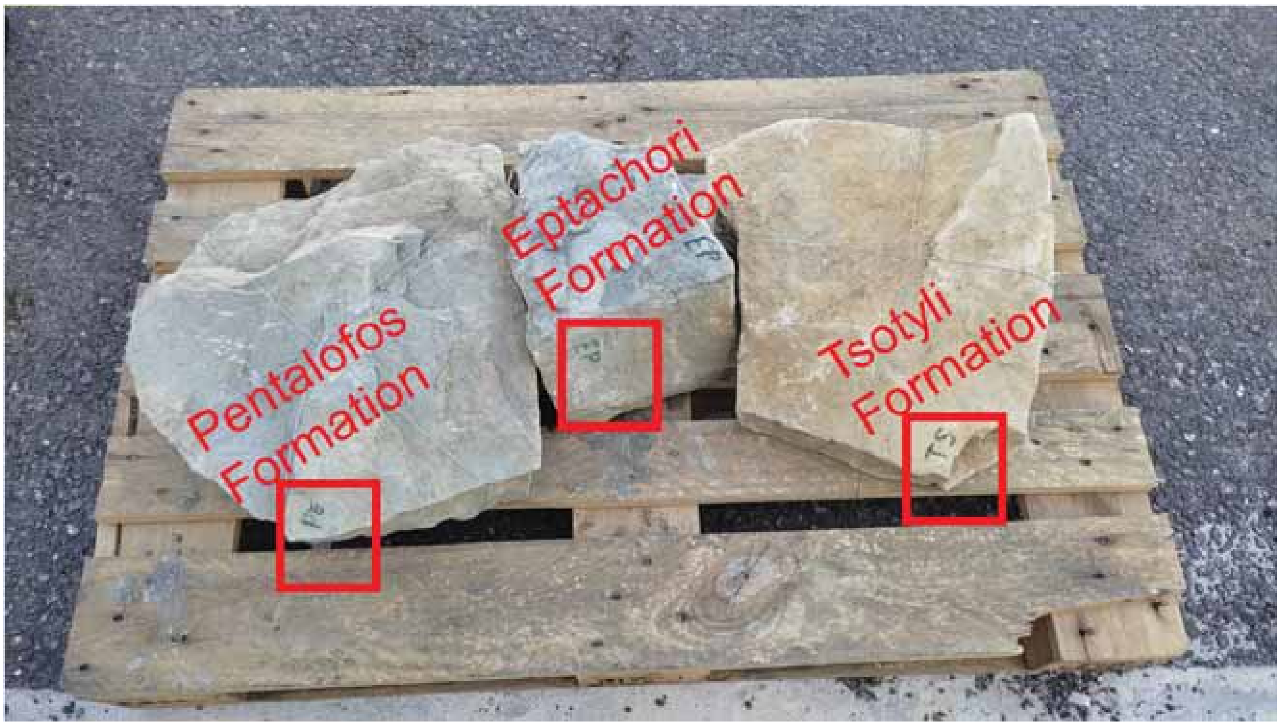

Figure 7.2.: Bulk samples collected during the initial walk over survey and sent to France: IFP Energies nouvelles – Earth Sciences and Environmental Technologies, Scotland: School of GeoSciences University of Edinburgh Grant Institute, Portugal: Departamento de Geociências Universidade de Évora.

The PilotSTRATEGY project has received funding from the European Union's Horizon 2020 research and innovation programme under grant agreement No. 101022664

CERTH is committed to open data and metadata sharing sample information in an effort to promote a workplace of collaboration. Therefore, data from the samples collected are open and accessible as follows:

Tsotyli formation https://app.geosamples.org/sample/igsn/IE5770001

Pentalofos formation https://app.geosamples.org/sample/igsn/IE5770002

Eptachori formation (https://app.geosamples.org/sample/igsn/IE5770003)

7.1 Petrophysical measurements: results

The petrophysical laboratory investigation for the Mesohelenic basin samples was conducted by the IFPEN. The permeability was measured with brine (NaCl 20g/l). All permeabilities were too low to be measured in the device used. An upper limit is given instead. The Formation factor FF was measured during permeability estimation while a single point cementation exponent m such as $FF=\Phi^{-m}$ was adopted.

7.1.1 Petrophysical results for Tsotyli formation

Table 7-1 and Figure 7.**3** present the petrophysical results for the Tsotyli Formation (Lower Miocene, estimated thickness 1700 m).

Table 7-1.: Petrophysical laboratory results for sample TSO 1-3 collected from the Tsotyli formation.

Petrophysical Properties	**Values**	**Sample code: TSO-1-3** **WGS84 Lat : 40.3075** **WGS84 Long : 21.3354**
Porosity (%)	6.0	
Water Permeability (mD)	<0.01	
Formation Factor/m	273/1.99	
Clay bound water (fraction)	0.87	

The PilotSTRATEGY project has received funding from the European Union's Horizon 2020 research and innovation programme under grant agreement No. 101022664

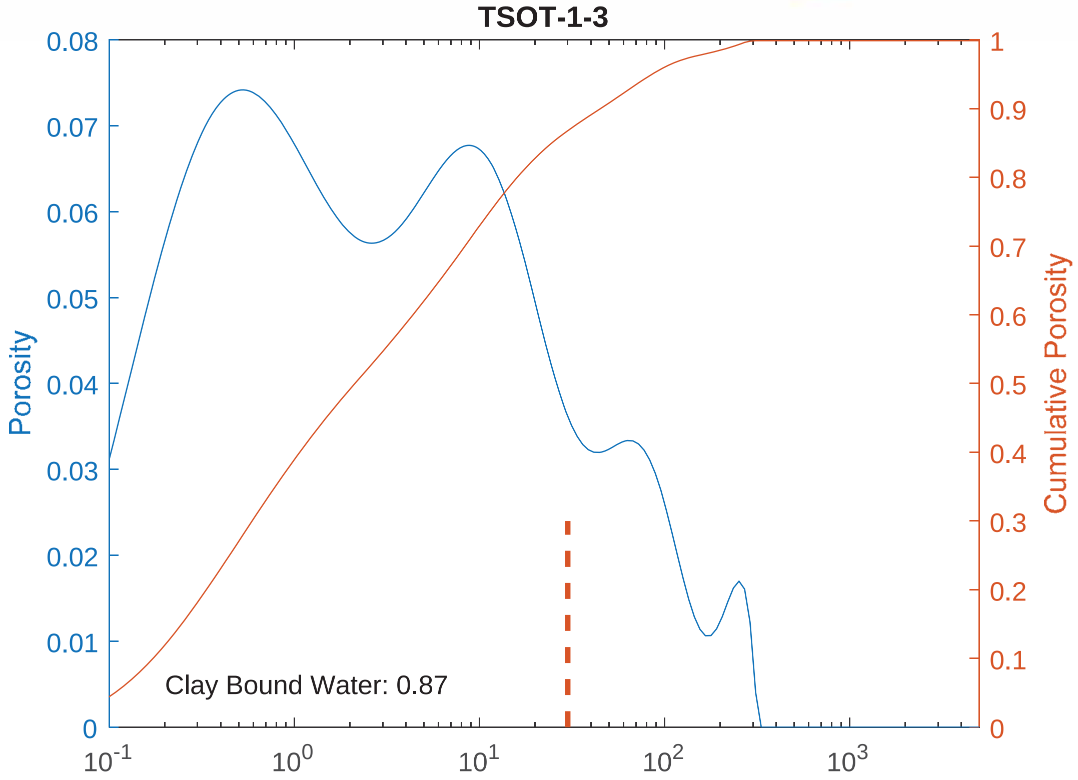

Figure 7.3.: Porosity and cumulative porosity values for sample TSOT-1-3 (Tsotyli formation), time-cut off at 30 ms.

The PilotSTRATEGY project has received funding from the European Union's Horizon 2020 research and innovation programme under grant agreement No. 101022664

7.1.2 Petrophysical results for Pentalofos formation

For the Pentalofos formation three samples were cored from the bulk sample and extracted for petrpophysical investigation. Since and the three samples come from the same batch, they share the same geographical coordinates. Table 7-2**Table 7-1** and Figure 7**.4** present the petrophysical results for the sample Pent 3-1 from the Pentalofos Formation (Upper Oligocene - Lower Miocene, estimated thickness 2500 m).

Table 7-2.: Petrophysical laboratory results for sample PENT-3-1 collected from the Pentalofos formation.

Petrophysical Properties	Values	Sample code: PENT 3-1 WGS84 Lat : 40.1332 WGS84 Long : 21.1997
Porosity (%)	5.0	
Water Permeability (mD)	<0.01	
Formation Factor/m	112/1.58	
Clay bound water (fraction)	0.96	

The PilotSTRATEGY project has received funding from the European Union's Horizon 2020 research and innovation programme under grant agreement No. 101022664

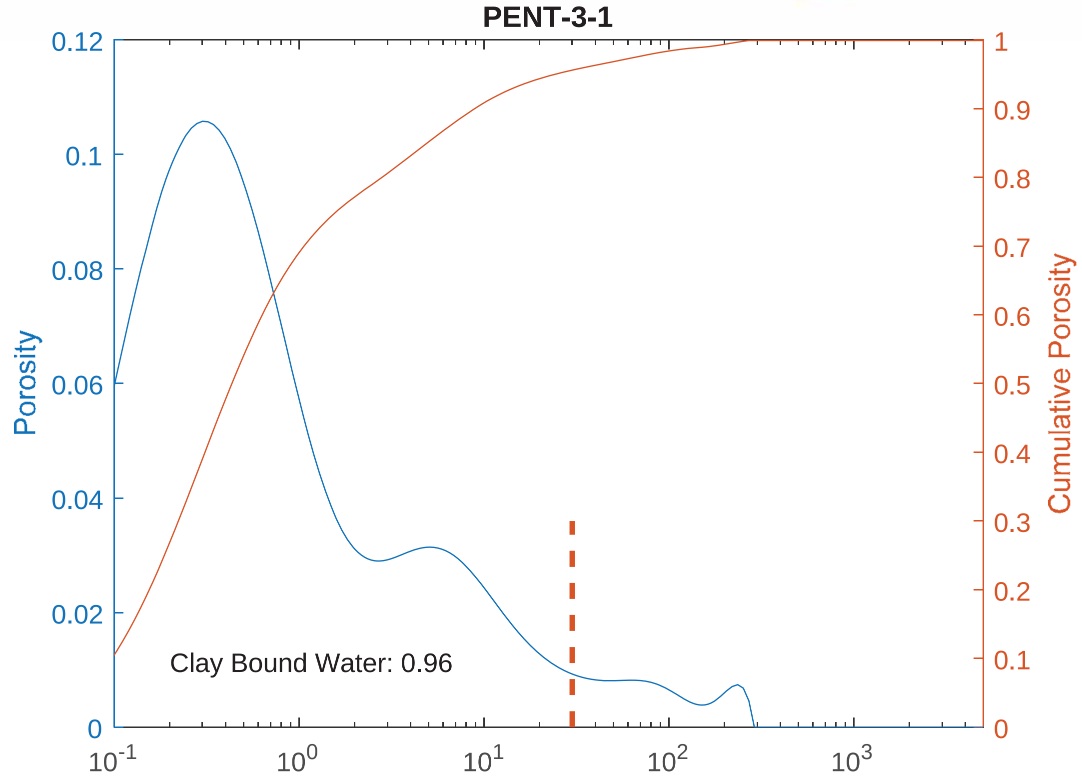

Figure 7.4.: Porosity and cumulative porosity values for sample PENT-3-1 (Pentalofos formation), time-cut off at 30 ms.

The PilotSTRATEGY project has received funding from the European Union's Horizon 2020 research and innovation programme under grant agreement No. 101022664

Table 7-3 **Table** 7-1 and Figure 7.**5** present the petrophysical results for the sample Pent 3-2 from the Pentalofos Formation.

Table 7-3.: Petrophysical laboratory results for sample PENT-3-2 collected from the Pentalofos formation.

Petrophysical Properties	**Values**	**Sample code: PENT 3-2** **WGS84 Lat : 40.1332** **WGS84 Long : 21.1997**
Porosity (%)	10.8	
Water Permeability (mD)	<0.01	
Formation Factor/m	46/1.72	
Clay bound water (fraction)	0.91	

The PilotSTRATEGY project has received funding from the European Union's Horizon 2020 research and innovation programme under grant agreement No. 101022664

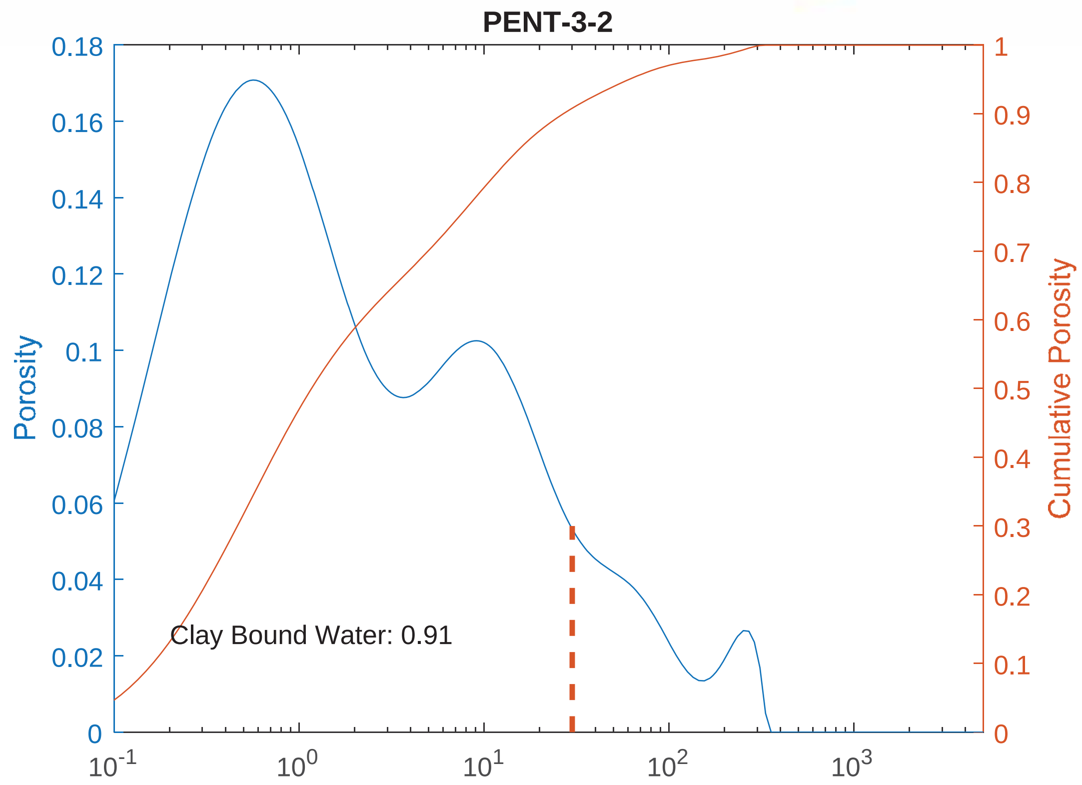

Figure 7.5.: Porosity and cumulative porosity values for sample PENT-3-2 (Pentalofos formation), time-cut off at 30 ms.

Table 7-4, **Table 7-3**, **Table 7-1** and Figure 7**.6** present the petrophysical results for the sample Pent 3-3 from the Pentalofos Formation.

Table 7-4.: Petrophysical laboratory results for sample PENT-3-3 collected from the Pentalofos formation.

Petrophysical Properties	**Values**	**Sample code: PENT 3-3** **WGS84 Lat : 40.1332** **WGS84 Long : 21.1997**
Porosity (%)	4.9	
Water Permeability (mD)	<0.01	
Formation Factor/m	157/1.68	
Clay bound water (fraction)	0.94	

The PilotSTRATEGY project has received funding from the European Union's Horizon 2020 research and innovation programme under grant agreement No. 101022664

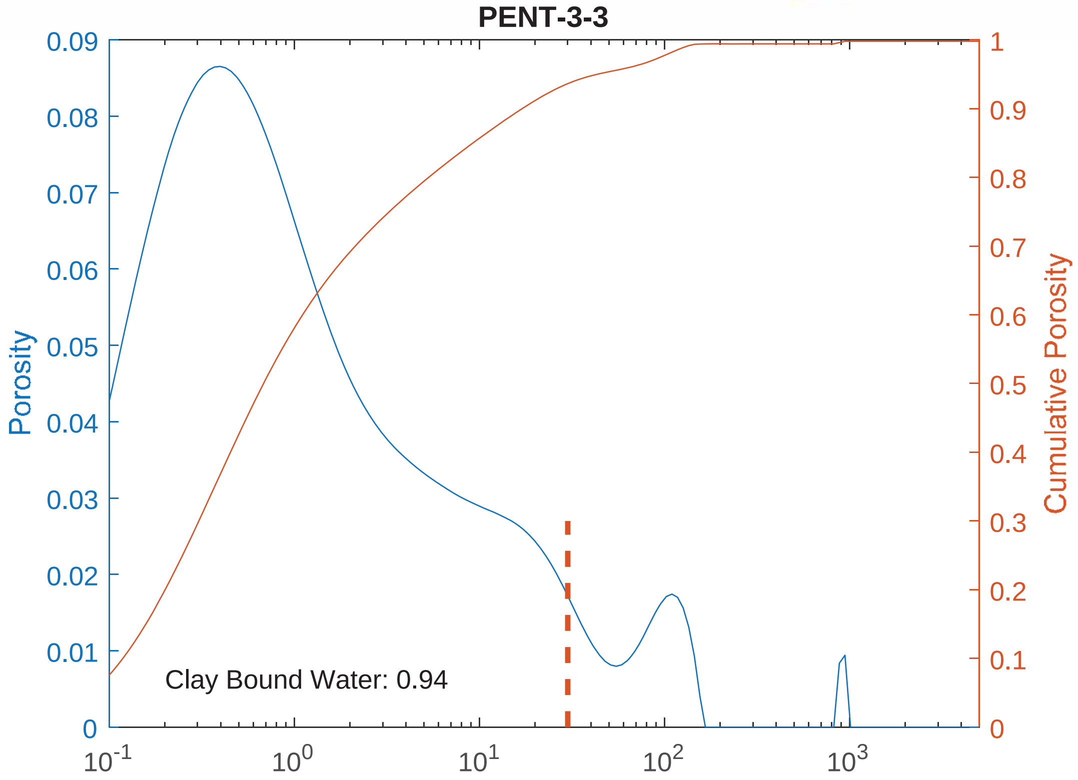

Figure 7.6.: Porosity and cumulative porosity values for sample PENT-3-3 (Pentalofos formation), time-cut off at 30 ms.

The PilotSTRATEGY project has received funding from the European Union's Horizon 2020 research and innovation programme under grant agreement No. 101022664

7.1.3 Petrophysical results for Eptachori formation

For the Pentalofos formation one sample was cored from the bulk sample and extracted for petrophysical investigation. Table 7-5 and Figure 7.**7** present the petrophysical results for the sample EPT 2-3 from the Pentalofos Formation (Upper Oligocene - Lower Miocene, estimated thickness 2500 m).

Table 7-5.: Petrophysical laboratory results for samples collected from the Eptachori formation.

Petrophysical Properties	**Values**	**Sample code: EPT-2-3.** **WGS84 Lat : 40.1535,** **WGS84 Long : 21.0824**
Porosity (%)	7.4	
Water Permeability (mD)	<0.01	
Formation Factor/m	123/1.46	
Clay bound water (fraction)	0.97	

The PilotSTRATEGY project has received funding from the European Union's Horizon 2020 research and innovation programme under grant agreement No. 101022664

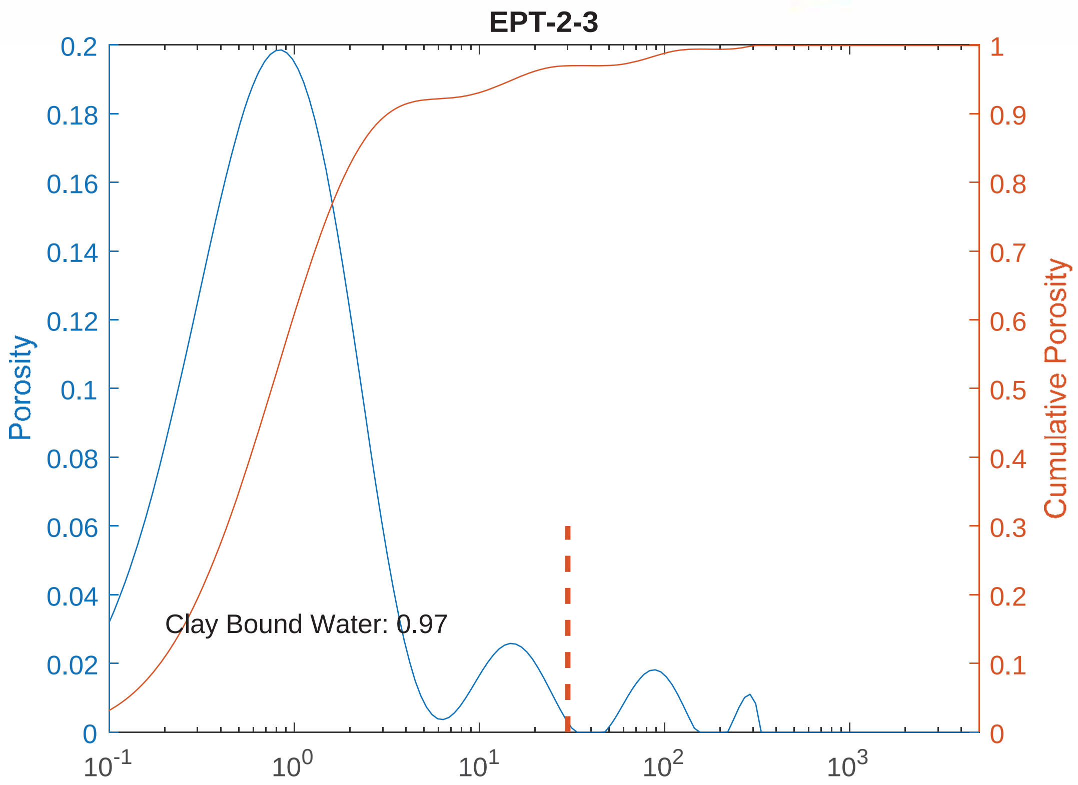

Figure 7.7: Porosity and cumulative porosity values for sample EPT-2-3, time-cut off at 30 ms.

The PilotSTRATEGY project has received funding from the European Union's Horizon 2020 research and innovation programme under grant agreement No. 101022664

7.2 References

Ciccotti, M., F. Mulargia, Differences between static and dynamic elastic moduli of a typical seismogenic rock, Geophysical Journal International, Volume 157, Issue 1, April 2004, Pages 474–477, https://doi.org/10.1111/j.1365-246X.2004.02213.x

Koukouzas, N., Tyrologou, P., Karapanos, D., Carneiro, J., Pereira, P., Lobo Veloso, F.M., Koutsovitis, P., Karkalis, C., Manoukian, E., Karametou, R., 2021, Carbon Capture, Utilisation and Storage as a Defense Tool against Climate Change: Current Developments in West Macedonia (Greece). Energies, 14, 3321; https://doi.org/10.3390/en14113321

Perras, M.A., Diederichs, M.S. A Review of the Tensile Strength of Rock: Concepts and Testing. Geotech Geol Eng 32, 525–546 (2014). https://doi.org/10.1007/s10706-014-9732-0

Christaras, B., Auger, F. & Mosse, E. Determination of the moduli of elasticity of rocks. Comparison of the ultrasonic velocity and mechanical resonance frequency methods with direct static methods. Materials and Structures 27, 222–228 (1994). https://doi.org/10.1007/BF02473036

The PilotSTRATEGY project has received funding from the European Union's Horizon 2020 research and innovation programme under grant agreement No. 101022664

8. Conclusion

1) Petrophysical data were successfully measured from subsurface samples, or from analogue surface samples, or calculated from borehole logs for all regions.

2) For the Paris Basin area, core samples from 2 wells were analysed. Neither well is in the study area, but the reservoir and seal are laterally homogeneous, and the wells are close. For the target reservoir, the reservoir section is not uniform vertically in terms of petrophysical properties and contains several barriers of low porosity and permeability. Permeability is governed by the amount of macroporosity. For the Vulaines 1 well, some porosity and permeability data are available from a database courtesy of the Vermilion oil company; the measurements performed in this study are consistent with these data.

3) For the onshore Ebro Basin (Spain), petrophysical characterization was carried out by both laboratory and on-site tests. Samples were from the Peñas Royas Section, the Torre de las Arcas outcrop and the Chiprana well. All are outside of the target structure but are thought to be representative of the reservoir and seal lithologies.

4) For the offshore Ebro area, samples of reservoir and seal were mostly taken from the Amposta Marino C2 well core, plus cuttings were available. Petrophysical analysis was conducted using available well logs and the results obtained were calibrated with the measured data. Porosity curves calculated with the neutron-density and density methods are very similar and calibrate well with core data.

5) For the Lusitania Basin (Portugal), outcrop samples from both reservoir complexes were collected onshore due to a lack of core samples. 13 wells were analysed, 7 offshore and 5 onshore; these are old and there are uncertainties in the calculate data. Samples covered three reservoirs of interest: Silves Group, Alcobaça Formation, Torres Vedras Formation. The Late Triassic Silves Group, has very low N/G, and overall low porosity that does not exceed 10%. The early Cretaceous Torres Vedras Formation has better N/G results, although with a large variability. The Torres Vedras Formation presents very good porosities, with an average value of 20%, this is the best reservoir target.

6) For West Macedonia (Greece), samples were collected from surface exposures of the Tsotyli, Pentalofos and Eptachori formations. All permeabilities of potential reservoirs were too low to be measured (< 0.01 mD).

The PilotSTRATEGY project has received funding from the European Union's Horizon 2020 research and innovation programme under grant agreement No. 101022664

9. ANNEXES

9.1 Ebro Basin - Spain

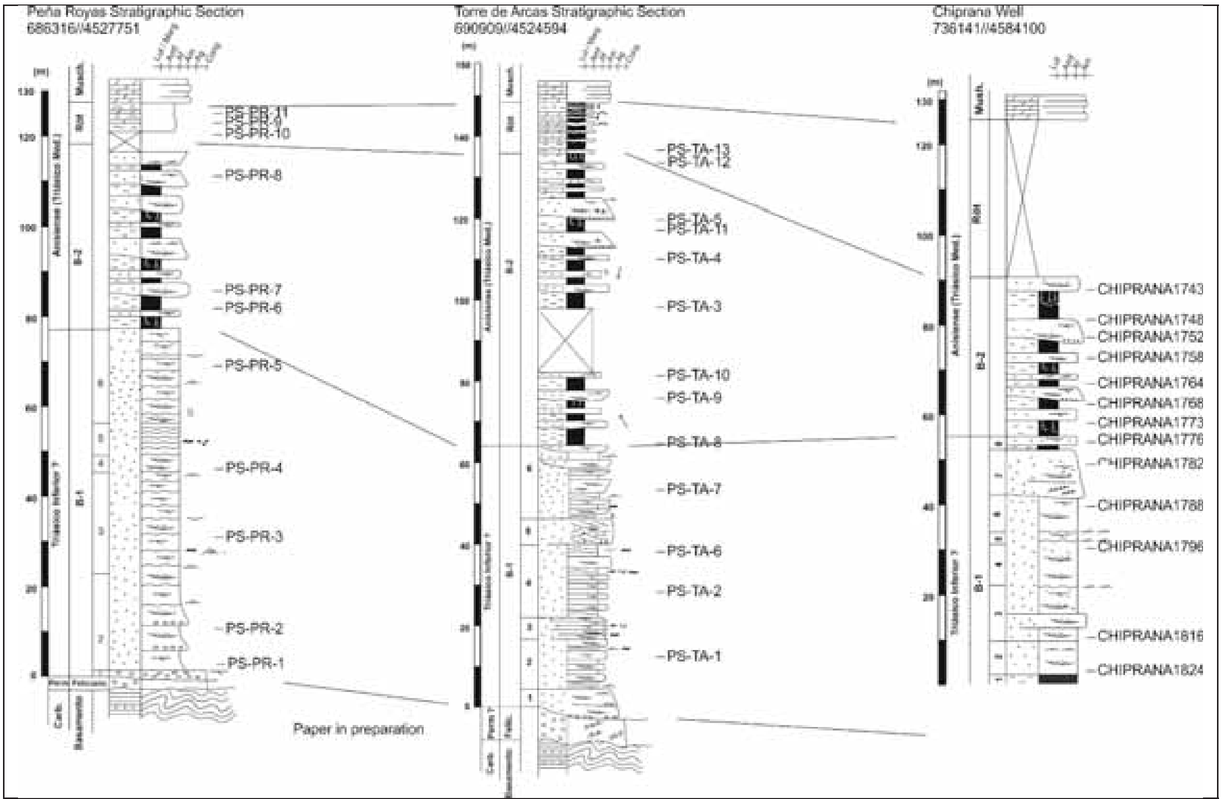

Localization of studied samples .

The PilotSTRATEGY project has received funding from the European Union's Horizon 2020 research and innovation programme under grant agreement No. 101022664

Samples of Peña Royas Section

The PilotSTRATEGY project has received funding from the European Union's Horizon 2020 research and innovation programme under grant agreement No. 101022664

Samples of Torre de Arcas Section

The PilotSTRATEGY project has received funding from the European Union's Horizon 2020 research and innovation programme under grant agreement No. 101022664

9.2 Portugal – Lusitanian Basin

Table – Studied samples from outcrops.

	**ARS-19** – Triassic Reservoir
	**ARS-20** – Triassic Reservoir

The PilotSTRATEGY project has received funding from the European Union's Horizon 2020 research and innovation programme under grant agreement No. 101022664

	**ARS-22** – Triassic Reservoir
	**CC-CV-4** – Triassic Reservoir

The PilotSTRATEGY project has received funding from the European Union's Horizon 2020 research and innovation programme under grant agreement No. 101022664

	**PRVT-23** – Triassic Seal
	**PPV-HT-28** – Triassic Seal

The PilotSTRATEGY project has received funding from the European Union's Horizon 2020 research and innovation programme under grant agreement No. 101022664

	**RNA-16** – Cretaceous Seal
	**FR-SIB-26** – Cretaceous Seal

The PilotSTRATEGY project has received funding from the European Union's Horizon 2020 research and innovation programme under grant agreement No. 101022664

	**CD-DARN-14** - Cretaceous Reservoir
	**PAJ-29** – Upper Jurassic Reservoir

The PilotSTRATEGY project has received funding from the European Union's Horizon 2020 research and innovation programme under grant agreement No. 101022664

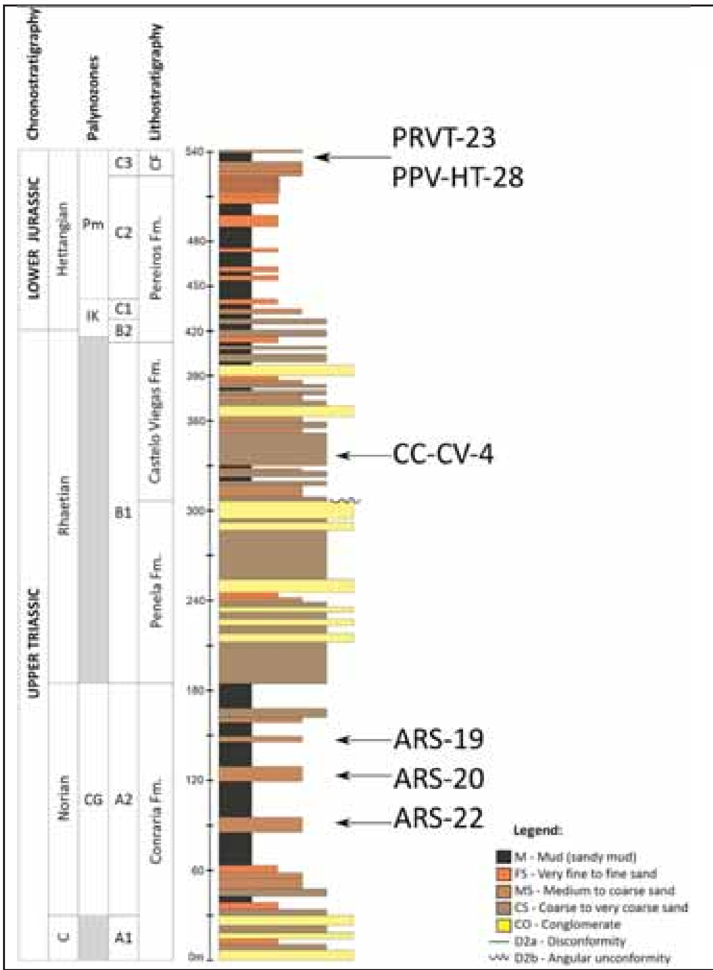

Figure … - Lithostratigraphic column of the Triassic storage complex, with location of the studied samples (adapted from Vilas-Boas et al., 2021).

The PilotSTRATEGY project has received funding from the European Union's Horizon 2020 research and innovation programme under grant agreement No. 101022664

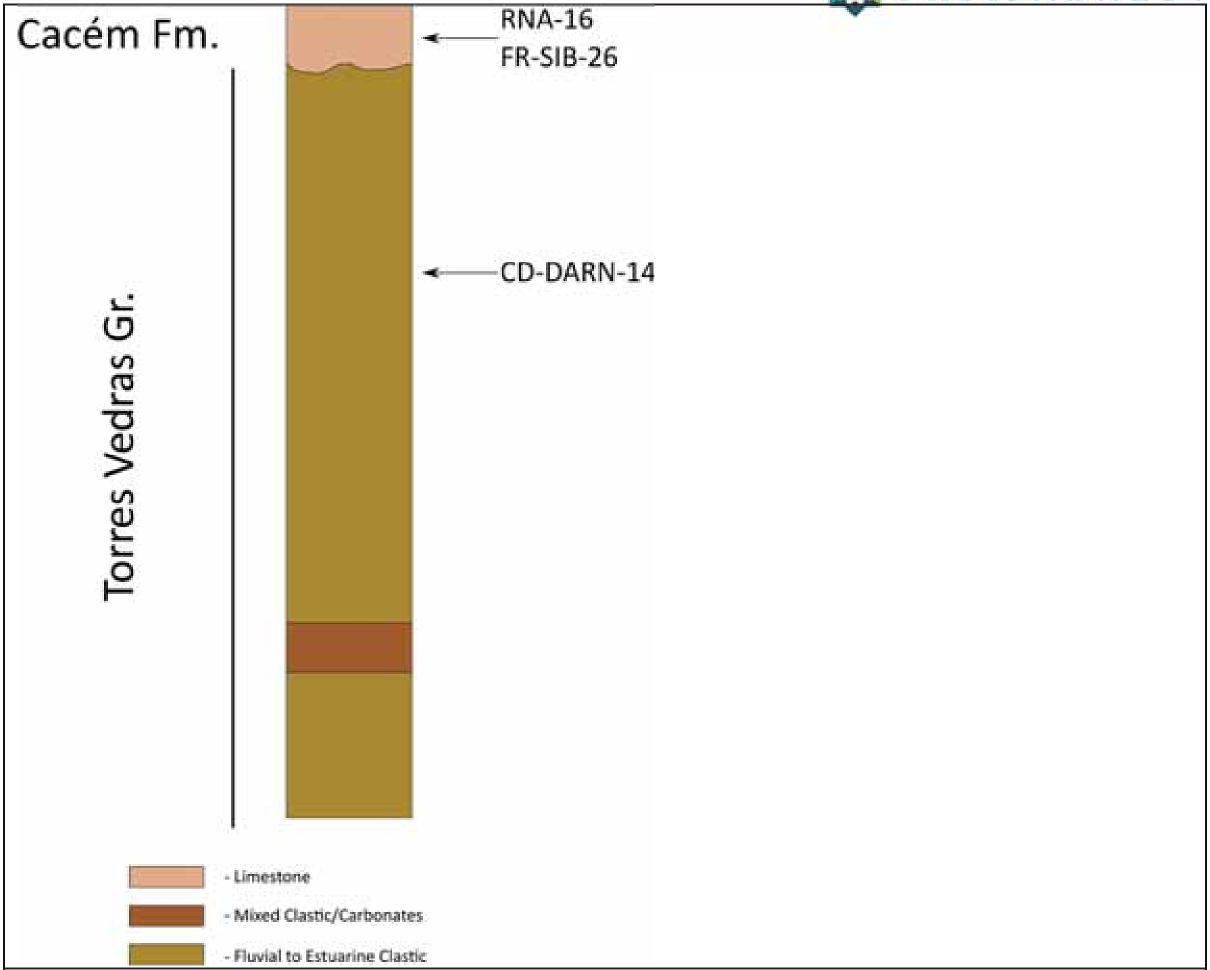

Figure … - Lithostratigraphic column of the Cretaceous storage complex, with location of the studied samples (adapted from Rey et al., 2006).

The PilotSTRATEGY project has received funding from the European Union's Horizon 2020 research and innovation programme under grant agreement No. 101022664

9.3 France – Paris Basin

The PilotSTRATEGY project has received funding from the European Union's Horizon 2020 research and innovation programme under grant agreement No. 101022664

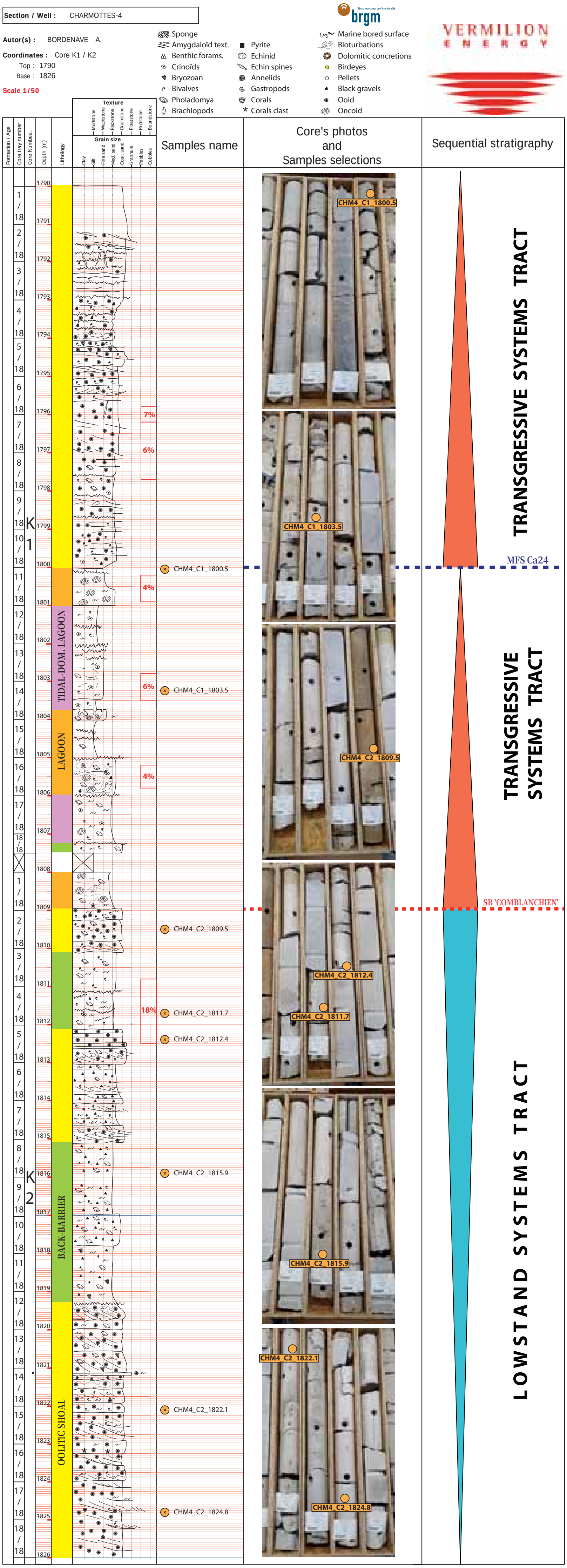

Section / Well : CHARMOTTES-4
Autor(s) : BORDENAVE A.
Coordinates : Core K1 / K2
Top : 1790
Base : 1826
Scale 1/50
brgm
VERMILION ENERGY
Sponge
Amygdaloïd text.
Benthic forams.
Crinoids
Bryozoan
Bivalves
Pholadomya
Brachiopods
Pyrite
Echinid
Echin spines
Annelids
Gastropods
Corals
Corals clast
Marine bored surface
Bioturbations
Dolomitic concretions
Birdeyes
Pellets
Black gravels
Ooid
Oncoid
Formation / Age
Core tray number
Core Number
Depth (m)
Lithology
Texture
Mudstone
Wackestone
Packstone
Grainstone
Floatstone
Rudstone
Boundstone
Grain size
Clay
Silt
Fine sand
Med. sand
Coar. sand
Granule
Pebbles
Cobbles
Samples name
Core's photos and Samples selections
Sequential stratigraphy
K1
K2
TIDAL-DOM. LAGOON
LAGOON
BACK-BARRIER
OOLITIC SHOAL
7%
6%
4%
6%
4%
18%
CHM4_C1_1800.5
CHM4_C1_1803.5
CHM4_C2_1809.5
CHM4_C2_1811.7
CHM4_C2_1812.4
CHM4_C2_1815.9
CHM4_C2_1822.1
CHM4_C2_1824.8
TRANSGRESSIVE SYSTEMS TRACT
MFS Ca24
TRANSGRESSIVE SYSTEMS TRACT
SB 'COMBLANCHIEN'
LOWSTAND SYSTEMS TRACT

Section / Well : VULAINES-1

Autor(s) : ISSAUTIER B.

Coordinates : Cores K6 / K7 / K8 / K9 / K10 K/11

Top : 1790
Base : 1826

Scale 1 / 50

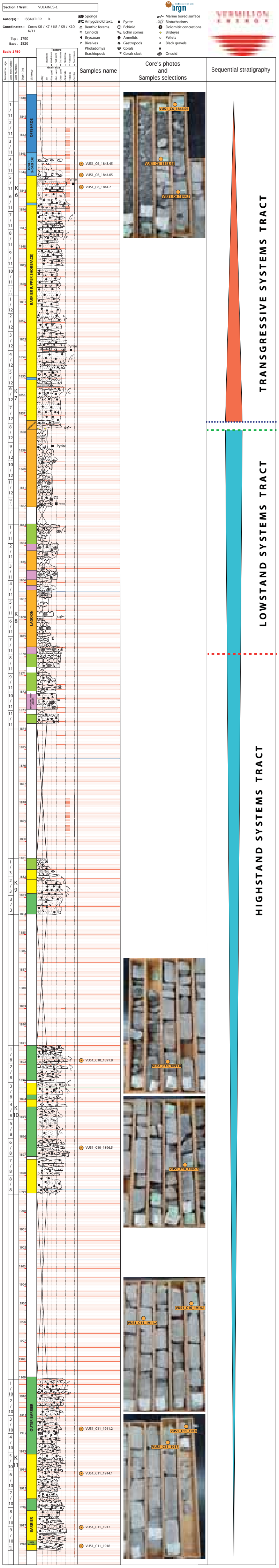

10. Appendix: experimental set-ups, measurement methodologies

10.1 Permeability and formation factor measurements (IFPEN)

The permeability was measured at room temperature on brine saturated samples (20 g/l NaCl) in an individual cell (Figure 10.1). At least three flow rates Q were imposed while measuring the corresponding stabilized pressure drop ΔP. Permeability is then obtained from the slope of Q vs ΔP by a linear regression, taking into account the brine viscosity at the measurement temperature.

The formation factor was measured simultaneously with permeability using a classical face to face two electrode system at ambient laboratory temperature (Figure 10.1). The conductivity of the brine was measured at the outlet of the core holder using a conductivity meter in which a temperature sensor was included. The formation factor was then determined from the ratio of brine to sample conductivity ($FF=C_w/C_0$) measured at the same temperature. The sample conductivity C_0 was determined using the measured resistance R and the sample length L and diameter D by the formula $C_0=L/(R\ \pi\ D^2/4)$.

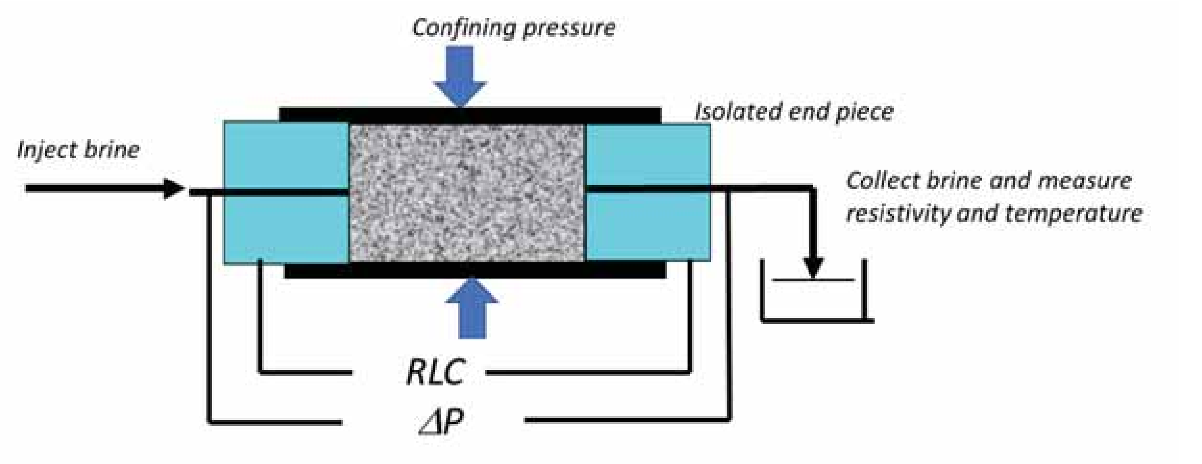

Figure 10.1: Schematic of the experimental set—up to measure permeability and formation factor

The above device was available only on 40 mm diameter sample. Indeed, due to the lack of enough rock material, smaller samples had to be cored (25 and 10 mm in diameter) but could formation factors could not be measured on these samples.

Interpretation of formation factor: cementation exponent

We provide a single point estimation of the cementation exponent according to:

$$m = -\frac{\log(FF)}{\log(F)}$$

where Φ is the porosity expressed in fraction. However, other relationships are possible such as:

$$FF = a\ F^{-m}$$

The PilotSTRATEGY project has received funding from the European Union's Horizon 2020 research and innovation programme under grant agreement No. 101022664

In these cases, adjusting a and m by regression need multiple data points with some porosity variations. Also, in clayey sandstones, the formation factor may need to be calculated differently from the conductivity measurements described above. For example in the Waxman-Smits model:

$$FF = \frac{C_{clay} + C_w}{C_0}$$

where C_{clay} is the excess conductivity due to the clays. Adjusting C_{clay} needs a series of measurement in which the conductivity of the sample is measured with different salinities. This was however not planned initially.

10.2 Centrifuge test (IFPEN)

Saturated samples were desaturated under air in a centrifuge with the objective of measuring the irreducible water saturation Swi, i.e. the asymptotic value of the capillary pressure curve (Figure 10.2). The spinning rotation speed ω was chosen such as to reach a capillary pressure Pc function of the radius of rotation and the sample length according to (Figure 10.3).:

$$P_C\,(R) = \frac{1}{2}\omega^2\left(R_{\max}^2 - R^2\right)\left(\rho_w - \rho_g\right)$$

The indicated capillary pressure are calculated at the inlet face of the sample R_{min} (about 7 bar for most samples). Since several samples of different length were centrifuged at the same time, the maximum Pc value can vary from one sample to another. To minimize the saturation profile, the sample was placed on a ceramic porous plate (Figure 10.3).

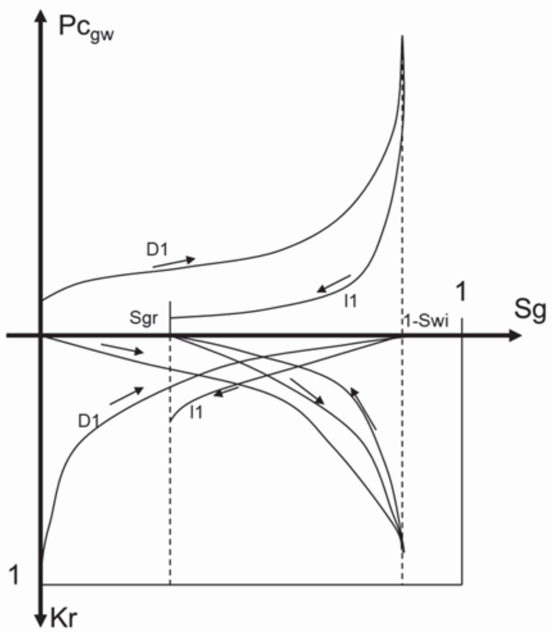

Figure 10.2: General shapes of capillary pressure curves and relative permeabilities in drainage (D1) and imbibition (I1). The irreducible water saturation Swi can be defined as the asymptotic value of the Pc curve.

The PilotSTRATEGY project has received funding from the European Union's Horizon 2020 research and innovation programme under grant agreement No. 101022664

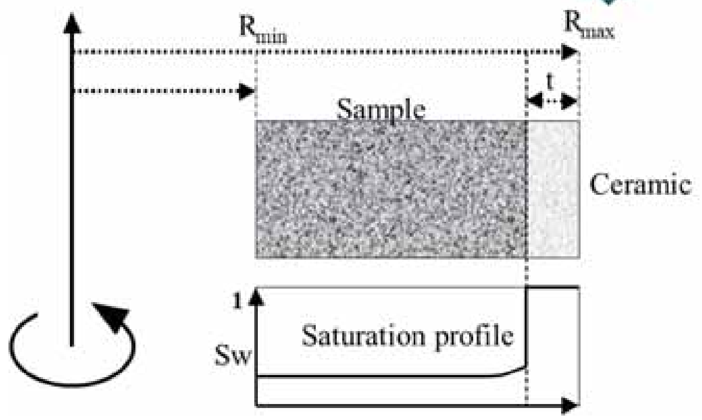

Figure 10.3: Schematic of the centrifuge set-up.

10.3 NMR measurements (IFPEN)

NMR measurements were performed using two low-field instruments (Magritek and Oxford Instruments) operating at 2 MHz for plugs with a diameter of 40 mm and 21 MHz for plugs with a diameter of 10 mm. NMR porosity and T_2 relaxation time distributions were calculated using a in-house software from the measured magnetization M(t). The plotted distribution corresponds to the amplitudes A according to :

$$M(t) = \sum_{i=1}^{i=200} A_i \exp\left(\frac{-t}{T_{2i}}\right)$$

where T_{2i} is a predefined table of 200 values spaced logarythmically between 0.1 ms and 5000 ms. The amplitudes Ai correspond to the number of water molecules at a relaxation time T_{2i}. Hence the total number of water molecules in the sample is the sum of all amplitudes; in the graphs, the amplitudes Ai are expressed in units of porosity, i.e. a measured water volume divided by the total geometric volume of the cylindrical sample, so that distributions measured on small or large samples of similar porosity can be compared and plotted in the same graph.

NMR T_2 relaxation time distributions can be interpreted as a pore-size distribution according to:

$$\frac{V}{S} = \rho_2 \left(\frac{1}{T_2} - \frac{1}{T_{2B}}\right)^{-1}$$

where ρ_2 is a surface relaxivity, V and S is the volume and surface of a pore, respectively, and T_{2B} represents the bulk water relaxation (about 3 s at 30 °C). However this conversion is usually not performed because the exact values of the surface relaxivity are not known. For subsurface porous rocks, there exist some general guidelines for calculating the so-called “Clay Bound Water” (CBW) for sandstone formation, and microporosity for carbonates (f_{micro}). (Dunn et al., 2002). These important parameters are calculated from the T_2 distribution according to

$$CBW\ , f_{micro} = \frac{\sum_{i=1}^{i=c} A_i}{\sum_{i=1}^{i=200} A_i}$$

The PilotSTRATEGY project has received funding from the European Union’s Horizon 2020 research and innovation programme under grant agreement No. 101022664

where the index c corresponds to a cut-off value T_{2c}. The default values of T_{2c} are, for sandstones, T_{2c} ~30 ms and for carbonates T_{2c} ~150 ms. Essentially, we calculate with this formula the amount of water in the smallest pores normalized by the total amount of water.

NMR measurements have also been performed using centrifuge de-saturated plugs. Since the imposed capillary pressure is quite large (about 7 bar for most samples), we have a measure of the irreducible water saturation Swirr. Hence we can calculate another value T_{2c}' such as (index c')

$$Swirr = \frac{\sum_{i=1}^{i=c'} A_i}{\sum_{i=1}^{i=200} A_i}$$

This calibrated cut-off corresponds more precisely to the smallest pores that cannot be desaturated during the CO_2 injection. A sketch of a measured distribution on shaley sandstone along with a summary of the significance of the provided numbers is given is

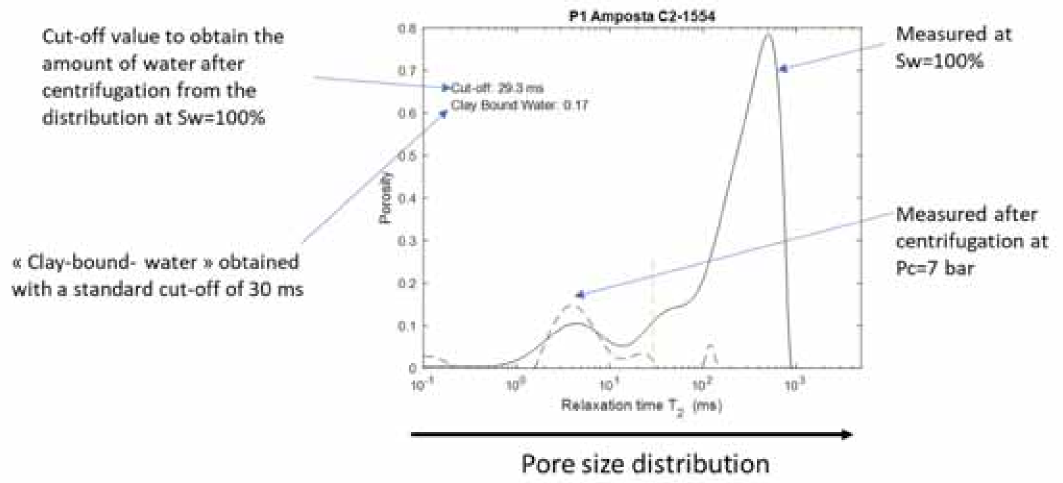

Figure 10.4: Example of two measured NMR distributions (at Sw=100% and Swirr).

10.4 Low and ultra-low permeability measurements (IFPEN)

The steady state method was used (Boulin et al., 2012). In the steady state method, a pressure gradient is applied and the corresponding water flux is measured. The water permeability k (m^2) is deduced from Darcy's law:

$$Q = S \cdot \frac{k}{\mu} \cdot \frac{P_u - P_d}{L}$$

where Q is the water flux (m3/s), S the sample surface (m2), µ the water viscosity (Pa.s), L the sample length (m), Pu the upstream pressure (Pa) and Pd the downstream pressure (Pa). The experimental set-up included two pistons (A and B on Figure 10.5). Piston A maintains the upstream pressure. Downstream pressure, maintained by piston B, was chosen to be lower than Pu, in order to create a flow of water from A to B. Displacements of pistons A and B provide measurements of the water flux Q (push-pull mode) using high precision pumps.

The PilotSTRATEGY project has received funding from the European Union's Horizon 2020 research and innovation programme under grant agreement No. 101022664

Upstream and downstream pressures were maintained independently by each piston. Upstream pressure was set to 7.5, 8 and 8.5 MPa, and corresponding downstream pressure was set respectively to 6.5, 6 and 5.5 MPa in such a way that the pore pressure was maintained at a mean value of 7 MPa, and the pressure gradient was set to 1, 2, and 3 MPa (each pressure gradient lasted three hours).

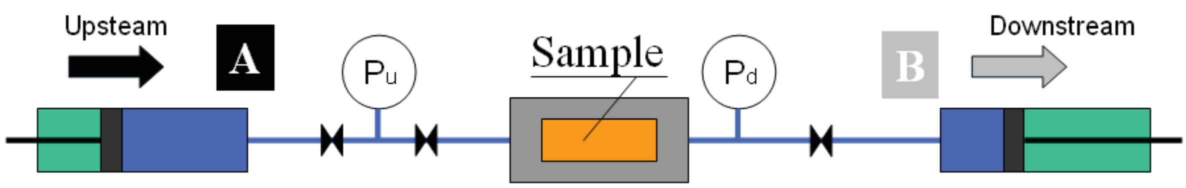

Figure 10.5: Simplified diagram of the experimental set-up. A and B represent the two pistons of the high precision pumps used upstream and downstream. The assembly is placed in an oven in which the temperature is regulated within 0.2 °C.

10.5 Entry pressure measurements (IFPEN)

Two measurement techniques were used. First, the standard method (Li et al, 2005) in which an upstream gas pressure is increased step by step until water is displaced at the outlet. The duration of the respective steps should be long enough to allow for observation of downstream water production (3 to 4 days). The water production itself is recorded by a pump placed downstream. The second method follows the dynamic approach presented by Egermann et al. (2006). Here, gas is injected upstream at a constant pressure P_g, gas pressure is chosen above the entry pressure. Upstream, gas displaces water until gas is in contact with the sample's surface. As the downstream pressure is maintained to be constant, two different flow rates are observed: before and after gas entry. The flow rate difference is related to the entry pressure value. Before conducting the caprock entry-pressure experiments, the permeability was measured using the steady state method (three flow rates at three different pressure gradients, see previous paragraph).

The PilotSTRATEGY project has received funding from the European Union's Horizon 2020 research and innovation programme under grant agreement No. 101022664

10.6 Refererences

Boulin P.F., Bretonnier P., Gland N., Lombard J.M. (2012), Contribution of steady state methods to water permeability measurement in very low permeability porous media, Oil Gas Sci. Technol. 67, 3, 387-401.

Egermann, P [P.], Lombard, J.-M., & Bretonnier, P. (2006). A fast and accurate method to measure threshold capillary pressure of caprocks under representative conditions. International Symposium of the Society of Core Analysts.

Dunn, K.-J., Bergman, D. J., & Latorraca, G. A. (2002). Nuclear magnetic resonance: Petrophysical and logging applications (1st ed.). Seismic exploration: v. 32. Pergamon.

Li S., Dong M., Li Z., Huang S., Qing H., Nickel E. (2005) Gas breakthrough pressure for hydrocarbon reservoir seal rocks: implications for the security of a long-term CO2 storage in the Weyburn field, Geofluids 5, 326-334.

The PilotSTRATEGY project has received funding from the European Union's Horizon 2020 research and innovation programme under grant agreement No. 101022664